In presenting the dissertation as a partial fulfillment of the requirements for an advanced degree from the Georgia Institute of Technology, I agree that the Library of the Institute shall make it available for inspection and circulation in accordance with its regulations governing materials of this type. I agree that permission to copy from, or to publish from, this dissertation may be granted by the professor under whose direction it was written, or, in his absence, by the Dean of the Graduate Division when such copying or publication is solely for scholarly purposes and does not involve potential financial gain. It is understood that any copying from, or publication of, this dissertation which involves potential financial gain will not be allowed without written permission.

7/25/68

A LASER DOPPLER VELOCIMETER SYSTEM FOR JET FLOW STUDIES

A THESIS

Presented To

The Faculty of the Graduate Division

by

Ram Priya Chaturvedi

In Partial Fulfillment

of the Requirements for the Degree

Master of Science in Mechanical Engineering

Georgia Institute of Technology

September 1971

A LASER DOPPLER VELOCIMETER SYSTEM FOR JET FLOW STUDIES

Approved:

Chairman

Date approved by Chairman July 27, 1971

ACKNOWLEDGMENTS

I wish to thank my thesis advisor, Dr. P. V. Desai, who proposed the research problem and provided guidance throughout this study. I also wish to express my gratitude for Dr. James H. Rust for providing valuable help in conducting the experimental investigation and for participating as a member of the thesis reading committee. My appreciation is extended to Dr. P. Durbetaki for his interest and participation as a member of the thesis reading committee.

I am indebted to two of my cohorts, Mr. William Evans and Mr. Larry Mathews for their timely help during the critical phase of this research.

TABLE OF CONTENTS

LIST OF TABLES

LIST OF ILLUSTRATIONS

Figure Page

NOMENCLATURE

a	= distance between focal point and receiver lens, Figure 2.7.
b	= distance between receiver lens and field stop, Figure 2.7.
b_o	= jet pipe radius.
B	= a quantity defined by equation 2.21.
B_d	= Doppler signal bandwidth.
B_N	= effective noise bandwidth.
B_p	= phototube bandwidth.
B_s	= spectrum analyzer bandwidth.
C	= channel number.
d	= distance between the particle and first scattered wavefront.
d_o	= jet pipe diameter.
D'	= field stop diameter.
D_A	= aperture diameter.
D_h	= heterodyne volume diameter
D_{11}, D_{22}, D_{33}	= lens diameters.
D_t	= pipe diameter.
e_1, e_2, e_3, e_m	= unit direction vectors.
E, E'	= laser beam diameter.
f_D	= Doppler signal frequency.
f_1	= frequency of the incident radiation.
f_o	= free-running frequency.

NOMENCLATURE (Continued)

f_{1A}	= apparent frequency of the incident radiation, equation 2.4.
f_{LO}	= frequency of the local oscillator.
f_{i1}, f_{i3}	= lower end of the capture range of a phase locked loop.
f_{i2}, f_{i4}	= upper end of the lock range of a phase locked loop.
f_s	= frequency of scattered radiation.
f_{iF}	= intermediate signal frequency in a spectrum analyzer.
f_{sig}	= input signal frequency.
F_1, F_2	= focal lengths.
FR	= friction factor.
FS	= field stop.
g	= acceleration due to gravity.
G	= phototube current gain
h	= Plank's constant
h_f, H_f	= head loss
i	= a quantity defined by equation 2.23.
I	= photomultiplier output current.
I_s	= Doppler signal current.
$I_1, I_2, I_3,$ $I_{\Delta B}, I_{A/C}; I_{DC}$	= various electrical currents.
j	= channel number.
k	= Boltzmann constant.
K	= proportionality constant of equation (2.14).
l	= pipe length

NOMENCLATURE (Continued)

L	= lens.
M	= mirror.
n,n'	= index of refraction.
N_d	= number of particles in heterodyne volume.
N_j	= number of counts in channel number j.
N_{Re}	= Reynolds number.
O( )	= of the order of.
p, p_d, p_i, p_r, p_s	= various power levels.
P	= scattering particle.
r_1	= signal to background noise ratio.
r	= radial coordinate.
r_{pot}	= potential core radius.
r_p	= scattering particle radius.
R	= load resistance.
t	= time.
T	= signal period.
T°	= absolute temperature.
U_r, U_{rr}, U_s, U_{ss}	= electrical wave functions.
$u_j, u_x, u_o, u_{x_{max}}, u'$	= flow velocities associated with a jet velocity field.
v_e, v_d, v_l, v_o, v_s	= voltages.

NOMENCLATURE (Continued)

V_f	= pipe flow velocity.
$V_1, V_2, V_{21}, V_{23}, V_m$	= velocities associated with the light scattering phenomenon of Doppler shift.
w_1	= wavefront.
W	= scattered radiation intensity.
x	= axial coordinate.
A_1, A_2	= apertures.
BS	= beam splitter.
CRT	= cathode ray tube.
ADC	= analog to digital converter.
DDM	= differential Doppler method.
DM	= discriminator.
DV	= digital voltmeter.
HP	= high pass filter.
kHz	= kilohertz.
LDV	= laser Doppler velocimeter.
LS	= laser source.
MA	= multichannel analyzer.
MHz	= megahertz.
OX	= optical axis.
PHA	= pulse height analysis.
PM	= photomultiplier tube.
RBA	= reference beam approach.
SNR	= signal to noise ratio.

NOMENCLATURE (Continued)

TAC	= time to amplitude converter.
VS	= high voltage supply.
α	= angle subtended by the field stop at receiver lens, Figure 2.7.
α_{min}	= minimum angle of resolution of a lens.
η	= efficiency.
θ	= angle between the two incident beams in a DDM system.
θ_d	= laser beam divergence angle.
θ_m	= maximum allowable misalignment between two beams, equation 2.22.
θ_R	= angle between incident and scattered beam directions.
λ_1	= wavelength of incident radiation.
λ_{10}	= vacuum wavelength of incident radiation.
λ_s	= wavelength of scattered radiation.
μ	= micron.
ϕ_o	= angle as shown in Figure 2.8.
ψ_o	= angle as shown in Figure 2.8.
ω_r, ω_s	= angular frequencies.
Ω_s	= solid angle.

SUMMARY

This thesis presents an exploratory investigation of a laser Doppler velocimeter system suitable to study liquid jet flow fields. The investigation has been carried out in two phases. The first phase includes a careful examination of optical configurations of the velocimeter applicable to jet flow studies, as well as an evaluation of an appropriate electronic readout system. Results of the first phase of investigation have been applied to develop a specific system configuration consisting of suitable optics, electronics and the jet flow loop. Calibration and computation procedure for quantitative evaluation of jet velocities have been outlined.

CHAPTER I

INTRODUCTION

1.1 Anemometry in Fluid Flow Fields

Experimental investigation of a fluid flow field often necessitates accurate and high response velocity sensors. Commonly employed techniques of fluid velocity determination employ an actual measurement of one or more of such secondary quantities as the fluid pressure, the temperature, the density, and the convective heat transfer. An inherent limitation of many techniques of velocity measurement can be traced to the disturbance that the sensing probe generates when introduced into the flow field. Compensatory analyses and calibrations are often needed to account for the flow disturbance prior to the actual determination of local velocity. Among the commonly employed velocity measurement instruments are the Prandtl-Pitot probe, the hot-wire or hot-film anemometer, as well as several flow visualization systems.

Perhaps the simplest and most often used velocity probe is the Prandtl-Pitot tube, originally conceived by Henri Pitot and later modified by Ludwig Prandtl. Fluid velocity is determined by this probe from measured values of the stagnation and the static pressures. Factors that contribute to measurement errors include, (i) a misalignment of the tube axis with the velocity vector, resulting in incorrect values of registered static and stagnation pressures, and (ii) a finite tube diameter resulting in a crowding of streamlines over the probe as

compared to the unstretched streamlines in the actual undisturbed flow field. Furthermore, the difficulties associated with fluctuating, as well as two- orthree-dimensional flow fields render the application of the probe suitable for steady one-dimensional flow fields. For flow fields exhibiting very low Reynolds numbers the Prandtl-Pitot tube becomes specially inappropriate due to the influence of viscous stresses at the stagnation pressure hole.

Hot wire and hot film anemometers have been commonly used in fluctuating or turbulent flow fields, which are quasi-steady, or steady on the mean. Such probes employ the cooling effect of a fluid stream blowing over an electrically heated surface. Of the two varieties of a hot wire anemometer, the constant temperature type employs a very fine metallic resistance wire carrying an electric current, which is introduced within the flow field to be measured. A portion of the internal heat generated within the wire is lost to the fluid flowing past it by convective heat transfer from the wire surface. The amount of current required to maintain the wire temperature and, hence, its resistance constant is a measure of the flow velocity. In a constant current type of hot wire anemometer, a constant amount of internally generated heat, together with the cooling capacity of the flow field, determine an equilibrium wire temperature or resistance. The voltage drop across the resistance becomes a measure of the flow velocity. For sufficient accuracy, a hot wire anemometer needs to be separately calibrated for specific applications. Such calibrations involve extensive electronic compensating circuitry, resulting in a rather complex measurement system. Due to its fine size the sensor wire has very limited aerodynamic strength.

This has led to a less frequent use of the hot wire technique in liquid flow systems as compared with its use in gaseous flow fields. Frequent calibrations of the wire become necessary due to the change in wire resistance caused by contaminants in the flowing fluid. A recurring problem of wire burnout due to any sudden decrease in local velocity is caused by the fact that a typical wire temperature is considerably higher than that of the surrounding fluid.

A hot-film transducer is a modification of a hot-wire anemometer to attain better strength characteristics for a wide range of flow situations. In a hot film device, a thin film of platinum deposited over a glass base is utilized to replace the fine resistance wire of a hot wire anemometer. The basic measurement circuitry is essentially the same as that used in constant temperature hot wire anemometer. Due to the increased dynamic and thermal strength, hot film anemometers often find applications in high temperature environments such as combustion chambers.

It is interesting to note that in compressible flow investigations, the direct readout of a hot wire or a hot film instrument is a measure of the local mass flow rate. This necessitates a further knowledge of the density variation before information regarding flow velocities can be obtained. A frequently encountered problem of measuring time dependent velocity profiles has not been satisfactorily resolved by hot wire or hot film techniques without compromising the structural integrity of the sensor and adding complex compensating circuitry.

Use of illuminated or self-luminous particles added to the flow system and other such flow visualization methods, as well as several tracer techniques are primarily intended for overall or qualitative investigations, rather than a detailed survey of the local flow fields.

Nevertheless, flow visualization by optical methods offers the advantage that it does not disturb the fluid flow field. While shadowgraphs and Schlieren techniques are mainly employed for temperature measurements, interferometers have been used in velocity measurements. However, their application is limited, since they measure the local density to obtain the fluid velocity. It might be pointed out that for surveying supersonic flow fields in the presence of shocks, an interferometer serves as a very useful tool.

Recently, there has been an increasing interest in an entirely novel optical technique for fluid velocity measurements. Commonly referred to as laser Doppler velocimetry (LDV), the technique uses a continuous wave laser as the source of incident radiation, portion of which is subsequently scattered by microscopic contaminants flowing with the fluid in a flow system under investigation. Optical mixing, at a photocathode surface, of the scattered portion with a portion of the unscattered radiation, produces an electrical signal at the Doppler frequency. The Doppler frequency equals the difference in frequencies of the scattered and the unscattered radiations. The Doppler frequency is directly related to the local flow velocity, as well as other system parameters. This technique directly measures local fluid velocities without disturbing the flow, since no physical sensor needs to be introduced in the flow field. Moreover, the method maintains a high sensitivity of measurement over a wide range of fluid velocities.

Two basic optical arrangements have been used in velocity measurements with LDV. These are referred to as the Reference Beam Approach (RBA) and the Differential Doppler Method (DDM). In a typical RBA ar-

rangement, the scattered radiation is optically mixed with a portion of unscattered radiation. This process is termed as optical heterodyning, which produces a periodic signal at the difference or Doppler frequency. A DDM configuration optically mixes two scattered beams with unequal Doppler shifts in their frequencies from the incident unscattered beam frequency. This results in a Doppler signal at a frequency equal to the difference in frequencies of the two scattered radiations. The main advantage of using a DDM system over a RBA arrangement lies in the fact that the alignment of optics is less critical in a DDM. Moreover, since the Doppler signal frequency is independent of scattering direction, scattered light may be collected over a wide range of directions to achieve the required intensity. This is achieved without broadening the Doppler signal spectrum. The RBA approach, on the other hand, has excellent discrimination characteristics against the background light. In principle it is possible to use three phototubes in three mutually perpendicular directions to measure total velocity vectors in the flow field.

1.2 A Brief Survey of Pertinent Literature

A pioneering effort in fluid flow measurement, which eliminated the disturbance of the flow field resulting from the technique of measurement, was reported in May 1964 by Yeh and Cummins [1][(1)]. In a report entitled, "Localized fluid flow measurement with an He-Ne laser spectrometer", they demonstrated that fluid velocities of the order of 3×10^{-4} feet per second ($N_{Re} = 0(10)$) could be measured by using a laser

---

(1) Numbers in square brackets represent the references in the bibliography.

spectrometer to examine the Doppler shift in the Rayleigh scattered light. Their scheme of measurement, shown in Figure 1.1, basically consisted of a Helium-Neon laser source, an arrangement of lenses and mirrors, a fluid flow loop with 30,000 parts of water by volume flowing with one part of 0.5 micron polystyrene spheres acting as scattering sources, and a photomultiplier tube. Their results showed a need to examine the importance of several quantities such as the size and concentration of the scattering particles, the range and geometry of measurable flow regimes, the fineness of the laser beam, alternative optical configurations, and data recording systems.

Foreman et al [2] extended the Yeh and Cummins technique to velocity measurement in gaseous flow fields. Initially using a glass tube and later a wind tunnel, they established the feasibility of the new technique in gaseous flows contaminated with smoke particles of random sizes and shapes acting as scatterers. By employing an analog frequency meter and a spectrum analyzer, they made measurements of Doppler frequencies corresponding to velocities as high as 1,000 feet per second ($N_{Re} = O(10^6)$). They observed Doppler signals for speeds up to 1,500 feet per second. Higher velocity measurements were restricted due to limited accuracy of their readout system and the nature of their flow system. The main problem being generation and injection of enough smoke particles into the flow field.

An important contribution by Davis [3] on the influence of system parameters on the performance of an LDV gave a new impetus to examine such a technique in further details. He demonstrated the importance of the coherency of the scattered and unscattered radiation in realizing the

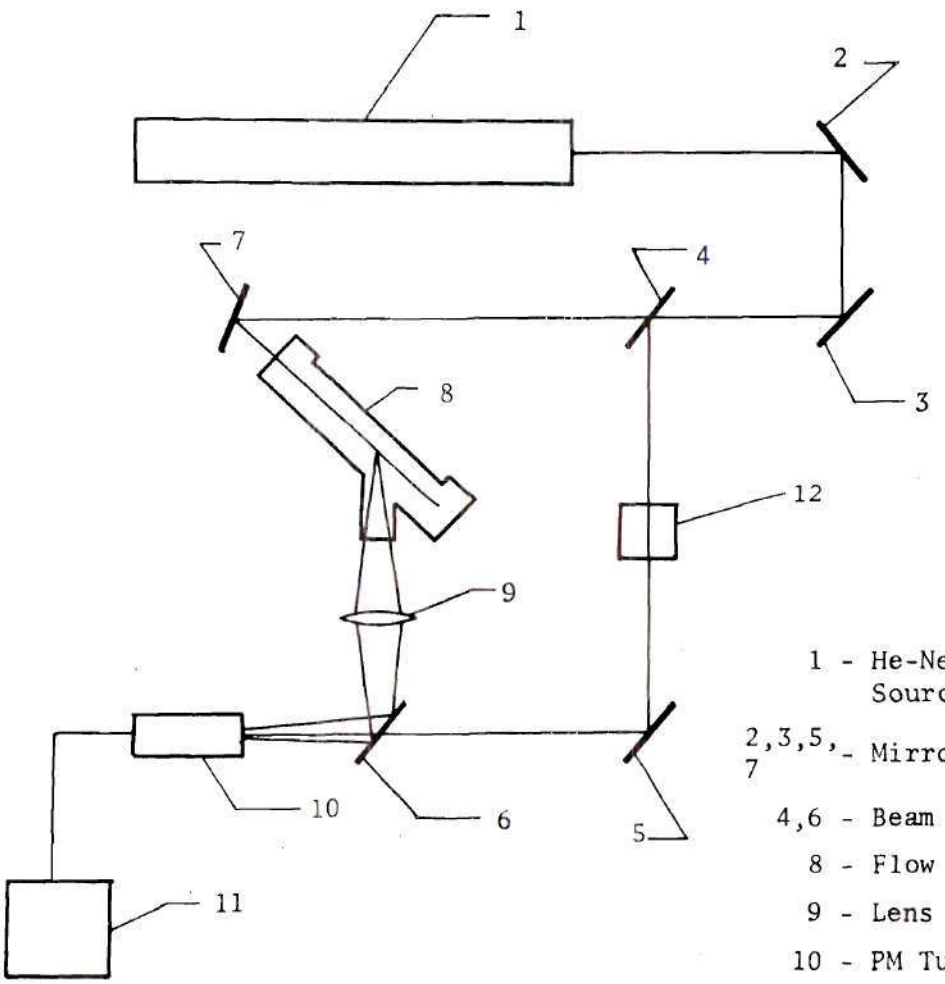

Figure 1.1. Yeh and Cummins' Laser Spectrometer

maximum conversion gain from the heterodyning process. His results indicated that a reduction in the size of the volume over which the measurements are averaged resulted in an undesirable increase in the bandwidth around the average Doppler frequency, f_D. Since the local fluid velocity is directly related to the central Doppler frequency, Davis proceeded to examine the phenomenon in further detail. He concluded that the three factors contributing to the broadening of Doppler bandwidth are (1) pulse modulation due to the finite time for passage of the scattering particle through the heterodyne volume, (2) an angular spread of the incident and the scattered beams from their true directions, and (3) the broadening of the signal spectrum due to amplitude and frequency modulation of the output power of the laser source. Davis obtained an expression for the fractional bandwidth, $\frac{\Delta f}{f_D}$, in terms of the spot size d, the laser wavelength λ, and the angle between particle velocity direction and the scattering direction, ϕ, as

$$\frac{\Delta f}{f_D} = \frac{\lambda}{d \text{ Cos } \phi} \quad . \tag{1.1}$$

This equation allowed him to select the size of the heterodyne volume for an allowable bandwidth.

Briefly, the study by Davis demonstrated that the spot size was a function of system optics, laser wavelength, and beam divergence. The smallest spot diameter was limited to about 10μ for the laser source. A reduction in coherency between signal and reference beams at the photocathode resulted in larger power levels for the two beams for noise suppression. It was observed that the scattering particle density required

for a given signal power varied inversely with both the incident beam power density and the spot volume.

Grant and Donaldson [4] extended the range of velocity measurements to velocities of the order of 6×10^4 centimeters per second (Mach number 2.8) in a small coldflow nozzle. Utilizing a high power argon laser and a special image transfer system which transferred a sharp image on the face of the aperturing plate onto the most favorable position on the photocathode, they established the superiority of the laser Doppler technique over conventional techniques for the specialized application to flow velocity measurements in high-velocity, high-enthalpy gas flows where any physical probe deteriorated rapidly. Use of a high power argon laser reduced the amount of scattering contaminants required to obtain good heterodyne signals and incorporation of an image transfer system simplified the alignment procedure. By equating the drag force in a laminar flow to the accelerating force on a scatterer particle, they established the relationship between stream velocity and particle velocity. A second relationship between the Doppler frequency and particle velocity was established to give a direct interpretation of the Doppler signal frequency in terms of actual stream velocity. They showed that the power ratio of the laser source appeared as a direct increase in the output at the detector. Furthermore, they pointed out that photocathode was more sensitive to shorter argon wavelengths than to longer He-Ne wavelengths and that shorter argon wavelengths had a pronounced favorable influence on the amplitude of the forward scattered light. Use of a large collimating lens masked off to give two slits on the face of the lens, along with the image transfer system, resulted in smaller beam di-

vergence angles and hence more efficient heterodyning with reduced alignment problems. The maximum velocity measured was limited due to characteristics of the flow system. Their overall test arrangement schematic is shown in Figure 1.2.

Huffaker [5] reported a laser Doppler detection system capable of simultaneously measuring three velocity components at a point in the flow field. He successfully operated the instrument in wind-tunnel flows at Mach numbers of the order of 2.0. Furthermore, with an argon ion laser he obtained turbulence and mean velocity data in the flow field generated by a 1.27 centimeter diameter subsonic jet (N_{Re} = 47,000). There was a good correlation with hot wire measurements down the centerline of the nozzle in the potential core region. He employed an optical single sideband modulator to eliminate the problem of 180 degree ambiguity in the direction of the flow. His readout system, shown in Figure 1.3, consisted of a frequency compressive feedback loop which used a tape deck with a frequency tracker which provided a d-c voltage corresponding to the mean flow velocity and an a-c voltage corresponding to the turbulent velocity fluctuations. The readout system could track carrier frequencies in the range 5 MHz. to 200 MHz. and deviation frequencies of the order of 0 to 50% of the carrier frequency at modulation frequencies up to 100 kHz. His readout system had an accuracy of the order of $\pm$ 3% of the carrier frequency for the d-c output and $\pm$(100 kHz $\pm$ 3% of deviation frequency) for the a-c output. He reported an average uncertainty in the LDV data of 8% and limited his measurements to radial positions up to Y/R = Radial position/Radius = 0.96 due to limited accuracy of the frequency tracker. He cited inaccurate positioning and flow

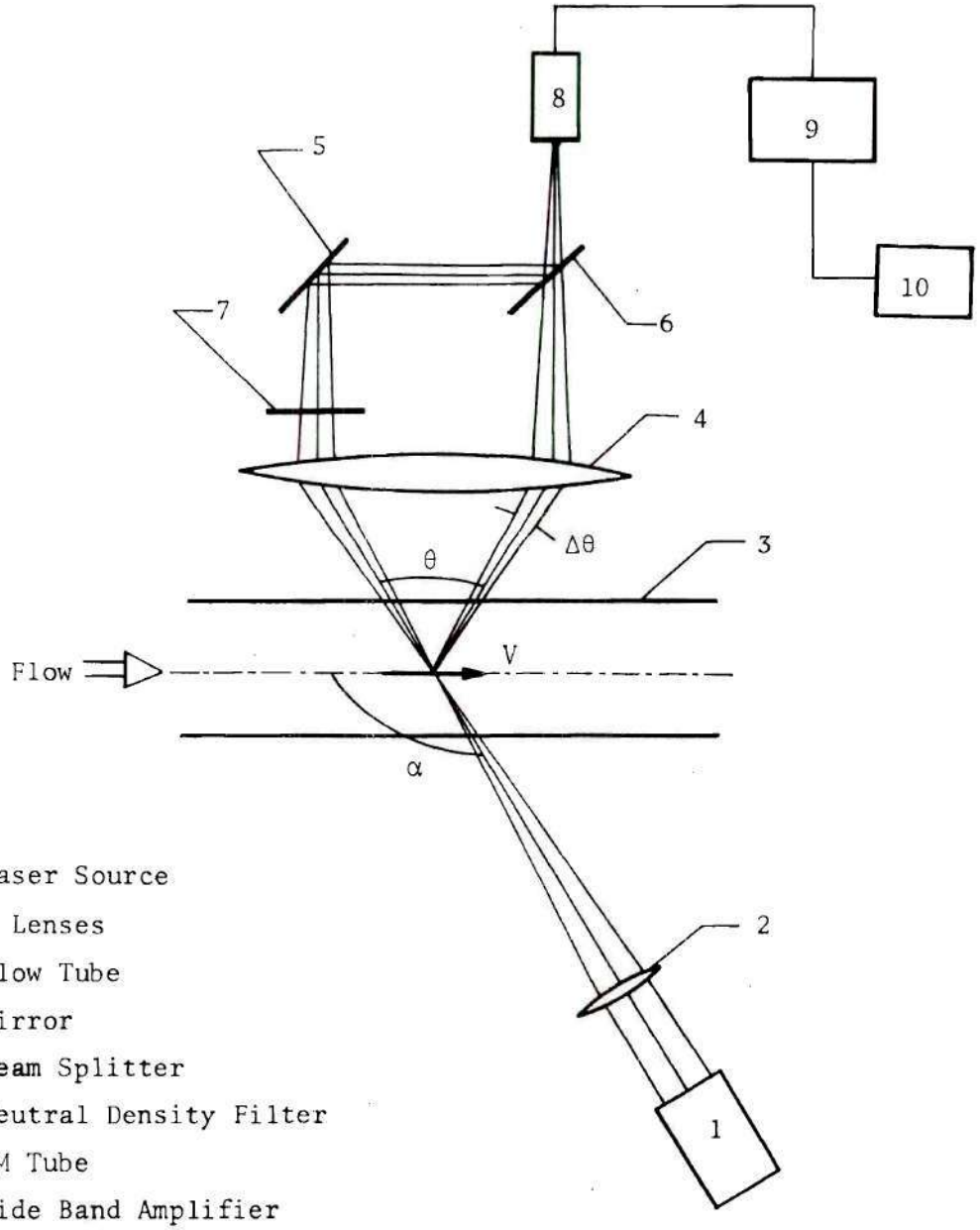

1 - Laser Source
2,4 - Lenses
3 - Flow Tube
5 - Mirror
6 - Beam Splitter
7 - Neutral Density Filter
8 - PM Tube
9 - Wide Band Amplifier
10 - Spectrum Analyzer

Figure 1.2. Grant and Donaldson's System.

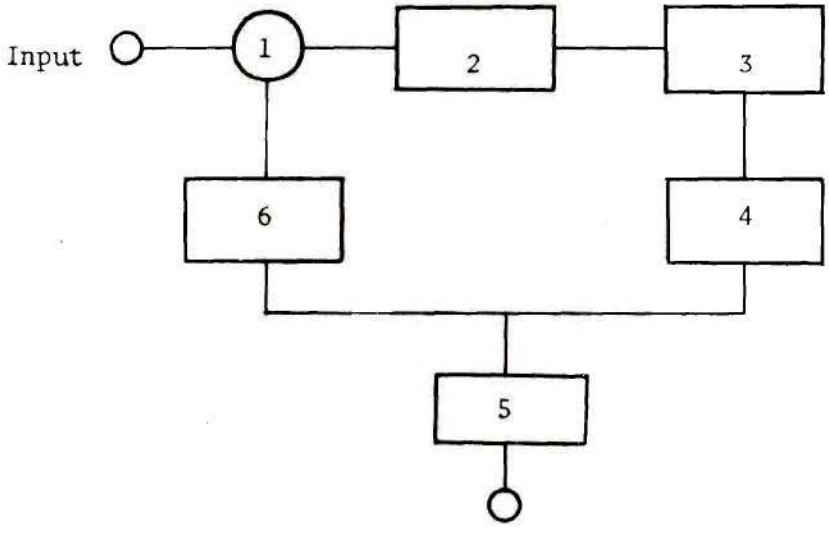

1 - Mixer

2 - IF Amplifier and Filter

3 - Frequency Modulator

4 - Base Band Amplifier

5 - Output Filter

6 - Voltage Controlled Oscillator

Figure 1.3. **Huffaker's Readout System**

variations as main sources of error in his measurements.

Huffaker also used his LDV system for atmospheric applications in wind velocity measurements. He demonstrated the feasibility of utilizing a cw monostatic CO_2 laser system for measuring wind velocities at a range of 35 meters, using natural contaminates in the air as the scattering medium.

Along with reported measurements of gaseous flow fields with a LDV system, several researchers made measurements in liquid flow systems. Foreman, Lewis et al. [6] made studies in a glass flow tube with ordinary tap water flowing through it. They measured laminar velocity profiles in the flow tube for a centerline velocity of 5.35 centimeters per second (N_{Re} = 0(1,000)). They also made measurements for radial positions up to about 88% of tube radius, while Yeh and Cummins had confined their data to radial positions from centerline of the tube up to about 10% of the tube radius. Foreman, Lewis et al. used the peak of a spectrum analyzer display and amplitude of the recorder trace of a phase-lock loop to determine the Doppler frequency. Their study established the feasibility of making flow measurements in most liquids with a LDV system, without a need for adding external contaminants. The limited range of accurate response of their readout system restricted the use of the LDV system to limited measurements of velocity fluctuations.

In a later report, Lewis, Foreman et al. [7] measured velocity profiles in a flow tube for N_{Re} = 5,000, using ordinary tap water and they obtained instantaneous velocity records up to N_{Re} = 6,500. Using a narrow band tracking filter with a strip chart recorder, they measured

local turbulent and mean velocities in low Reynolds number, unsteady flows.

Goldstein and Kreid [8] made velocity measurements in a steady flow field of contaminated water, flowing with 1:50,000 concentration by volume of 0.557 μ. polystyrene spheres through a square duct. Their study provided one of the first measurements of a developing laminar flow field in a square duct and established that a greater length of duct was required for development of the velocity profile than the theoretically predicted value. Furthermore, their investigation, made in a range of Reynolds numbers between 69 and 387, demonstrated the high precision of velocity measurement with a LDV system - with a reported accuracy of 0.1%. They utilized two apertures such that both the scattered and reference beams passed through the test section and were manipulated to pass through the same two apertures before reaching the photomultiplier tube. Consequently, their optical arrangement met heterodyning requirements with an easier beam alignment procedure. The Doppler frequency was read off the recorded output from a spectrum analyzer.

Most of the LDV systems discussed used optical arrangements based on the reference beam approach and concentrated their efforts on improving the range of their application to a versatility of flow regimes with increasingly suitable readout systems. The approach of differential Doppler method for its possible advantages over the reference beam arrangement was initially investigated by Penney [9]. He employed a differential Doppler arrangement for measurement of speeds of extended moving surfaces. His investigation was based on an optical heterodyne

measurement of the difference between two Doppler shifts, produced in the light scattered through two different angles by the moving surface. Utilizing a spectrum analyzer for the readout, he obtained signal-to-noise-ratios (SNR) of the order of 200 and observed that SNR was inversely proportional to both the surface speed as well as the diameter of the illuminated spot. Furthermore, he noted that SNR was independent of the detector-surface distance over a wide range and was proportional, within a factor of 2, to the intensity of light scattered in the direction of the detector. The differential Doppler signal was strongly modulated in phase and amplitude - the later made it difficult to obtain an accurate indication of the signal frequency by counting it directly. His arrangement, shown in Figure 1.4, provided convenient measurement of velocity components tangential to extended, optically rough surfaces with absolute accuracies of the order of 0.1% and relative accuracies of 0.04%.

Mazumder and Wankum [10] compared the relative merits of the differential Doppler method to the reference beam approach and developed a symmetrical method of optical heterodyning of the Doppler shifted signal with minimum instrumental spectral broadening and high SNR. Their experimental arrangement basically consisted of a He-Ne laser source, a rotating disc painted with uniform size pigment particles, and a spectrum analyzer. They pointed out that a differential Doppler arrangement utilizing two scattered beams to generate the signal was advantageous over a reference beam method in that it resulted in a Doppler frequency, f_D, such that f_D was sensitive only to one velocity component meeting certain requirements and that spatial superposition of the two

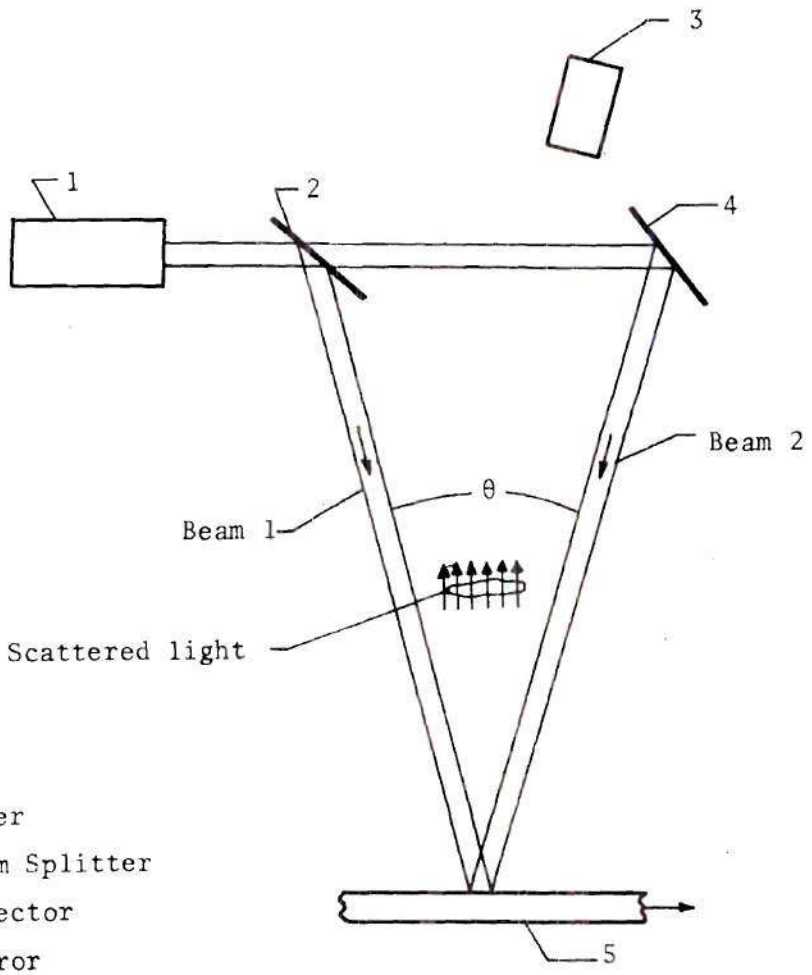

1 - Laser
2 - Beam Splitter
3 - Detector
4 - Mirror
5 - Moving Surface

Figure 1.4. Penney's Differential Doppler Arrangement

beams resulted in the same difference frequency, f_D, across the photocathode surface, thus cancelling the aperture broadening. They further observed that the heterodyning efficiencies of both the reference beam approach and two-scattered-beams differential method were highly dependent on the beam alignment.

Mazumder and Wankum overcame the limitations of these two methods by utilizing two incident beams instead of two scattered beams in a differential Doppler arrangement and referred to it as the symmetrical system of second type. They observed that such an arrangement required no further beam mixing as the scattered beam directly generated the Doppler signal. The f_D thus obtained was independent of scattering angle, spatial position, and area of receiving aperture. Consequently, the receiver aperture area could be increased to obtain the desired level of signal strength without additional signal broadening. The optical alignment was thus simplified. Moreover, the SNR values obtained with differential Doppler arrangement of second type were higher or equal to those achieved in a reference beam arrangement with the advantage that the former suffered negligible loss in its heterodyning efficiency due to beam misalignment. Only sources of instrumental spectral broadening in such a differential method were the transmission aperture, finite scattering volume, and finite signal lifetime. In brief, advantages of the differential Doppler method could be employed as long as signal power could be appreciably increased by increasing the receiver aperture area. Conversely, the reference beam approach was advantageous when aperture broadening of the signal was insignificant for scattering sites located at large distances.

Mazumder [11] further developed a differential Doppler system employing two incident beams such that velocities in any set of orthogonal axes could be measured without the directional ambiguity of 180 degrees. Using a rotating diffraction grating or a Bragg cell, he obtained two incident beams of different frequencies. He observed that this frequency bias could be adjusted for the maximum expected value of the velocity to be measured and the resultant Doppler signal was not an even function of the velocity. With an aim to measure two point cross correlations of velocity in a turbulent flow field, he thus developed a LDV technique applicable to any system where the direction of velocity could reverse itself.

Mayo [12] and Bedi [13] reported simplified optical arrangements for a laser Doppler velocimeter system. Mayo described a simple, efficient optical system which he claimed required almost no optical heterodyne alignment and which was stable and insensitive to stress and vibration. He utilized a properly coated parallel-face optical flat as a beam splitter to obtain two parallel beams from one without any appreciable loss of optical power. The only alignment requirement of his system was that the incident beam be collimated which he satisfied by using a typical commercial laser. By proper choice of the coating on splitter flat, he could obtain any desired ratio of power in the two beams and by further utilizing suitable locations of the detector optics, he could operate his system in either the reference beam or the differential Doppler mode. Although no data was presented, the author claimed to have demonstrated the improved simplicity of alignment and insensitivity to vibration. His input optics is shown in Figure 1.5.

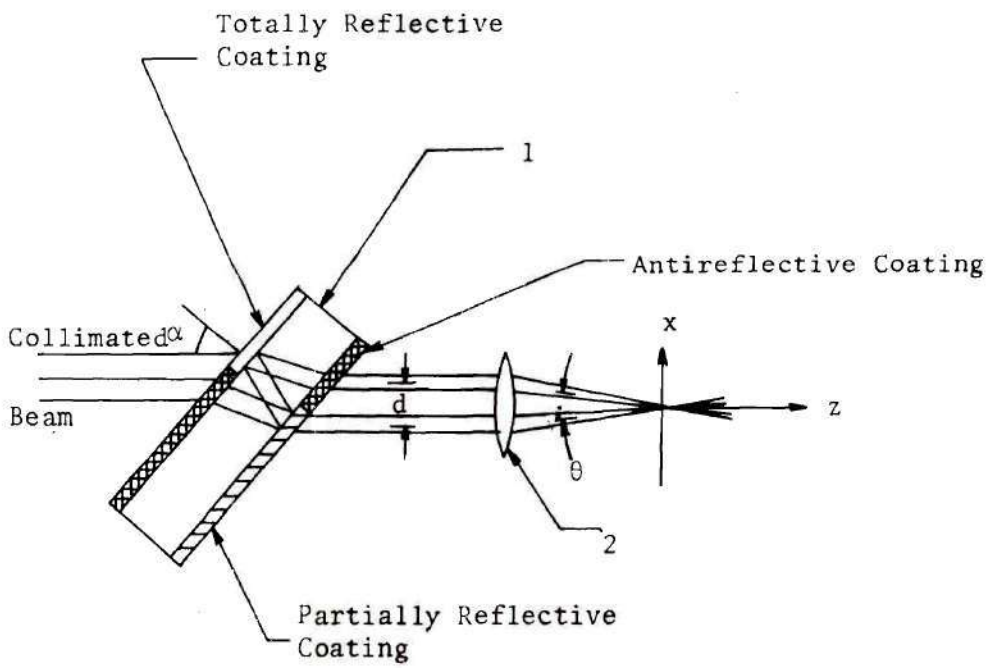

1 - Parallel-Face Optical Flat

2 - Lens

Figure 1.5. Mayo's Input Optics

Bedi [13], on the other hand, utilized three standard right-angle prisms, as shown in Figure 1.6, to obtain two parallel beams - the weaker beam transmitted through the prisms with about 5% of incoming light while the stronger beam with remaining incident light was reflected and brought parallel to the weaker beam. The author, without presenting measurement data, claimed the following advantages for his system: (a) two-dimensional flows could be measured in one setting without disturbing the optical alignment, (b) system provided quick and easy optical set-up, (c) the flow system could be easily traversed by simply moving the lens which provided rigidity and stability to the system, (d) system required no heterodyning alignment, and (e) it could perform measurements in complex flow systems. Furthermore, the system was not affected by any linear motion or such vibration of the beam splitter and there was no loss of available laser light.

Thompson [14] described a simple laser velocimeter and utilized it to measure velocities of the order of 200 meters per second by using the naturally occurring dust particles in a wind tunnel flow system. He employed a Kösters prism to obtain two beams of approximately equal intensity from a He-Ne laser source. The scattered light was collected by a lens system and detected by a photomultiplier tube. By measuring the time interval between the two pulses generated at the photomultiplier output and knowing the separation of the two laser beams, he was able to calculate the particle velocity directly. His readout consisted of an oscilloscope to measure the time interval between the pulses. The oscilloscope was set for single sweep operation and the time base was triggered by the first pulse of each pair of pulses. Three main factors

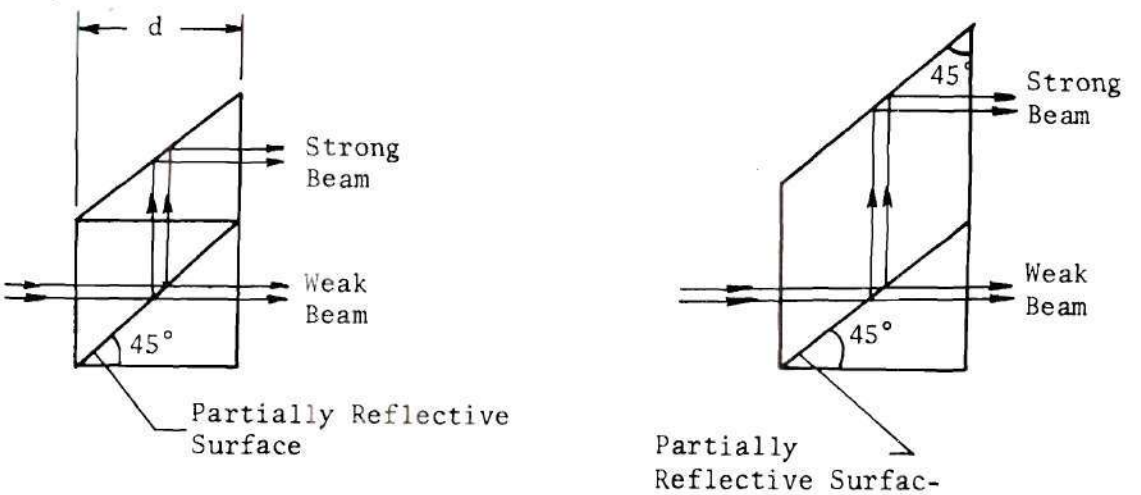

(a)
Three Piece Design

(b)
Two Piece Design

Figure 1.6. Bedi's Three Standard Right-Angle Prism Arrangement.

limited the accuracy of his measurements. These were (a) accuracy of measurement of the separation of the two beams, (b) accuracy of measurement of time of flight of the particle between the beams, and (c) fidelity with which the particle velocity represented the fluid velocity. Main advantage of his system was that it measured velocity directly requiring no complicated readout system or calibration.

1.3 Statement of Thesis Problem

The present study is an exploratory investigation of a laser differential Doppler velocimeter system suitable for measurements in liquid jet flow fields. Various possible optical configurations and electronic readout systems are examined to evolve a specific system configuration consisting of suitable optics, electronics and the jet flow loop. Procedures of calibrating the readout system and interpretation of data in terms of flow velocities are discussed.

CHAPTER II

THEORY OF OPERATION OF LASER DOPPLER VELOCIMETER

2.1 The Phenomena of Doppler Shift

The optical operation of a laser Doppler velocimeter in fluid flow studies can be explained by examining the technique of optical heterodyning of two signals, one of which is Doppler shifted with respect to the other. The technique of the fluid velocity measurement utilizing the phenomenon of Doppler shift of an optical signal can be illustrated by an examination of Figure 2.1. A light radiation along the direction of a unit vector, e_1, with a frequency f_1, a wavelength λ_1, and a speed V_1 is shown to be striking a particle moving with a speed V_2 along a unit vector e_2 at a fixed instant of time. For non-relativistic particle speeds considered in this investigation,

$$V_2 \ll V_1. \tag{2.1}$$

The component of V_2 in the direction of V_1 can be expressed as

$$V_{21} = (e_1 \cdot e_2 V_2) = (e_1 \cdot e_2) V_2. \tag{2.2}$$

As a result, the difference between the speed of incident radiation and the component of particle velocity in the direction of e_1 is given by

$$V_1 - V_{21} = V_1 - (e_1 \cdot e_2) V_2. \tag{2.3}$$

As observed by the moving particle, the apparent frequency of the inci-

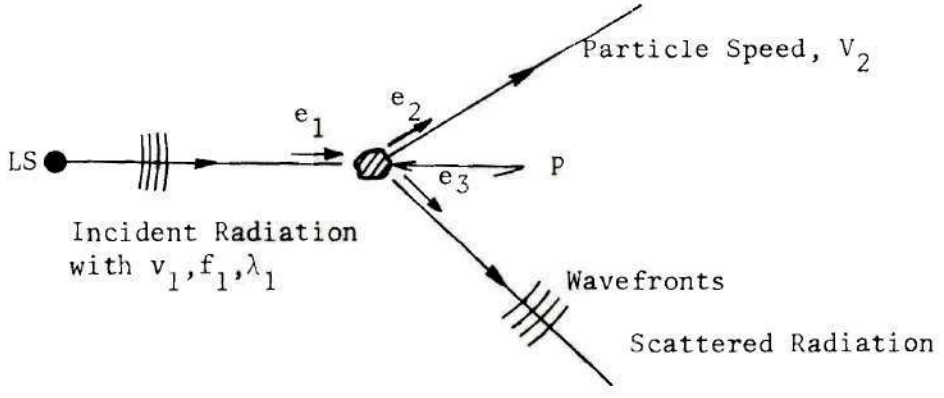

LS - Source of Radiation

P - Moving Particle

e_1, e_2, e_3 - Unit Vectors

Figure 2.1. Light Scattered Off A Moving Particle.

dent radiation is

$$f_{1A} = \frac{V_1 - V_{21}}{\lambda_1}, \text{ or}$$

$$f_{1A} = \frac{1}{\lambda_1} [V_1 - (e_1 \cdot e_2) V_2], \tag{2.4}$$

which is also the apparent frequency of the radiation scattered off the particle as seen by the moving particle. Part of this scattered radiation can be collected by a suitable receiver located along the direction e_3 with respect to the particle. At a specific instant of time, the particle scatters a wavefront along e_3. The component of the particle velocity along e_3 is given by

$$V_{23} = (e_2 \cdot e_3) V_2. \tag{2.5}$$

After a time interval equal to $\frac{1}{f_{1A}}$, following the initiation of the first wavefront, the moving particle scatters off a second wavefront. The distance d, between the particle and the first scattered wavefront along e_3 at the time when second wavefront is initiated, is given by

$$d = \frac{[V_1 - (e_2 \cdot e_3) V_2]}{f_{1A}} \tag{2.6}$$

A look at Figure 2.2 indicates that this is also the distance along e_3 between the first and the second wavefronts scattered by the particle. Therefore, the distance d represents the wavelength of the scattered radiation as observed by a fixed receiver along e_3. In other words,

$$\lambda_S = \frac{[V_1 - (e_2 \cdot e_3) V_2]}{f_{1A}} \tag{2.7}$$

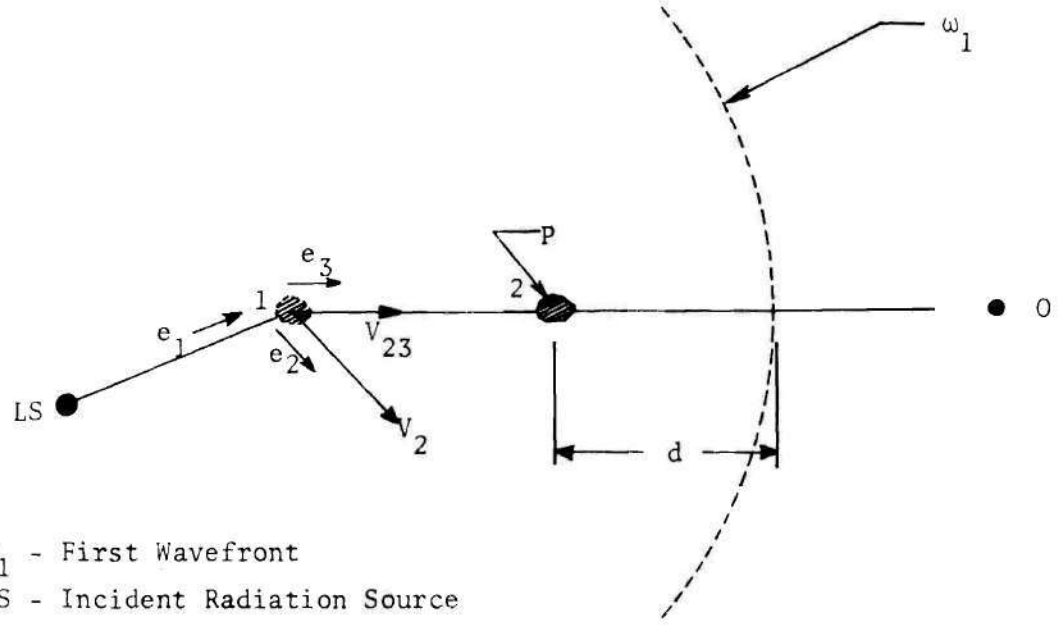

ω_1 - First Wavefront

LS - Incident Radiation Source

O - Fixed Receiver

P - Moving Particle

1,2 - Particle Positions at Two Instants Considered

e_1, e_2, e_3 - Unit Vectors

Figure 2.2. Schematic Representation of Scattered Beam Wavelength.

Incorporation of the expression for f_{1A} from equation (2.4) into the equation (2.7) gives

$$\lambda_S = \frac{[V_1 - (e_2 \cdot e_3)\, V_2]}{[V_1 - (e_2 \cdot e_1)\, V_2]} \quad \lambda_1, \tag{2.8}$$

with the corresponding frequency given by

$$f_S = \frac{V_1}{\lambda_1} \quad \frac{[V_1 - (e_2 \cdot e_1)\, V_2]}{[V_1 - (e_2 \cdot e_3)\, V_2]}, \text{ or}$$

$$f_S = \frac{V_1}{\lambda_1} \quad \frac{1 - (e_2 \cdot e_1) \frac{V_2}{V_1}}{1 - (e_2 \cdot e_3) \frac{V_2}{V_1}} \tag{2.9}$$

The consequent Doppler shift between f_1 and f_s, the respective frequencies of the incident and scattered radiations, as seen by a stationary receiver along e_3 is given by

$$f_D = (f_s - f_1), \text{ or}$$

$$f_D = \frac{V_1}{\lambda_1} \quad \frac{1 - (e_2 \cdot e_1) \frac{V_2}{V_1}}{1 - (e_2 \cdot e_3) \frac{V_2}{V_1}} \quad - f_1, \tag{2.10}$$

which further simplifies to

$$f_D = \frac{1}{\lambda_1} \quad \frac{e_2 \cdot (e_3 - e_1)\, V_2}{1 - (e_2 \cdot e_3) \frac{V_2}{V_1}} \quad . \tag{2.11}$$

For $V_2 << V_1$, equation (2.11) becomes

$$f_D = \frac{n}{\lambda_{10}} [e_2 \cdot (e_3 - e_1)] V_2, \qquad (2.12)$$

where λ_{10} is the vacuum-wavelength of the incident radiation, and n is the index of refraction of the surrounding medium.

Equation (2.12) directly relates the particle speed V_2 with the resulting Doppler frequency f_D. In equation (2.12), the factor in the square brackets is determined for a specific system configuration by fixing the directions of incident radiation, the particle velocity, and the fixed receiver location, while n is a property of the medium in which the particle is moving. In the case of a fluid flow problem, unit vector e_2 in the direction of particle velocity coincides with the direction of fluid flow, provided the scattering particles in the flow field are of proper size and density to closely follow the flow-field of the fluid continuum.

2.2 Optical Heterodyne Technique

Optical heterodyning involves a comparison of two monochromatic, coherent light beams of different frequencies when they are simultaneously incident on the photosensitive surface of a photodetector. The photodetector, operating as a square-law device, generates an electrical signal of a frequency equal to the difference of the incident frequencies. The current output of a photomultiplier tube, operating in such a heterodyne mode, contains the Doppler frequency component as well as the DC signal.

When two monochromatic, coherent light beams, with their elec-

trical fields respectively designated by $U_r = U_{rr} \text{ Cos } \omega_r t$ and $U_s = U_{ss} \text{ Cos } \omega_s t$, simultaneously impinge on a photocathode surface, the resulting output current is given by

$$I = K(U_r + U_s)^2, \text{ or}$$

$$I = K[U_{rr} \text{ Cos } \omega_r t + U_{ss} \text{ Cos } \omega_s t]^2, \text{ or}$$

$$I = K[U_{rr}^2 \left(\frac{1 + \text{Cos } 2\omega_r t}{2}\right) + U_{ss}^2 \left(\frac{1 + \text{Cos } 2\omega_s t}{2}\right)$$

$$+ U_{rr} U_{ss} \{\text{Cos } (\omega_r + \omega_s)t + \text{Cos}(\omega_r - \omega_s)t\}], \qquad (2.13)$$

where K is a proportionality constant. If the frequency components ω_r, ω_s and $(\omega_r + \omega_s)$ are considerably higher as compared with the upper limit of acceptance of frequency by the phototube, referred to as frequency response of the phototube, the only output corresponding to these high frequencies is the time-averaged d-c current from the photomultiplier tube, for each of these components. The component at frequency $(\omega_r - \omega_s)$ on the other hand, results in an a-c output current from the phototube for values of $(\omega_r - \omega_s)/2\pi$ less than the limiting frequency of the tube. The output current from the phototube, in such an instance, is equal to

$$I = K \left[\frac{U_{rr}^2}{2} + \frac{U_{ss}^2}{2} + U_{rr} U_{ss} \text{Cos}(\omega_r - \omega_s)t\right]. \qquad (2.14)$$

In the present investigation, the two beams under comparison are the reference beam and the scattered beam, with their frequencies in the

optical frequency range well above the frequency response of the photo-tube.

A suitable optical configuration is of fundamental importance in a heterodyning arrangement. The major factors that make the process of heterodyning inefficient are: (i) imperfect optical components, (ii) angular misalignments in the optical arrangement, (iii) lack of spatial coherence of the two light beams, and (iv) incomplete overlap of the two light beams on the photocathode surface.

2.3 Laser Doppler Velocimeter

The technique of optical heterodyning monochromatic laser beam with its light scattered off a moving particle constitutes a useful basis for designing a flow measurement system. A look at Equation (2.12) indicates that a low value of the Doppler shift frequency, f_D, is associated with a low particle velocity. In order to detect such a low value of f_D with an acceptable resolution, it is of utmost importance to have the radiation source to radiate within a bandwidth which is several orders of magnitude smaller. A laser constitutes a suitable source of incident radiation,since it radiates essentially monochromatic radiation.

A fluid flow measurement system utilizing the Doppler shift of a monochromatic radiation primarily consists of (a) a suitable light source, (b) a proper configuration of lenses and mirrors, (c) a flow system, and (d) a read-out system. Since there have been several reported arrangements of optical components for specific applications, it is worthwhile to examine the basic features common to these applications. The so-called reference-beam-approach (RBA), and the differential-Doppler-method (DDM), both utilize the basic phenomena of Doppler shift,

but use different optical configurations for photomixing.

2.3.1 Reference Beam Approach (RBA)

Figure 2.3 shows a light beam from a laser source focussed at the point in the flow field of interest. Very small sized contaminants of the order of one micrometer flowing with the main fluid act as continuous sources for scattering the incident radiation in a preferred direction. As a particle passes through the focal point, P, part of the incident radiation is scattered off in several directions. Most of the incident radiation passes through the flow field without scattering and is focussed on the photocathode of a photomultiplier tube. The scattered light is Doppler shifted, resulting in a Doppler frequency given by Equation (2.12).

The receiving optics consisting of a lens and a beam splitter, as shown in Figure 2.3, focusses that part of the scattered light which is along the receiver direction. This occurs at the same spot as the unscattered light, resulting in optical heterodyning of the two beams, with subsequent output current from the phototube being a periodic signal superimposed on the noise signal. The frequency of this sine wave is the Doppler frequency associated with the particle velocity at the focal point P.

A mathematical expression for the Doppler frequency which is applicable to the RBA arrangement can be developed by considering the configuration of Figure (2.4). The general equation (2.12) for Doppler shift, when used for optical configuration shown in Figure (2.4), becomes

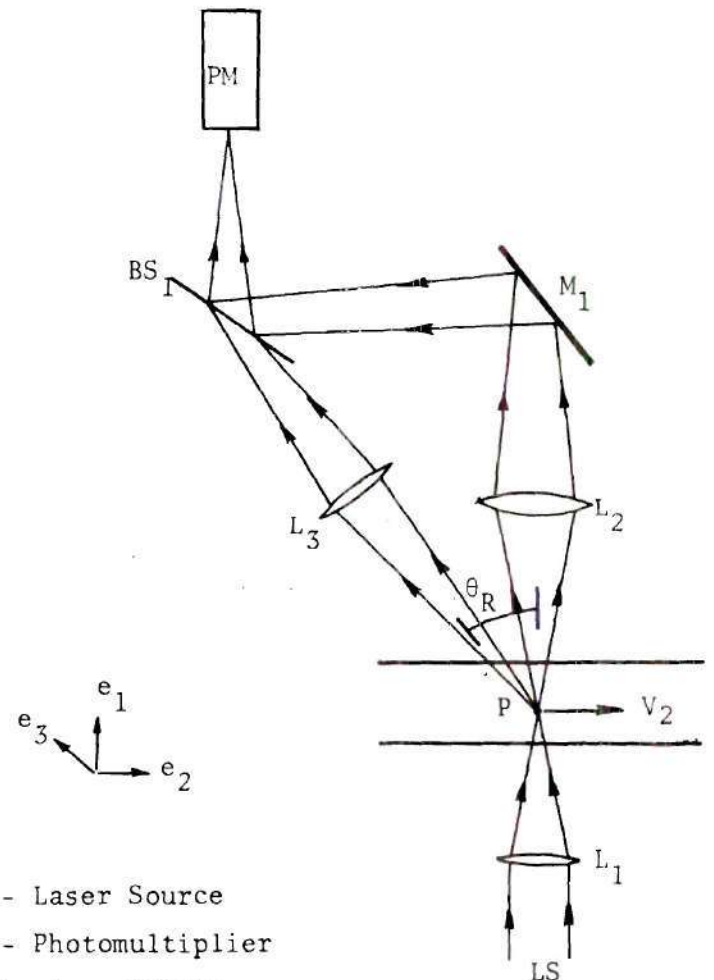

LS - Laser Source

PM - Photomultiplier

L_1, L_2, L_3 - Lenses

M_1 - Mirror

BS_1 - Beam Splitter

P - Focal Point

V_2 - Particle Speed

e_1, e_2, e_3 - Unit Vectors, in Incident, Particle Speed and Scattered Directions

Figure 2.3. Schematic of the Reference Beam Approach.

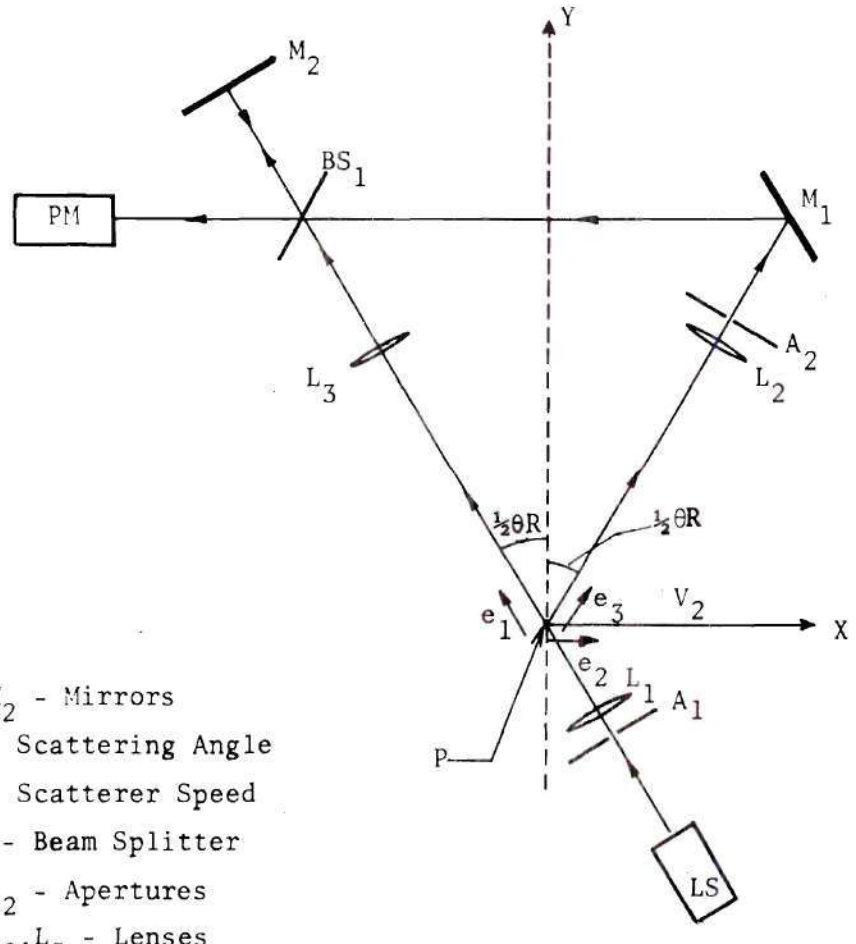

M_1,M_2 - Mirrors
θ_R - Scattering Angle
V_2 - Scatterer Speed
BS_1 - Beam Splitter
A_1,A_2 - Apertures
L_1,L_2,L_3 - Lenses
LS - Laser
PM - Photomultiplier Tube
e_1,e_2,e_3 - Unit Vectors

Figure 2.4. Derivation of Expression for f_D in RBA.

$$f_D = \frac{2nV_2}{\lambda_{10}} \quad \text{Sin} \quad \frac{\theta_R}{2} , \qquad (2.15)$$

and gives the speed V_2 of the particle in direction of x-axis directly as a function of the Doppler frequency and the angle θ_R which is fixed for the configuration. As an example, for a water medium, a 6328 Å laser radiation source, and a scattering angle θ_R equal to 10^o, equation (2.15) simplifies to $f_D = 3.66\ V_2$, where f_D is in KHZ, and V_2 in centimeters per second.

2.3.2 Differential Doppler Method (DDM)

The differential Doppler method measures speeds in a flow field by detecting the difference in Doppler shifts in frequencies of two incident light beams, simultaneously scattered from the same focal point, P, in the flow system. Radiation scattered in a specific direction contains two scattered components corresponding to the two incident beams, the components having experienced different Doppler shifts. As the two scattered components simultaneously emanate from the same focal point P in the flow field, they are well aligned and produce a strong heterodyne signal when optically mixed at the photocathode.

Figure 2.5 shows a schematic of the optical arrangement of a typical differential Doppler method of velocity measurement. Two incident light beams from the same laser source, along directions represented by unit vectors e_1 and e_2, with an angle θ between e_1 and e_2, are focused at a point P in the flow-field by the lens L_1. Light scattered from focal point P, along another unit vector, e_3, is collected using an aperture and focused by lens L_2 at the photocathode of a photomulti-

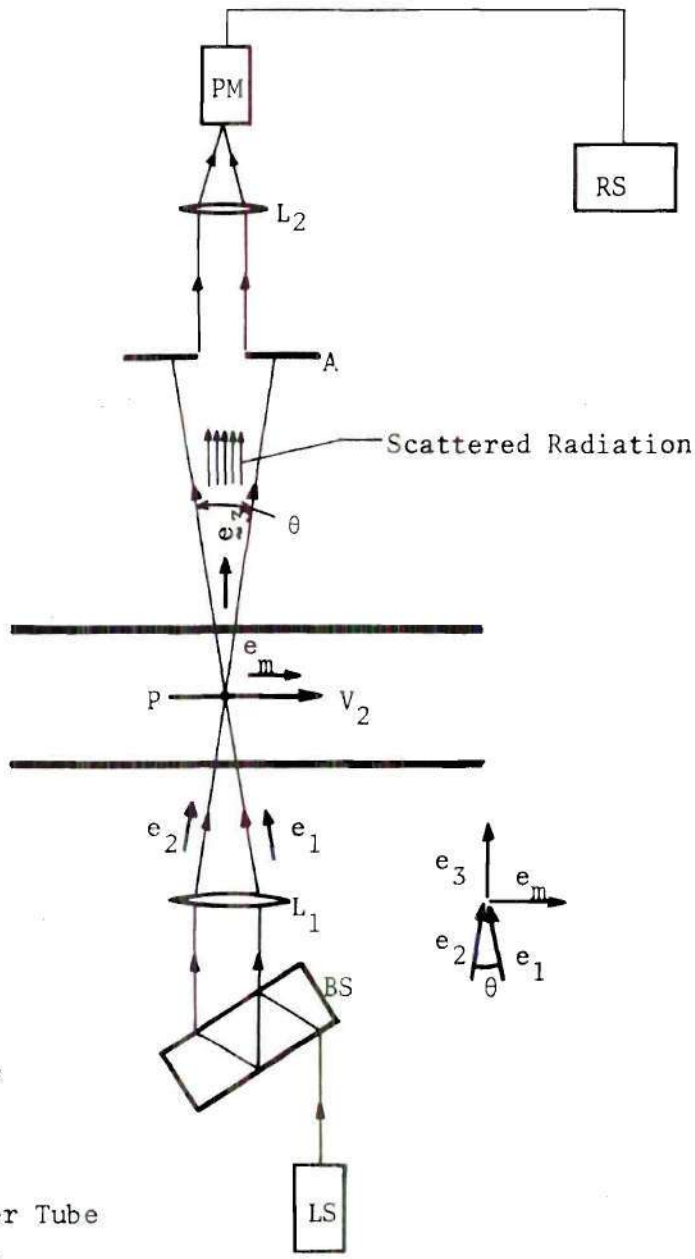

LS - Laser Source

BS - Beam Splitter

P - Moving Particle

A - Aperture

L_1, L_2 - Lenses

PM - Photomultiplier Tube

RS - Readout System

e_1, e_2, e_3, e_m - Unit Vectors

Figure 2.5. Optical Arrangement in DDM

plier tube. At the time of scattering, the contaminant particle at focal point P is moving with a speed V_2 along unit vector e_m.

Component of the scattered light, corresponding to incident beam along e_1, experiences a Doppler shift in its frequency, f_{D_1}, which can be written by using Equation (2.12) as

$$f_{D_1} = \frac{n}{\lambda_{10}} [e_m \cdot (e_3 - e_1)] V_2, \tag{2.16}$$

where λ_{10} is the vacuum-wavelength of the incident radiation while n is the index of refraction of flow-field medium. The corresponding Doppler shift, f_{D_2}, for incident beam along e_2 is similarly equal to

$$f_{D_2} = \frac{n}{\lambda_{10}} [e_m \cdot (e_3 - e_2)] V_2. \tag{2.17}$$

The resulting difference in the two Doppler shifts is

$$f_D = f_{D_2} - f_{D_1}, \text{ or}$$

$$f_D = \frac{n}{\lambda_{10}} [e_m \cdot (e_1 - e_2)] V_2. \tag{2.18}$$

Figure 2.6 shows a vector diagram associated with a DDM optical arrangement. For such an arrangement, bisector of the angle θ between the two incident beams is perpendicular to unit vector e_m in direction of particle speed. For such a configuration, Equation (2.18) simplifies to

$$f_D = \frac{2nV_2}{\lambda_{10}} \text{ Sin } \frac{\theta}{2}. \tag{2.19}$$

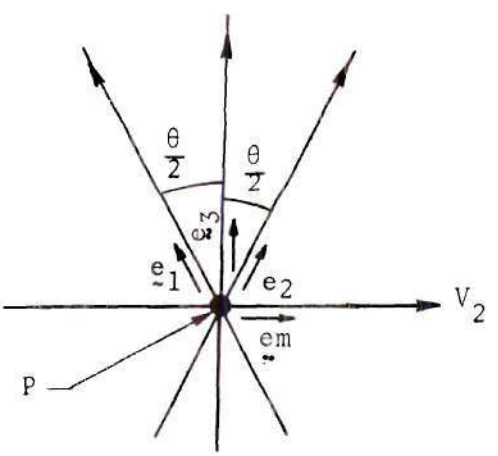

Figure 2.6. Vectors Associated With a DDM Arrangement

The two scattered radiation components at respective frequencies f_{D_1} and f_{D_2}, when optically heterodyned at the photocathode of photomultiplier tube, result in a periodic Doppler signal at a frequency, f_D, given by Equation (2.19), which also directly gives the corresponding speed, V_2, of the scattering particle at focal point P.

It is observed from Equation (2.18) that differential Doppler method of velocity measurement gives rise to a heterodyne signal with a frequency, f_D, which is independent of the scattering direction e_3. This observation is of utmost significance because it shows that the scattered light in a differential Doppler system can be collected over a wide range of scattering directions without broadening the spectral distribution of the signal. Also, it is relatively easier to align and adjust the optics in a differential Doppler method as compared to the relatively more cumbersome alignments associated with RBA.

2.4 Parametric Considerations of a LDV System

The performance of a laser Doppler velocimeter depends on several parameters, some of which are interrelated. The size and density of the contaminant particles, the size of the heterodyne volume, proper alignment, and the relative intensities of the incident and scattered radiation, and factors affecting the background noise level are factors that need to be considered in order to obtain a suitable system performance. It is worth noting that the total coherence and constant phase relationship, usually assumed between the incident and scattered beams, is considerably more difficult to attain in practice than is recognized in theoretical development of the operational equations. A

loss of gain and an increased noise level are two of the more common consequences of a lack of beam coherence.

The conversion efficiency of the photomixing process at the photocathode is mainly affected by the lack of coherence between the incident and scattered radiation. Lack of spatial coherence results from mechanical vibrations and misalignment between the beams while, a lack of temporal coherence is caused by time-varying mode patterns of the multimode laser. Mechanical vibrations are minimized by using a heavy base for the setup, lathe bed being the most common, while the optical misalignment problem is more involved as it is a function of several related optical parameters.

The problem of misalignment is specially critical in a LDV system where the two beams in question are of optical wavelengths and give rise to large errors for rather small misalignments due to the small values of their wavelengths. This relatively critical factor of misalignment between the beams may be examined by considering the expression for the conversion efficiency, η_1, developed by Ross [19] and given by

$$\eta_1 = \frac{\mathrm{Sin}(BD_A/2)}{(BD_A/2)} , \tag{2.20}$$

where

$$B = \frac{2\pi \ \mathrm{Sin}\ \theta_m}{\lambda} . \tag{2.21}$$

In Equation (2.21), θ_m is the angle between two plane waves of wavelength λ striking the photocathode of a diameter equal to D_A. It is

observed from Equation (2.20) that conversion efficiency is a function of $(BD_A/2)$ and high values of η_1 correspond to

$$\frac{BD_A}{2} \leq 1,$$

which, with the help of Equation (2.21) reduces to

$$\theta_m \leq \frac{\lambda}{\pi D_A}, \tag{2.22}$$

for small values of θ_m. Equation (2.22) gives the maximum allowable misalignment between the two beams and shows that a reduction in the aperture size, D_A, at the photocathode allows a larger misalignment without any significant reduction in efficiency. On the other hand, positioning a small pinhole accurately and maintaining its position present mechanical problems. The latter consideration, therefore, puts a lower limit on the size of aperture that can be used in practice to obtain high conversion efficiencies. It may be observed that a higher power-density associated with a smaller pinhole has a fatiguing influence on the photocathode.

Another significant factor influencing the performance of a LDV system is a set of parameters associated with the scattering particles. The effect of this set of parameters can be studied by consideration of a model for the particles which assumes those to be spheres of radius r_p and of index of refraction n^1. Such a particle scatters the incident radiation in the direction of the receiving lens, with an intensity given by [3]

$$W = \frac{\lambda^2 \, i(\alpha, n^1, \theta_R)}{4\pi^2} , \tag{2.23}$$

per unit solid angle and per unit incident power density. In Equation (2.23), $i(\alpha, n^1, \theta_R)$ is a quantity which is a function of the particle size, r_p, the index of refraction of particle, n^1, and the angle, θ_R, between incident and scattered beam directions. Also in Equation (2.23) the angle α is given as

$$\alpha = \frac{2\pi \, r_p}{\lambda} . \tag{2.24}$$

Figure 2.7 shows a schematic arrangement of the receiving optics. Total power, p_s, incident on the lens, L_2, is [3]

$$p_s = \frac{\lambda^2 \, i(\alpha, n^1, \theta_R)}{4\pi^2} \, \Omega_s \, p_d \, N_d , \tag{2.25}$$

where

$$\Omega_s \simeq \frac{\pi}{4} \left(\frac{D_A}{a}\right)^2 , \tag{2.26}$$

is the solid angle subtended by receiver lens L_2 at the point of scattering which is also the focal point of the incident beam. Incident power density p_d, at the point of scattering is [3]

$$p_d = \frac{p_i}{(\pi D_h^2/4)} , \tag{2.27}$$

where p_i is the output power of the laser source, and

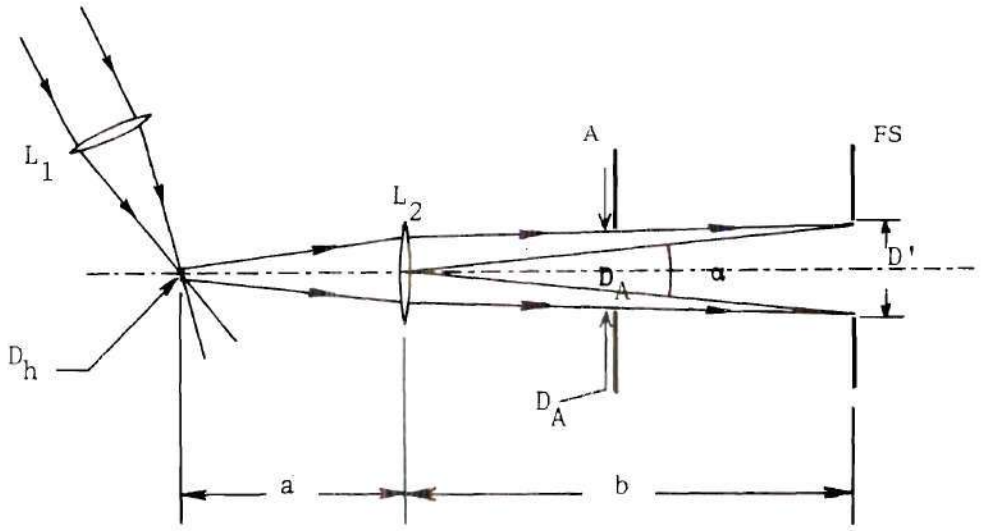

A - Aperture Stop

FS - Field Stop

L_1, L_2 - Lenses

D_h - Heterodyne Volume Diameter

D_A - Aperture Diameter

D' - Field Stop Diameter

Figure 2.7. Schematic Arrangement of a Receiving Optics.

$$D_h = \frac{a}{b} D', \tag{2.28}$$

is the diameter of the small volume over which the incident beam is focussed by lens L_1. An important parameter itself, this volume is commonly referred to as the heterodyne volume. In Equation (2.25), N_d represents the number of particles within the heterodyne volume.

An increase in particle density results in an increase in signal power. However, such an increase in power is not directly proportional to the particle density, due to the randomness of phase relationships between signals scattered from different particles within the heterodyne volume. The Doppler signal current for a completely random phase relationship between signals from different particles can be related to the total number of particles, N_d, in the heterodyne volume as [3]

$$I_s \propto N_d^{1/2}. \tag{2.29}$$

It is thus obvious that signal power per particle can be increased by either increasing laser source power, or the solid angle, Ω_s, subtended by the receiving lens aperture, or by decreasing the angle θ_R between incident and scattering directions. As seen from Equation (2.25), an increase in the laser power and solid angle Ω_s results in a corresponding increase in the signal power in a linear fashion. However, there also are some undesirable aspects associated with each one of the three possible ways of increasing signal power. More powerful laser sources are less coherent, a large Ω_s widens the Doppler frequency band and a decrease in the scattering angle θ_R re-

sults in reduced system accuracy as well as a reduced Doppler frequency. A systematic optimization of signal power per particle is a study in itself and is considered beyond the scope of this investigation.

Frequently, the performance of a LDV system is severely limited due to undesirable noise levels. By denoting the efficiency of the Doppler shift process as η_1, a condition imposed on the ratio of the signal to noise power levels p/p', can be expressed as [3]

$$\frac{p}{p'} > r_1 \eta_1^{-2} \tag{2.30}$$

where r_1 is the signal to background noise ratio. The corresponding a-c signal due to the Doppler frequency, $\eta_1 I_2$, when combined with the respective d-c levels of the incident and scattered beam current, I_1 and I_3, yields the total phototube output current. In other words,

$$I = I_1 + \eta_1 I_2 + I_3. \tag{2.31}$$

It may be noted that η_1 is directly dependent on the degree of coherence between the reference and scattered beams. Suitable electromagnetic shields and filters to reduce the noise power level, p', are almost always needed to supplement the system.

The problem of the photomultiplier thermal noise suppression can be sufficiently resolved by providing the reference beam power, p_r, such that [3]

$$p_r > G^{-2} \eta_2^{-1} \frac{5kT^{\circ}hf}{q^2R} \left(\frac{B_N}{B_s}\right), \tag{2.32}$$

where

G = phototube current gain,

k = Boltzmann constant,

T° = absolute temperature,

R = load resistance, and

B_N = effective noise bandwidth.

For phototube and spectrum analyzer bandwidths of B_p and B_s, respectively, the effective noise bandwidth can be approximated by [3]

$$B_N \simeq \sqrt{2B_pB_s} \quad . \tag{2.33}$$

The relative power levels of incident and scattered radiations are closely related to the resolution requirements of the spectrum analyzer. To study this relationship, the ratio of the magnitudes of the a-c signal current component and the d-c current component in the total phototube output is given by [3]

$$\frac{I_{A/C,\ peak}}{I_{DC}} = \frac{\eta_1 U_s U_r}{\frac{1}{2}(U_r^2 + U_s^2)} \quad . \tag{2.34}$$

For a reference beam considerably stronger than the signal beam,

$$U_r >> U_s \tag{2.35}$$

Equation (2.34) simplifies to [3]

$$\frac{I_{A/C,\ peak}}{I_{DC}} \simeq 2\eta_1 \frac{U_s}{U_r} \quad , \text{ or}$$

$$\frac{I_{A/C,\ peak}}{I_{DC}} \simeq 2\eta_1 \left(\frac{ps}{pr}\right)^{1/2}, \tag{2.36}$$

where (p_s/p_r) is the corresponding ratio of signal power to the reference beam power.

The current $I_{A/C,\ peak}$ is distributed over the bandwidth, B_d, of the Doppler signal. As a consequence, the current in a smaller bandwidth, ΔB_d is equal to $I_{\Delta B_d}$, where [3]

$$I_{\Delta B_d} = I_{A/C,\ peak} \left(\frac{\Delta B_d}{B_d}\right), \tag{2.37}$$

which essentially is the current measured by the spectrum analyzer, with a resolution equal to $(\Delta B_d/B_d)$.

An important parameter, particularly in fluid flow studies, is the heterodyne volume size. For local measurements of velocities, one attempts to make measurements over as small a fluid volume as practicable. However, attempts to reduce the size of the heterodyne volume may result in a reduced system performance. Examination of Figure 2.7 shows that

$$\alpha \simeq \frac{D'}{b}, \tag{2.38}$$

where b is the distance between receiver lens L_2 and the image plane which is the same as the plane of field stop in the Figure. Consequently, diameter of the heterodyne volume, D_h, in the object plane equals [3]

$$D_h = \frac{a}{b} D', \tag{2.39}$$

a being the distance between the focal point and lens L_2. Equation (2.39) is valid for all values of α greater than α_{min}, α_{min} being the minimum angle of resolution of receiver lens L_2, and is given by

$$\alpha_{min} = 1.22 \frac{\lambda_1}{D_A}. \tag{2.40}$$

In Equation (2.40) λ_1 is the incident radiation wavelength and D_A is the aperture diameter shown in Figure 2.7. D_h, as given by Equation (2.39), is the dimension of heterodyne volume, normal to the receiver axis along e_3. The dimension of the heterodyne volume along the receiver axis, on the other hand, is approximately equal to the diameter of the incident laser beam, E', at the focal point on the receiver axis, given by [3]

$$E' \simeq \theta_d F_1. \tag{2.41}$$

In Equation (2.41), θ_d is the laser beam divergence angle and F_1 is the focal length of lens L_1, which focusses the beam at the focal point. Divergence angle, θ_d, is given by [3]

$$\theta_d = 1.22 \frac{\lambda_1}{E}, \tag{2.42}$$

where E is the diameter of unfocussed incident beam. With the use of Equation (2.42), the expression for E' can be simplified to

$$E' \simeq 1.22 \frac{\lambda_1}{E} F_1. \tag{2.43}$$

For values of α less than α_{min}, the size of the heterodyne volume perpendicular to the receiver axis is limited by the resolution of lens L_2 and is given by [3]

$$D_h \simeq 1.22\left(\frac{\lambda}{D_A}\right) a. \qquad (2.44)$$

For the specified source of incident radiation, the size of the heterodyne volume is thus a function of the ratios (a/D_A), and (F_1/E); an attempt to make these ratios smaller to attain a smaller volume size results in reduced system accuracy. Further remarks concerning an experimental determination of the actual heterodyne volume for the system of the present investigation are included in Chapter V.

To conclude this subsection on the discussion of the influence of various parameters on the operation of a LDV system, consideration must be given to two factors which frequently contribute to possible errors in the measurement of particle speeds by this technique.

One such factor is the Doppler signal bandwith. It is related to the phenomenon of pulse-modulation which causes broadening of the Doppler signal spectrum. A particle passing through the heterodyne volume produces a pulse of scattered radiation, of a width corresponding to the time of residence of the particle within the heterodyne volume. This results in a fractional bandwidth, $\left(\frac{\Delta f_D}{f_D}\right)$, in the Doppler signal which is inversely proportional to the size of the heterodyne volume, D_h, normal to the receiver axis. As a result, small heterodyne volume sizes correspond to larger signal bandwidths, making it cumbersome to determine the central Doppler frequency, f_D. Pulse modulation can only

be eliminated by achieving a constant phase relationship between signals generated by the particles in the heterodyne volume. Since this is not an attainable task for any finite size of the heterodyne volume, and for any reasonable concentration of particles, one must accept a finite bandwidth of the Doppler signal, rather than the desirable single central frequency.

In an existing LDV system it is often difficult to ascertain an accurate relationship between the directions of the unit vectors representing the directions of incident and scattered radiations, and the particle velocity. This leads to the second factor contributing to a decreased overall accuracy of measurement. An examination of Figure 2.8 further illustrates this point.

In order that the incident beam power density is sufficiently high, a pencil of smaller incident beamlets is bundled together, resulting in a spread in the incident beam direction, e_1. A similar spread in the direction, e_3, of the scattered beam further contributes to a fractional shift in Doppler frequency. An expression relating this fractional shift to the associated angles may be written as [3]

$$\frac{\Delta f_D}{f_D} \simeq \frac{\text{Sin } \phi_o \, \Delta\phi_{max} + \Delta\psi_{max}}{\text{Cos } \phi_o} \qquad (2.45)$$

for $\psi_o \simeq 90^o$ and for small values of $\Delta\phi_{max}$ and $\Delta\psi_{max}$. From the geometry of the figure,

$$\Delta\phi_{max} \simeq \frac{D_A/2}{a} \qquad (2.46)$$

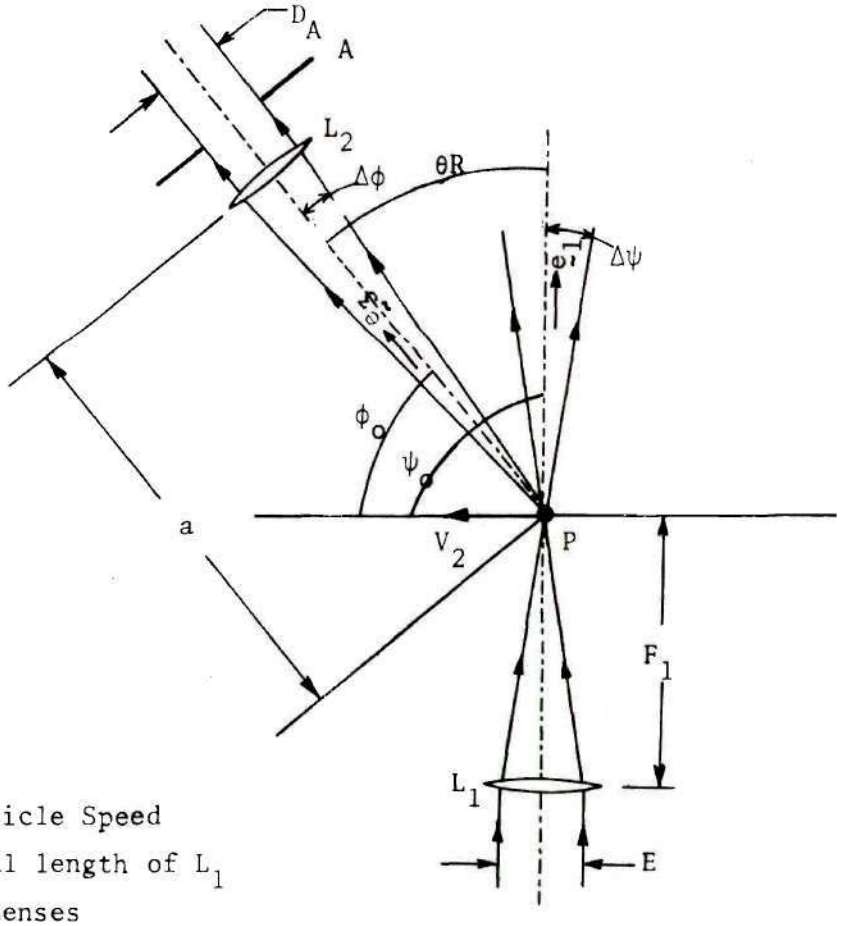

V_2 - Particle Speed

F_1 - Focal length of L_1

L_1,L_2 - Lenses

A - Aperture Stop

P - Moving Particle

Figure 2.8. Angular Spread In Incident And Scattered Beam Direction Vectors.

and $$\Delta\psi_{max} \simeq \frac{E/2}{F_1}$$

A decrease in a/D_A and F_1/E to achieve smaller heterodyne volume thus results in increased values of $\Delta\phi_{max}$ and $\Delta\psi_{max}$. This in turn, leads to the undesirable Doppler bandwidth.

CHAPTER III

THE ELECTRONIC READOUT SYSTEM

3.1 The Phase Locked Loop

Two readout systems used in the analysis of LDV signals are the phase locked loop and spectrum analyzer. It is often inaccuracy and restricted applicability of the readout system that limits the operation of the LDV system. A brief explanation of the two basic readout systems is presented here before describing a more versatile digital readout system used in this investigation.

The phase locked loop is a frequency feedback system. It consists primarily of a phase comparator, a low pass filter, an error amplifier in the forward signal path, and a voltage-controlled oscillator (VCO) in the feedback path. Grebene [15] has provided an excellent description of the phase locked loop (PLL). Consider Figure 3.1, where the error voltage, v_d, equals zero for no input applied to the system. The reference frequency, f_o, at which the VCO operates is called a free-running frequency. The phase comparator generates an error voltage, $v_e(t)$, by comparing the reference frequency with the input signal frequency, f_{sig}, and its phase angle. The feedback nature of PLL causes the VCO to "lock" with the incoming signal for $f_{sig} \simeq f_o$; except for the necessary phase angle to sustain the lock the two frequencies are identical. The "lock-range" defines the range over which the frequency lock can be maintained. The "capture-range", on the other hand, defines the

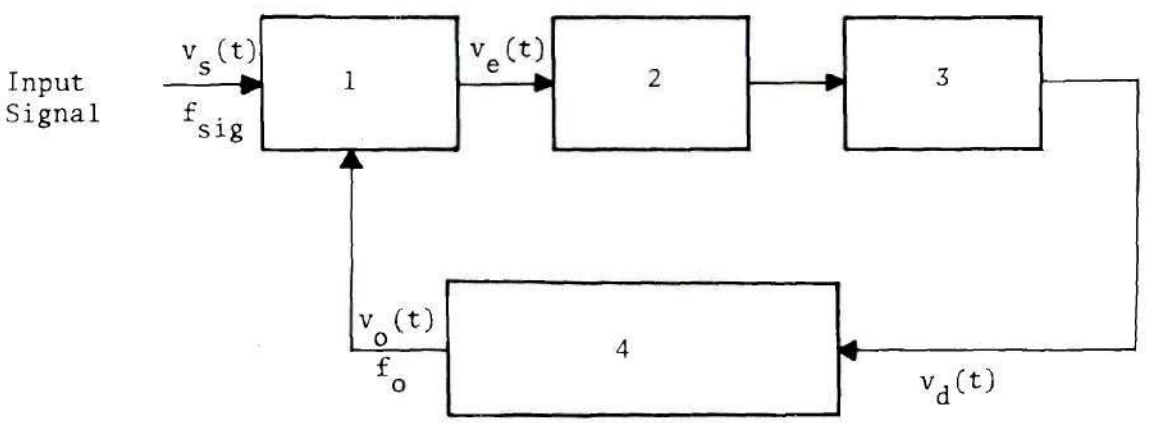

1 - Phase Comparator

2 - Low-Pass Filter

3 - Amplifier

4 - Voltage-Controlled Oscillator

Figure 3.1. Block Diagram of a Phase-Locked Loop

range of frequencies over which the PLL can acquire lock with the input frequency. The time elapsed to establish the lock is referred to as the "pull-in time".

Figure 3.2 illustrates the frequency to voltage transfer characteristics of the PLL. When the input signal reaches a frequency f_{i1}, corresponding to the lower end of the capture range, the loop suddenly locks on the input and tracks it until the input frequency reaches f_{i2}, the latter being the upper end of the lock range. Depending on whether the loop starts with or without an initial lock, the PLL responds to input frequencies separated from the reference frequency by less than Δf_c or Δf_l.

Three factors affect the applicability of phase locked loops [15].

a. Provided that the input amplitude is sufficient to maintain the lock, the PLL responds only to the input frequency and not the amplitude, thus filtering out only the frequency information, and not the amplitude.

b. The "harmonic lock effect" tends to make the PLL respond to harmonics and subharmonics of the input, thus degrading the system interference rejection.

c. The PLL proves to be of little value as a feedback gain control component, since it does not respond to the input amplitude.

3.2 The Spectrum Analyzer

A spectrum analyzer is basically a swept receiver, which may display a signal on an oscilloscope. The spectrum is presented as a

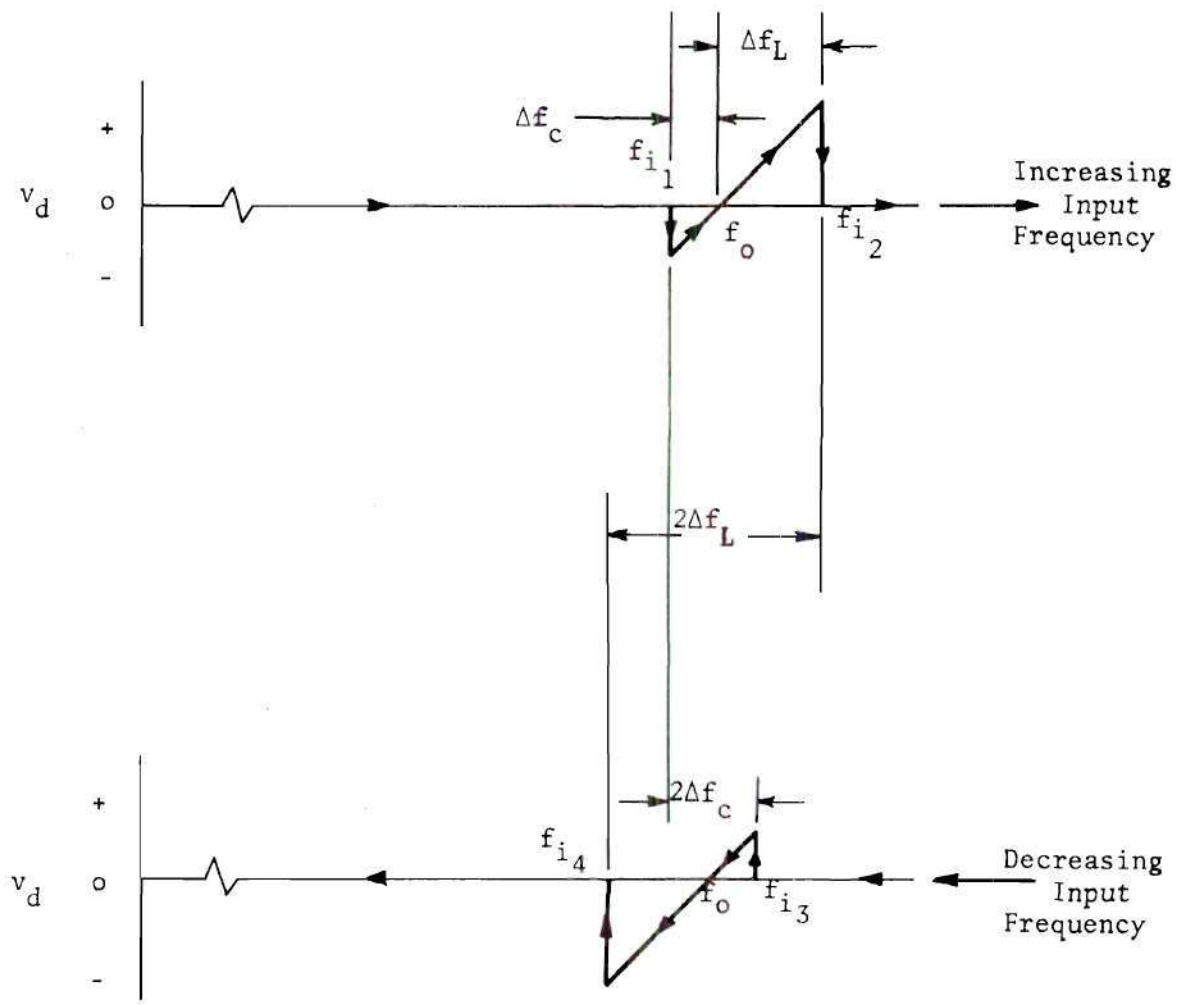

$2\Delta f_L$ - Lock Range

$2\Delta f_c$ - Capture Range

Figure 3.2. Typical PLL Frequency-To-Voltage Transfer Characteristics

plot of amplitude versus frequency, the amplitude being an indication of the signal energy. Examination of Figure 3.3 shows a block diagram representation of a spectrum analyzer as given by Grisell et al. [16].

Ramp voltage from the sawtooth generator is applied to a voltage-tunable local oscillator, LO, and the deflection plates of the CRT, simultaneously. Consequently, the horizontal position of the dot on the screen directly represents the frequency. As LO sweeps across a frequency band, the input signal is converted to an intermediate signal with a frequency f_{iF} which is amplified following the detection and subsequently applied to vertical deflection plates. The process results in an amplitude versus frequency display of the input signal.

A special problem is encountered when a spectrum analyzer is employed to analyze the output signal from a laser Doppler velocimeter. Laser Doppler velocimetry utilizes light scattered from discrete particles to generate the Doppler signal. Consequently, the Doppler signal is not a continuous sinusoid. Rather, it is a series of brief sinusoids of durations corresponding to the time of passage of a particle through the heterodyne volume. In the present investigation, this time period was of the order of 10 μsec. For higher flow velocities and smaller heterodyne volume sizes the durations of Doppler signals tend to be smaller. One solution to this problem, referred to as "dropout," is to increase the particle concentration in the flow. This, however, tends to attenuate the scattered light and thus degrades the Doppler signal. A spectrum analyzer determines the frequency of an input by comparing the input signal with an internal sweeping oscillator. When the input signal to the spectrum analyzer is at the same frequency as spec-

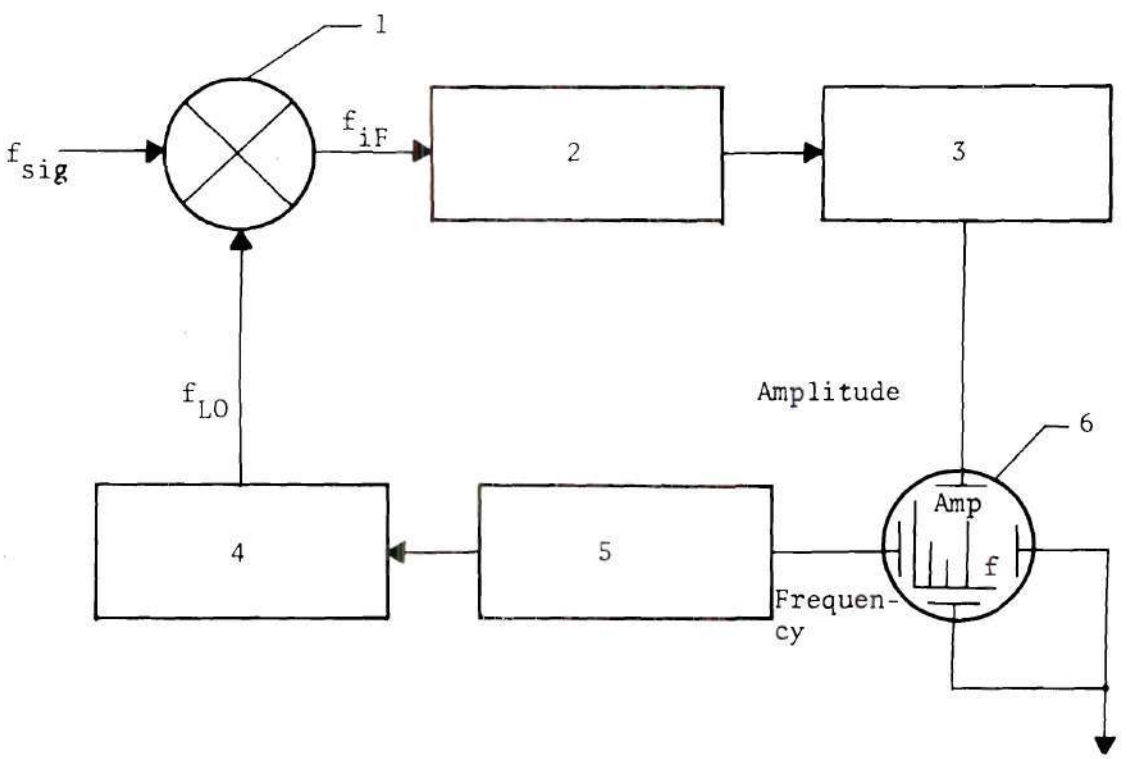

1 - Mixer

2 - IF Filter

3 - Detector and Video Amplifier

4 - Voltage - Tunable Oscillator

5 - Sawtooth Generator

6 - CRT

Figure 3.3. Spectrum Analyzer - A Block Diagram

trum analyzer's swept oscillator, which is changing frequency linearly with respect to time, there is a deflection on the screen. If the spectrum analyzer's sweeping oscillator is not at the frequency of the Doppler signal at some time during the brief interval between dropouts, no indication of the Doppler signal's frequency is obtained. Furthermore, the spectrum analyzer has to be recalibrated each time the signal changes from one range of frequencies to another so as to obtain the specified instrument accuracy.

3.3 The Digital Readout System

The preceding description of the phase locked loop and spectrum analyzer points to the need for a significantly improved readout system. This is particularly important in the study of turbulent fluid flow fields. A unique scheme of data analysis employed in this investigation makes use of a multichannel analyzer. A multichannel analyzer is often used by nuclear scientists to measure the distribution of pulse heights in the outputs of nuclear radiation detectors. In a typical experimental setup, the output of a detector is accumulated by a multichannel analyzer for a preset period of time. The resulting histogram is a spectrum, or energy distribution, giving radiation intensity (counts) versus energy (channel number).

Examination of Figure 3.4 shows a typical analyzer display and Figure 3.5 represents an elemental block diagram of the multichannel analyzer operating in its "pulse height analysis", (PHA), mode. In the PHA mode, the amplitudes of individual input pulses are digitized in an analog-to-digital converter. The analyzer has a typical memory capacity

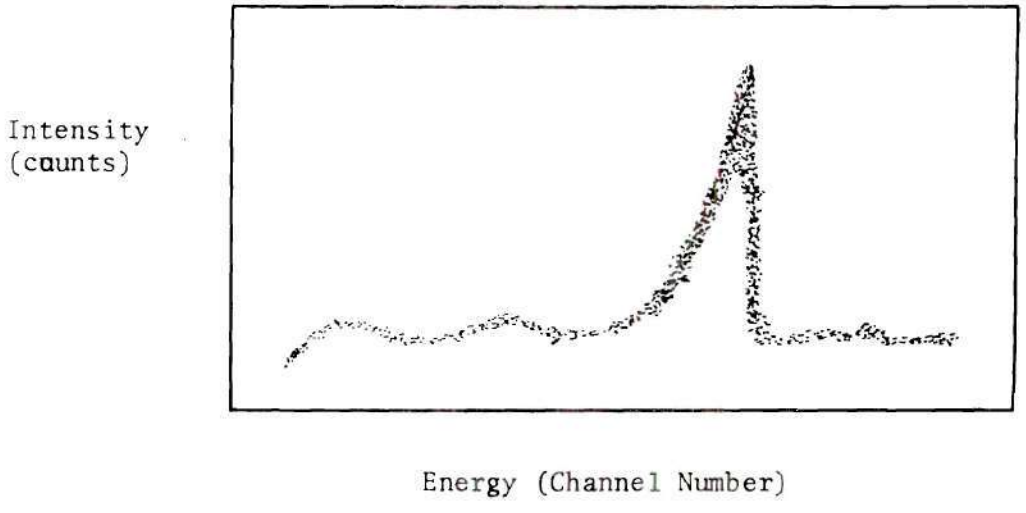

Figure 3.4. A Typical Multichannel Analyzer Display

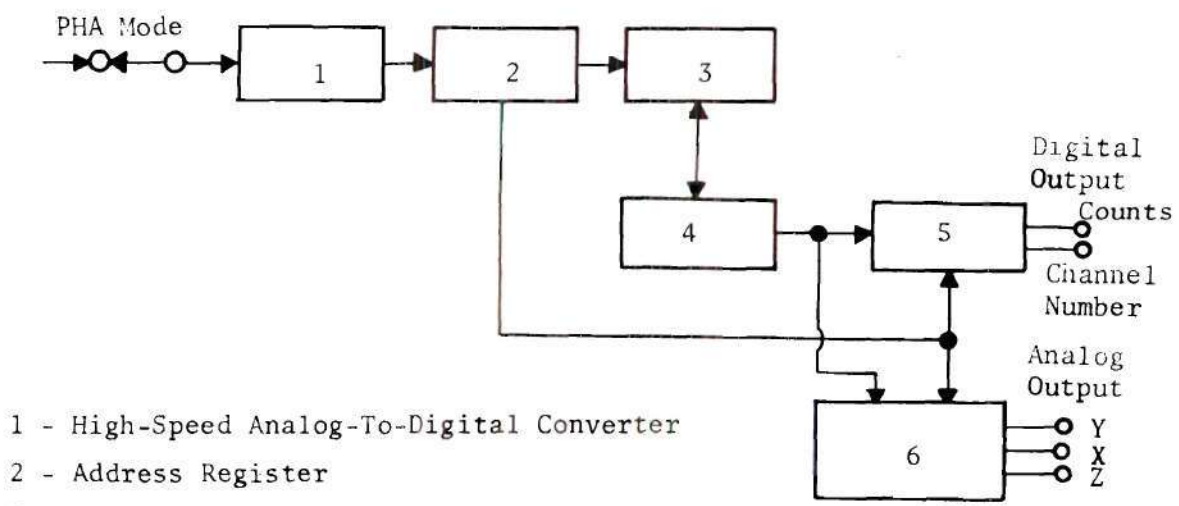

1 - High-Speed Analog-To-Digital Converter

2 - Address Register

3 - Memory

4 - Accumulator

5 - Digital Output Circuits

6 - CRT and Digital-To-Analog Converter

Figure 3.5. Block Diagram Representation of A Multichannel Analyzer

of 1024 words, each being a 6-decimal-digit (24-bit) word. In other words, the analyzer is capable of storing information for 1024 channels with up to 999,999 counts per channel. Output from the analyzer is normally fed to a printer, punch tape, or computer for analysis of the data.

Figure 3.6 shows a block diagram representation of the readout system used in this investigation. Output from the velocimeter is a current signal from the photomultiplier tube. This signal is converted to a voltage by passing the current through a 50 ohm resistor. In addition to the Doppler signal, the photomultiplier output contains d-c components and low frequency noise from various sources. The readout system functions to analyze this total output for its frequency components and their relative occurances. To accomplish this, the photomultiplier output is fed to a 20 kHz cutoff, high-pass filter which filters out the low-frequency noise. Subsequently, the signal is amplified, fed to a fast discriminator, a time-to-amplitude converter, and then to a multichannel analyzer.

3.3.1 The Discriminator

The discriminator operates on the input by putting out a negative spike, each time the input makes a zero transition going from a positive value to a negative one. To accomplish this, a variable knob on the unit is operated which presets the discriminator to a threshold or discriminator level such that a spike is produced each time the input signal goes more negative than the preset threshold value. This feature of the discriminator works to an additional advantage as it filters out some of the low amplitude noise accompanying the Doppler signal.

The "Threshold Control" is essentially a ten-turn potentiometer

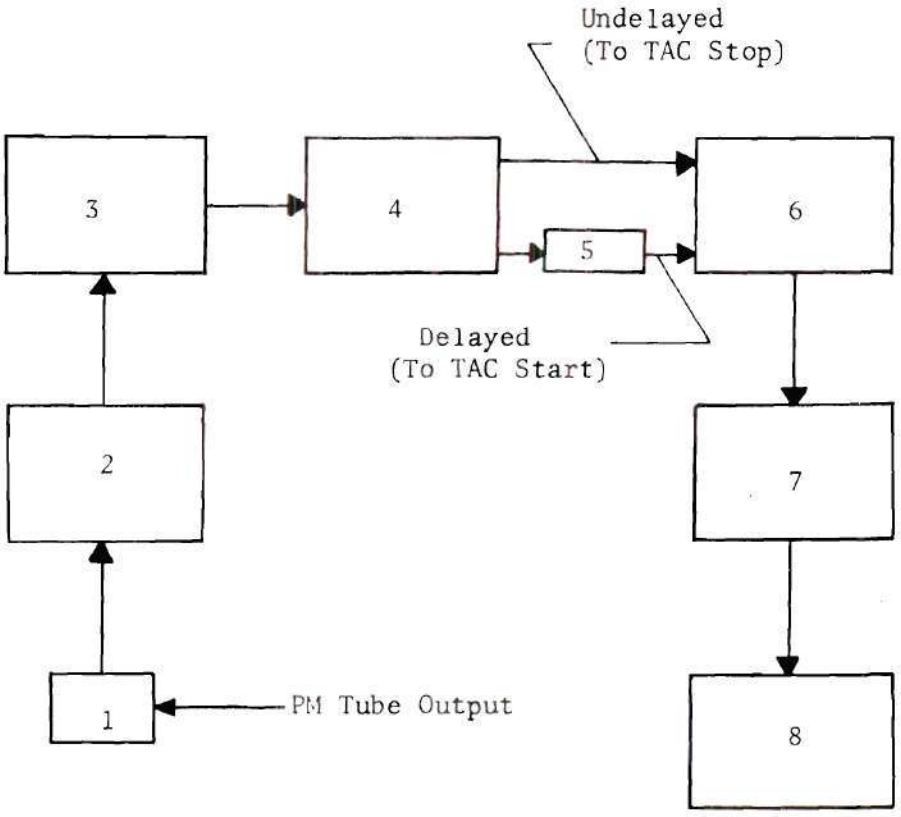

1 - 20 KHz High-Pass Filter

2 - Ortec Amplifier

3 - Discriminator

4 - Hewlett-Packard Amplifier

5 - Delay Cable

6 - Time to Amplitude Converter

7 - Multichannel Analyzer

8 - Teletype

Figure 3.6. Block Diagram of the Digital Readout System

with a calibrated dial. The control is calibrated in -50 millivolts per one milliampere of input current across an input impedence equal to 50 ohms. The minimum threshold setting is -100 millivolts or -2 milliamperes while the useful range extends to at least -500 millivolts or -10 milliamperes. Using an oscilloscope, the threshold control is set at the highest practical value so that much of the noise is eliminated without cutting out the main Doppler signal. The "Dual Updating Discriminator" used in the present system processes fast negative - going output signals from the photomultiplier.

Two modes of operation, "Input Clipped" and "Input DC", may be front panel switch selected. In the input clipped mode, an output of preset duration occurs after each threshold crossing, independent of signal duration above threshold, while the input d-c mode results in an output without interruption for the preset time over threshold, whichever is longer. The discriminator is calibrated with a slow risetime signal. A typical phototube signal has a risetime of the order of 2 to 5 nannoseconds. The "updating" timer on the discriminator guarantees the persistance of an output signal for a preselected time duration after the most recent input threshold crossing, independent of the previous operating history.

The output spikes from the discriminator are subsequently amplified by the linear amplifier. Approximately 45 feet of coaxial cable is used to delay part of the discriminator output, which is sent to the Time to Amplitude Converter (TAC) "start" input. The undelayed portion is fed directly to the TAC "stop" input.

3.3.2 Time-To-Amplitude Converter

The delayed and undelayed inputs to the TAC result in a standard time error Δt, which is equal to the cable delay time. This time error is compensated in the calibration of the TAC. The TAC produces an output signal whose amplitude is proportional to the time difference between start and stop input signals. Internal control logic and timing circuitry in the unit minimize invalid data by eliminating start-stop ambiguities and random input information. TAC overflow, caused by a start signal that is not followed by a timely stop signal, is not read out by the "pulse height analyzer", resulting in a quick TAC reset. In addition, valid readout data is delayed to allow other equipment to asses the data before it is read by the analyzer.

The TAC range selector knob can be set at a value ranging from 0.3 μsec to 30.0 μsec. The function of TAC selector knob is to assign the maximum voltage, (about 1 volt), to the amplitude of that TAC output signal which results from an input signal to the TAC having a period equal to the selector reading. Other TAC output signal amplitudes, corresponding to input signal periods lower than the selector reading, are assigned lower voltage values in direct proportion to their periods and the selector period reading. Signals with their amplitudes in the range between -200 to -400 millivolts are acceptable at TAC start and stop inputs. Figure 3.7 shows inputs and outputs from the TAC. A typical TAC cycle is shown in Figure 3.8. The following Figure 3.9 is a graphical representation of a typical input signal as it is processed by the readout system.

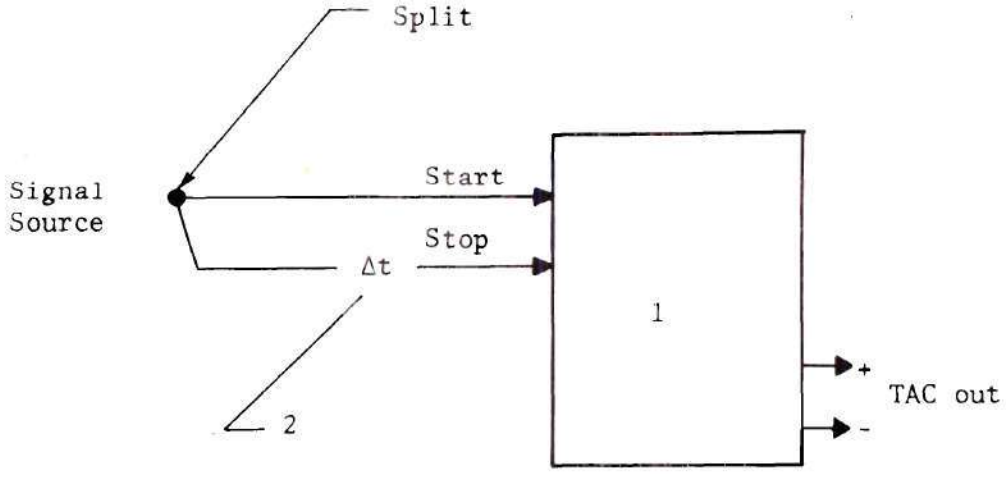

1 - Time-To-Amplitude Converter

2 - Δt Greater Than Signal Width

Figure 3.7. Method of TACing Sequential Signals On a Single Line

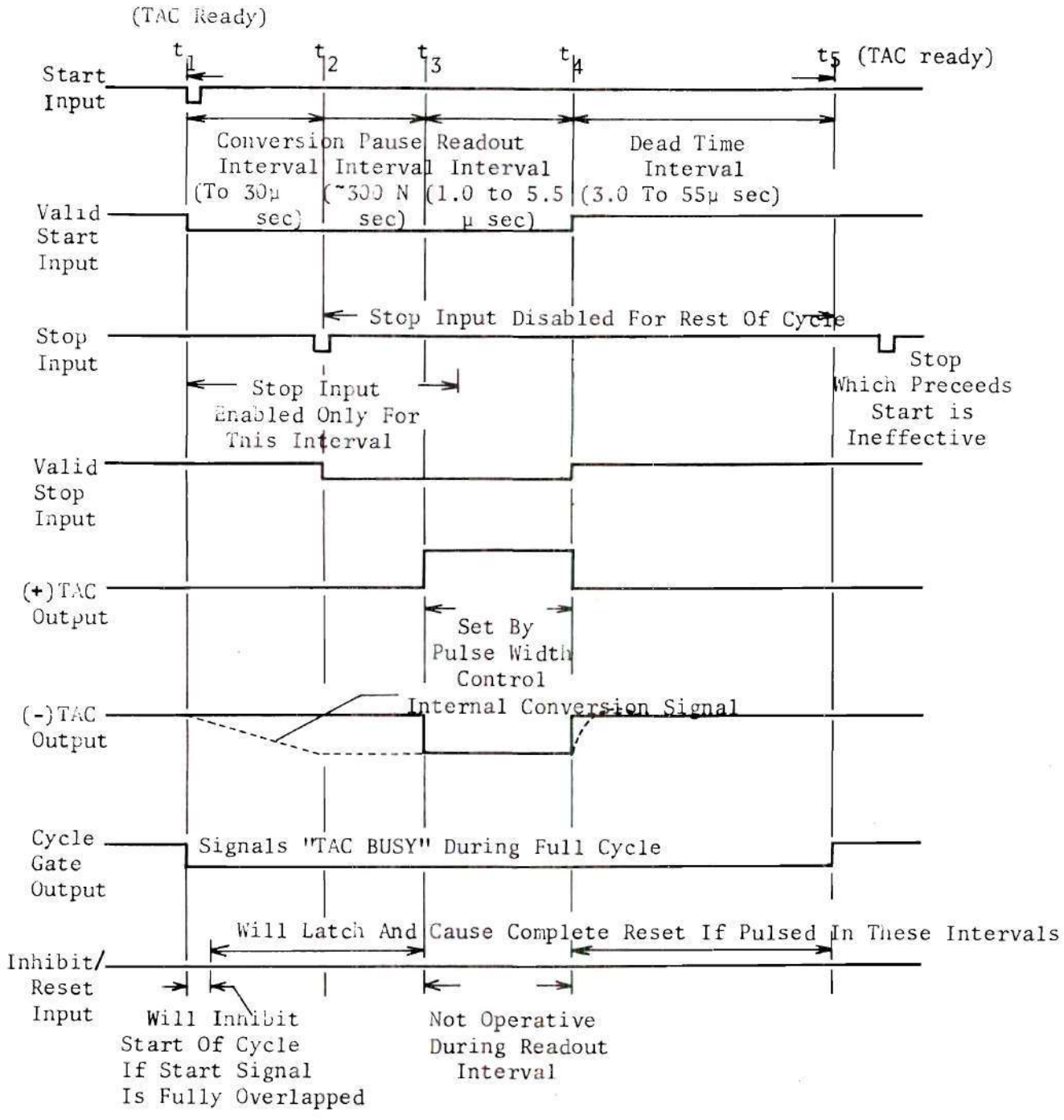

Assumed: TAC Reset At Time t_1

Full Scale Time: t_3

Figure 3.8 Typical Time-To-Amplitude Converter Cycle

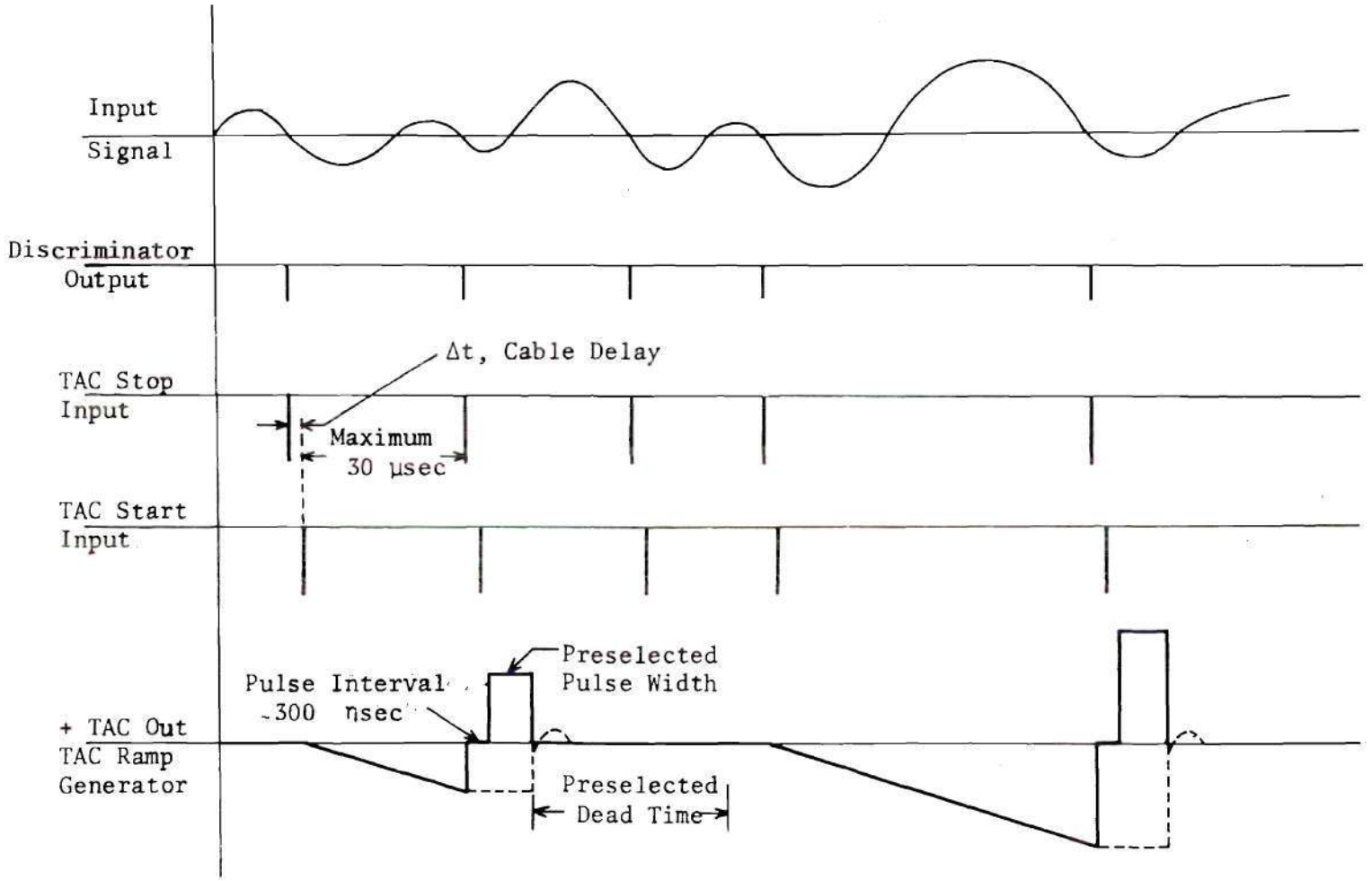

Figure 3.9. History of a Typical Input To the Readout System

3.3.3 The Multichannel Analyzer

The output of TAC is amplified and fed to the "Analog to Digital Converter", (ADC), module of the multichannel analyzer. Basically, the multichannel analyzer classifies input signals into amplitude groups and continuously totalizes the number in each amplitude group. For a series of pulses of random but bounded amplitudes the multichannel analyzer measures the distribution of the amplitudes as a function of the voltage. The pulses can be spaced as closely as a few microseconds and are resolved into groups up to a maximum of 256, although the absolute upper limit of groups may be several multiples higher. The 256 amplitude groups with incremental amplitude ranges correspond to the 256 channels between selected amplitude limits. The instrument measures the amplitude distribution of pulses, a process which is referred to as "pulse height analysis". Ross [17] describes this aspect of the analyzer.

In the PHA mode, the objective of the measurement is to obtain a distribution of the frequency of occurrence of the heights of a train of applied pulses. To obtain this distribution the incoming pulses are sorted for pulse height by the ADC into one of the 256 possible heights. The ADC is of a ramp type in which an arriving pulse first charges a capacitor to the peak pulse amplitude. The capacitor is then discharged linearly to a zero value by a constant current source. During the discharge, a binary counter counts a clock, resulting at full discharge in a counter reading representative of the initial capacitor charge or the pulse amplitude. This number represents a single channel in the analyzer's core memory, into which a count is now added.

To accomplish this, the counter reading is transferred into the

memory address register. A read-memory operation then causes the contents of the addressed channel to be loaded into the accumulator. Next, a single count is added to the accumulator count, which was the cumulative number of counts in the memory, of that amplitude. Following this step, the new accumulator content is written back into the same memory channel. The net effect of these operations is to increase the count by one in a particular channel of the memory. Each time a pulse is received by the ADC, the sequence is repeated, thereby compiling a distribution in which the channels correspond to particular pulse heights and the total count in each channel equals the number of pulses whose height corresponds to that channel.

A master control module contains facilities for establishing the primary operating modes of data acquisition, display, read-in and readout and all the data handling functions of the multichannel analyzer. In "live display" mode, the point to be stored is placed on the oscilloscope screen and the display oscillator starts sweeping from that point and continues until the next point to be analyzed. In "live/static display" mode, the point to be stored is placed on the oscilloscope screen and remains until the next point to be stored becomes available. After data has been acquired, front panel controls enable digital selection of memory groups for data storage, display, processing, and readout.

The read-in/out display module is capable of driving high speed digital printers and x-y plotters. A scanmaster control enables the spectrum of interest to be expanded in the x-axis for observation of peak separation during oscilloscope display readout. When the x-gain is increased, only a small segment of the displayed data appears on the face

of the 'scope. A ten-turn potentiometer allows movement of the entire expanded memory contents across the face of the 'scope. A digital read-out switch allows either all of the memory contents or only the information displayed on the 'scope during scanmaster operation to be read out.

In the present readout system, a teletype was utilized to obtain frequency data in a digital form of channel numbers versus counts.

CHAPTER IV

APPARATUS AND EQUIPMENT

4.1 Flow System Design

In order to generate a reference flow field against which experimental data might be compared it was decided to fabricate an axisymmetric free turbulent jet flow system. A schematic arrangement of the flow loop is shown in Figure 4.1. It consists of a small centrifugal pump, a flow regulating needle valve, a calibrated rotameter with a range of 0.0145 to 0.145 gallons per minute of water, a 2" x 2" cylindrical chamber upstream of the jet pipe to provide a stagnation volume of the order of 100 times the nozzle pipe volume, a 0.079 inch I.D. jet tube to generate a freely expanding axisymmetric turbulent jet, the container duct, and a return path for the flow of water. A heavy metal collar on the outlet end of the jet tube minimized vibrations at relatively high jet velocities. A mercury manometer measured the pressure inside the stagnation chamber. Water jet issuing from the nozzle expanded inside the six inch square cross section and two feet long plexiglass duct. The duct was initially filled with distilled water containing externally added contaminant particles. Well documented equations for a freely expanding jet of water were used to analytically predict the jet velocity field; this helped generate the needed reference flow field.

The flow loop was initially designed and fabricated for use beyond the present investigation of a freely expanding axisymmetric jet

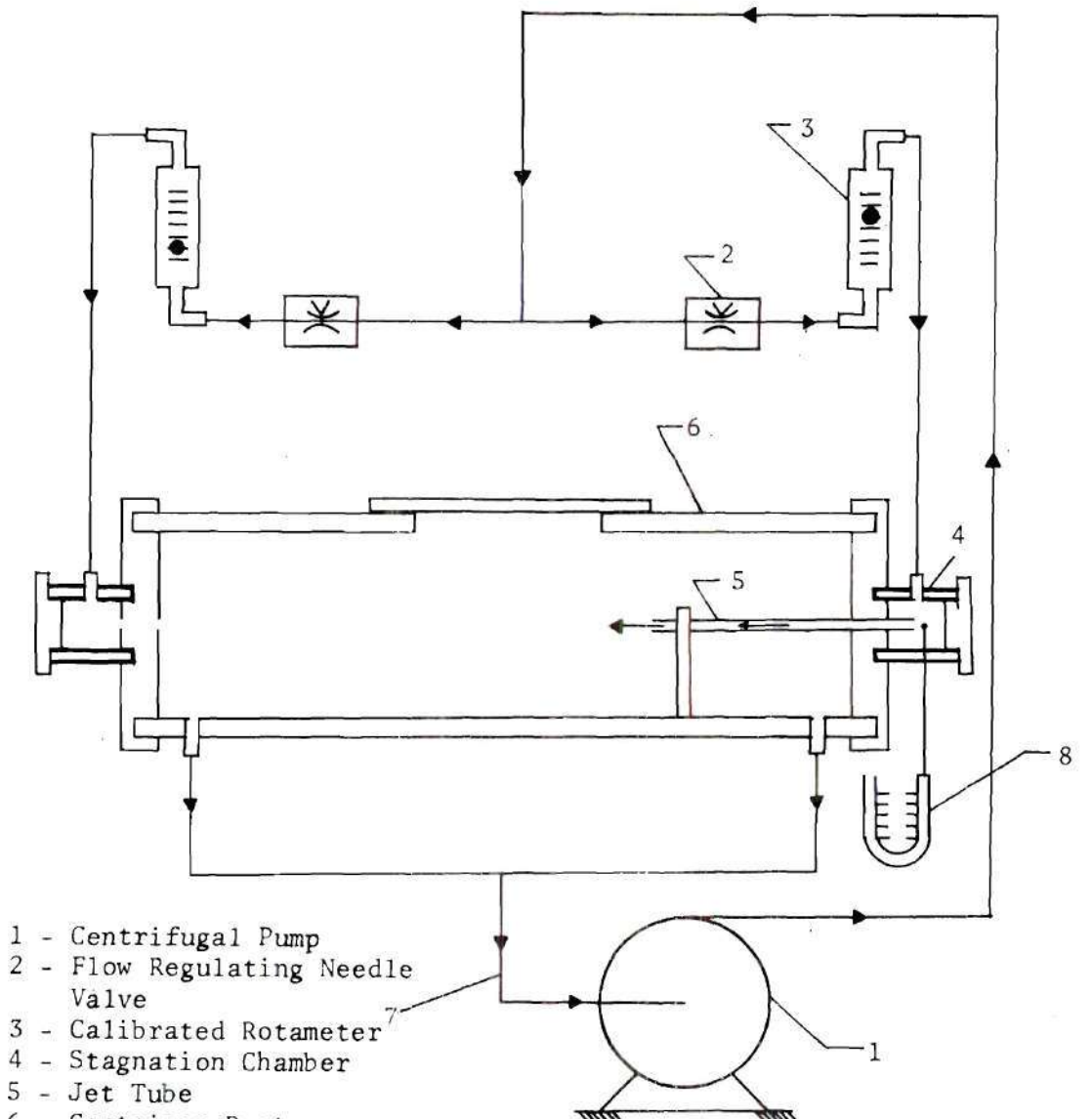

1 - Centrifugal Pump
2 - Flow Regulating Needle Valve
3 - Calibrated Rotameter
4 - Stagnation Chamber
5 - Jet Tube
6 - Container Duct
7 - Return Flow Path
8 - Mercury Manometer

Figure 4.1. Flow Loop Schematic

to the flow field of impacting jets. The selection of duct size was predicated on the basis of generating a truly free axisymmetric jet, which did not interact with the wall shear layer within the measured flow field. Furthermore, duct cross section had to be limited in order to accommodate the selected optical components for measurements across the entire flow field. Water leaving the jet flowed out through the duct outlets located at far ends, to be pumped back into the stagnation chamber. The velocity distribution in the fully developed flow field of an axisymmetric, turbulent free jet is given by [18]

$$\frac{u_x(x,r)}{u_{x_{max}}(x)} = \frac{1}{[1 + r^2/0.016x^2]^2}, \tag{4.1}$$

where $u_x(x,r)$ is the local axial velocity, $u_{x_{max}}(x)$ is the jet centerline velocity, and x, r, respectively, are the axial and radial coordinates at the point of measurement. Following the convention of defining the jet boundary by the equation

$$\frac{u_x(x,r)}{u_{x_{max}}(x)} = 0.01, \tag{4.2}$$

and substituting (4.2) into (4.1), a relation for jet radius was obtained as

$$r = 0.3795\ x. \tag{4.3}$$

Centerline velocity development of such a jet is given by [18]

$$\frac{u_{x_{max}}(x)}{u_o} = 6.4\ (\frac{d_o}{x}), \tag{4.4}$$

d_o being the nozzle diameter and u_o the jet velocity at nozzle exit. From Equation (4.4), at $x = 64\ d_o$, the axial velocity reduces to a value of 10% of u_o, and from Equation (4.2) this corresponds to a minimum jet velocity of $0.001\ u_o$ at the jet boundary. This value was considered sufficiently small to preclude a recirculation zone between the jet free shear layer and the duct wall. Furthermore, it was adjudged sufficient to provide a duct height at least 1 1/2 times the jet width at an axial distance of $64\ d_o$ from the nozzle exit. All the measurements were confined in this region. Geometrical as well as the flow parameters associated with the jet flow field are shown in Table 4.1. These values refer to the jet flow field shown in Fig. 4.2. It is seen that jet width at $x = 64\ d_o$ equals 3.8 inch. Hence a 6 inch square cross section duct provided a height more than 1 1/2 times the jet width at that station.

A jet pipe length of 4.72 inches provided a sufficient length to diameter ratio to yield a fully-developed turbulent pipe flow at its exit. A 5 inch long jet flow field within a 12 inch long duct section allowed a maximum jet pipe length of 6.963 inches.

The present LDV system resolution was of the order of 10^{-2} feet per second. Equating this value with the minimum jet velocity of $0.001\ u_o$ yielded the nozzle exit velocity of

$$0.001\ u_o = 10^{-2}, \text{ or}$$

$$u_o = 10 \text{ feet per second.} \qquad (4.5)$$

For u_o of the order of 10 feet per second inside the selected jet pipe gave the volume rate of flow through the jet pipe of the order of 1/6

TABLE 4.1 Geometrical and Flow Parameters Associated With the Expanding Jet.

x - Distance Along Jet Axis (inches)	r - Jet Radius (inches)	$\frac{u_{x_{max}}(x)}{u_o}$
6.4 d_o = 0.503	0.191	1.000
10 d_o = 0.787	0.298	0.640
20 d_o = 1.574	0.596	0.320
30 d_o = 2.361	0.894	0.213
40 d_o = 3.148	1.192	0.160
50 d_o = 3.935	1.490	0.128
60 d_o = 4.722	1.788	0.107
64 d_o = 5.030	1.907	0.100
70 d_o = 5.509	2.086	0.091

x - Streamwise Station From Nozzle Exit.

r - Jet Radius As Given by Equation 4.3.

$\frac{u_{x_{max}}(x)}{u_o}$ = Ratio of Centerline Velocity to Nozzle Exit Velocity.

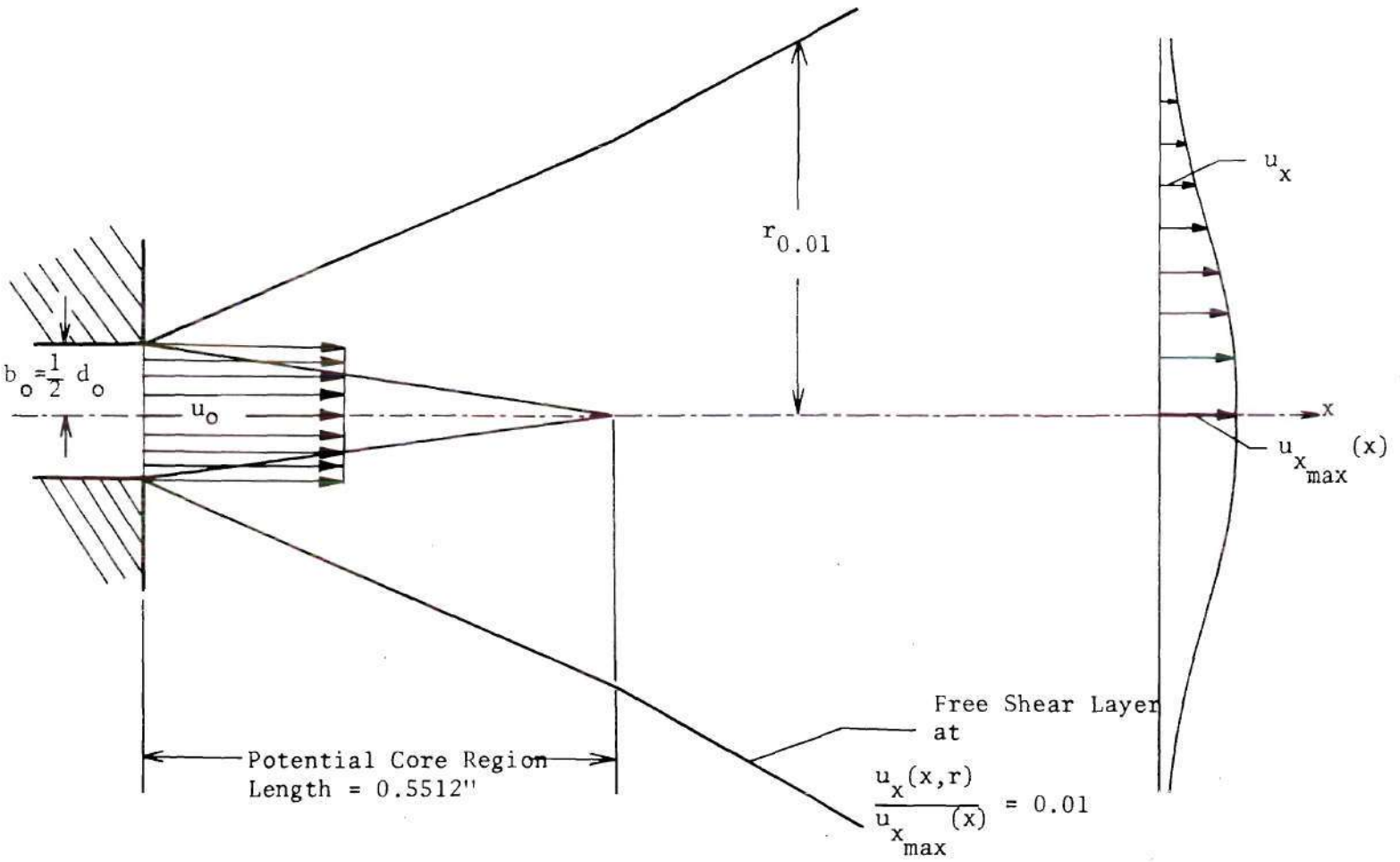

Figure 4.2. Axisymmetric Turbulent Free Jet Expanding Inside the Duct

gallon per minute; this established the pumping requirements.

The friction losses at the test Reynolds number (based on jet pipe diameter, u_o, and water temperature of 60°F.) of N_{Re} = 5465 were estimated as

$$h_{f_1} = FR' \frac{1}{D_t} \cdot \frac{V_f^2}{2g}, \text{ or}$$

$$h_{f_1} = 0.036 \times \frac{6.963}{0.0787} \times \frac{100}{2 \times 32.2}, \text{ or}$$

$$h_{f_1} = 4.946 \text{ feet of water,} \tag{4.6}$$

where h_{f_1} = head loss through the jet pipe. Velocity of water flow through the 1/4 inch return line was estimated to be about one foot per second, corresponding to a Reynolds number of 1720. Flow through the tygon return line being laminar, friction factor was calculated as

$$FR'' = \frac{64}{N_{Re}}, \text{ or}$$

$$= 0.0372. \tag{4.7}$$

Corresponding head loss was estimated to be

$$h_{f_2} = 0.294 \text{ feet of water.} \tag{4.8}$$

Total head loss, h_f, in the flow system (the sum of h_{f1}, h_{f2} and the friction loss through the flow regulating valve) was estimated to be of the order of 7.0 feet of water.

Finally, for 1.385 c.c. of 10% solid solution of 0.52 μ poly-

styrene particles added to a total volume of approximately 870 cubic inches of water in the flow loop, the volumetric concentration of contaminant particles in the water gave a ratio of 102,936 parts water to 1 part contaminant.

4.2 The Optical Configuration

Figure 4.3 shows the input and the receiving optical arrangement of the differential Doppler system developed for this investigation. A properly coated parallel-face optical flat utilized as the beam splitter, BS, generated two parallel beams, II and III, of approximately equal intensities, from the incident laser beam, I. Figure 4.4 is a photograph of the laser source, LS, mounted on a firm adjustable stand, AS_1, followed by the beam splitter, BS, mounted on an optical stand. All optical components were mounted on optical table, OT, capable of translation along the optical axis OX. A spirit level was utilized to horizontally level the optical table and the laser source. Subsequently, the laser source, the beam splitter, and the lens, L_1, were aligned with reference to the flow duct and the receiver optics. Purpose of this alignment process was to bring the bisector of the angle between beams II and III perpendicular to the length of the duct. Lateral movement of the duct perpendicular to the optical axis could be precisely measured off a scale (least count 1/64 inch) mounted along the rack-pinion duct stand AS_2. The axial translation of the optical table along OX, independent of duct travel, on the other hand, was measured with a precision dial indicator (least count of 0.001 inch).

The dual incident beams, II and III, were focussed at a point P

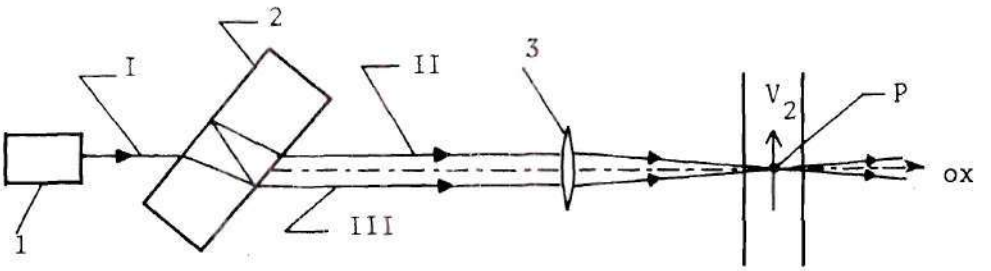

P - Focal Point

ox - Optical Axis

I - Incident Laser Beam

II - First Incident Beam

III - Second Incident Beam

1 - Laser Source, LS

2 - Beam Splitter, BS

3 - Input Lens L_1, F_1 = 87 mm
D_{11} = 35 mm

(a) Input Optics

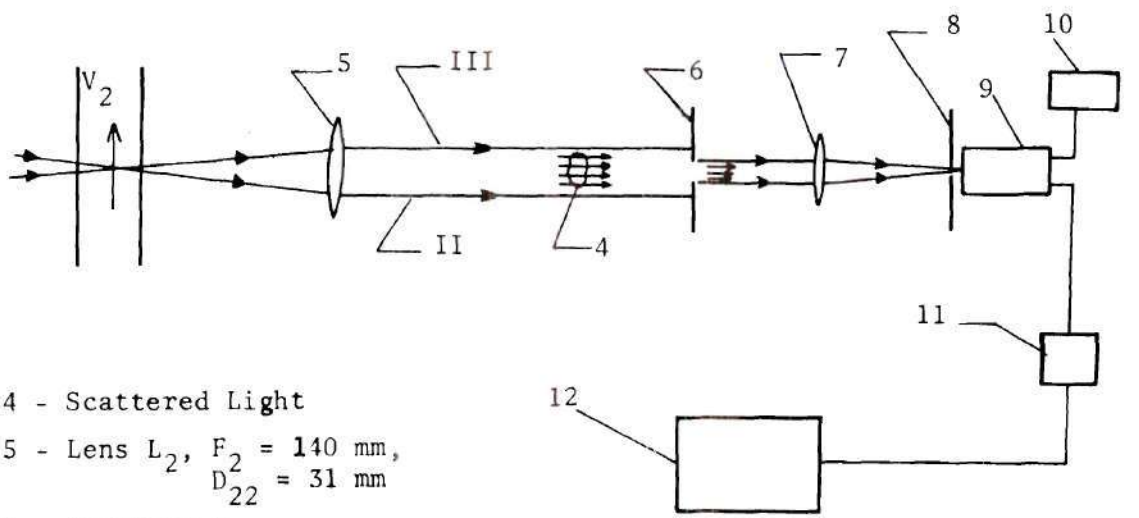

4 - Scattered Light

5 - Lens L_2, F_2 = 140 mm,
D_{22} = 31 mm

6 - Aperture A_1

7 - Lens L_3, F_3 = 103 mm,
D_{33} = 35 mm

8 - Pinhole A_2 With Micrometer Movement

9 - Photomultiplier, PM

10 - High Voltage Supply, VS

11 - High-Pass Filter, HP

12 - Readout System

(b) Receiving Optics

Figure 4.3. The Optical Configuration

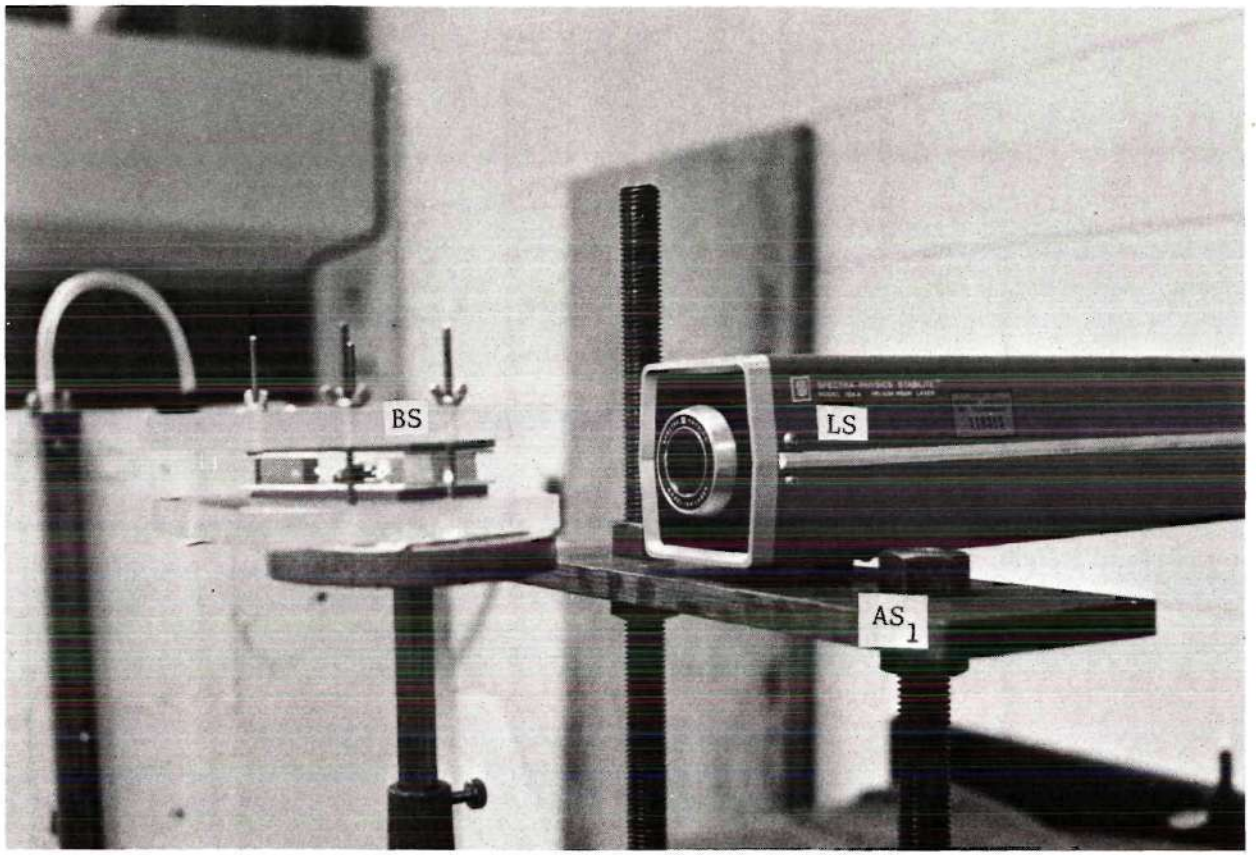

Figure 4.4 The Input Optics

inside the jet flow field by the input lens L_1. On the receiver optics end a collimating lens, L_2, was utilized to obtain the scattered parallel beams II and III. Following lens L_2, the main scattered beams were intercepted with an adjustable aperture A_1. Conversely, the relatively weak radiation between the beams, scattered off the moving particles at P, passed across A_1 to be focused by another lens L_3. Lens L_3 focused the weak scattered radiation via a pinhole, A_2, onto the photocathode of the photomultiplier tube, PM. The main function of the pinhole was to intercept the extraneous light from reaching the photocathode. The resulting output from the PM tube was a Doppler signal in form of brief pulses of sinusoids superimposed on low frequency noise signals. The PM tube output was filtered by the high-pass filter, HP, and fed to the readout system for further analysis. Figure 4.5 is a photograph showing the duct on its stand, the optical table, dial indicator, and the receiver optics consisting of lenses L_2 and L_3, apertures A_1 and A_2, and the photomultiplier tube.

4.3 The Readout System

Figure 4.6 shows a photograph of the digital electronic readout system employed with the LDV system of this investigation. Electrical signal output from the photomultiplier was filtered by the high-pass filter, amplified, and subsequently fed to the discriminator, DM. The output of DM was amplified and part of it delayed through the delay cable. Delayed and undelayed portions were subsequently fed to the TAC. Amplified TAC output was fed to the ADC module of the multichannel analyzer, MA. In addition, the photograph shows the master control and memory modules. The oscilloscope seen in the photograph was used to observe

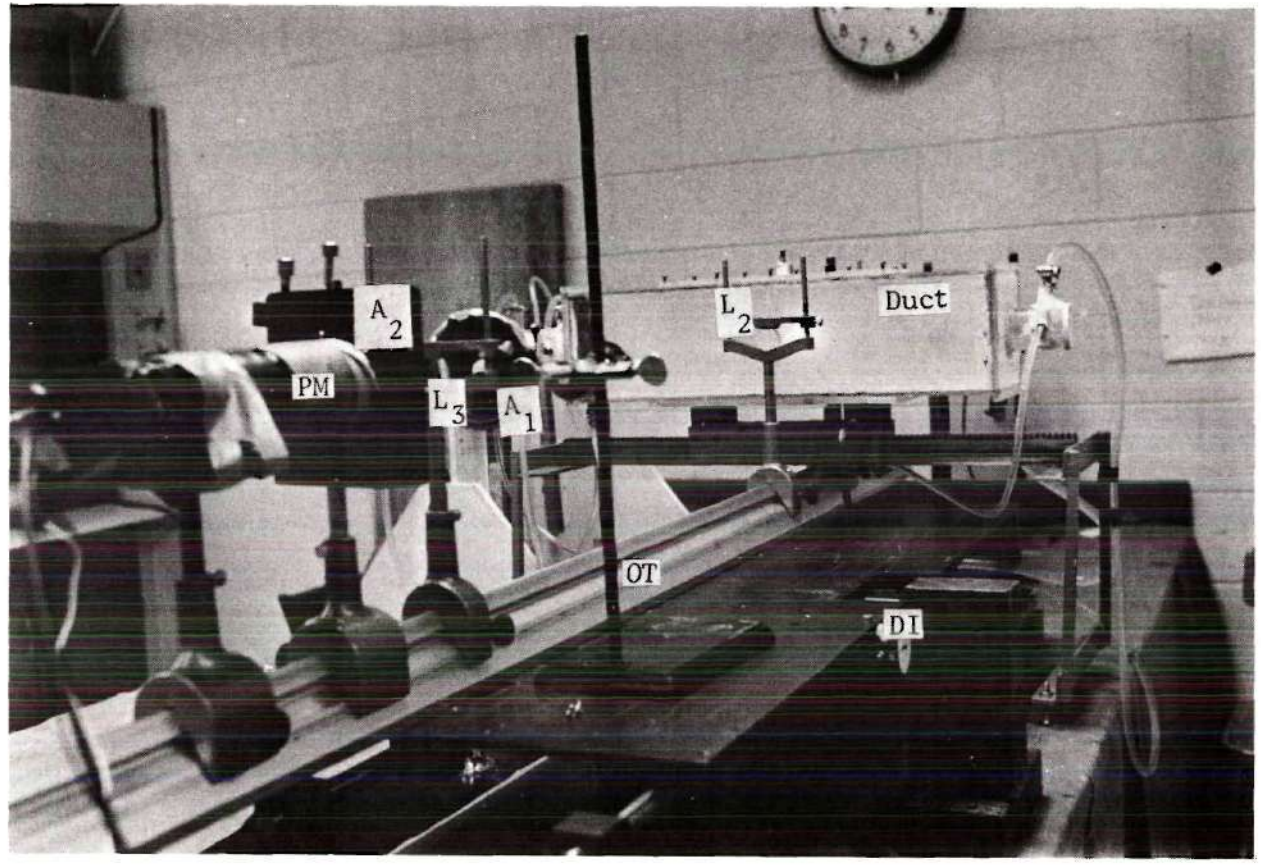

Figure 4.5 The Duct and The Optics

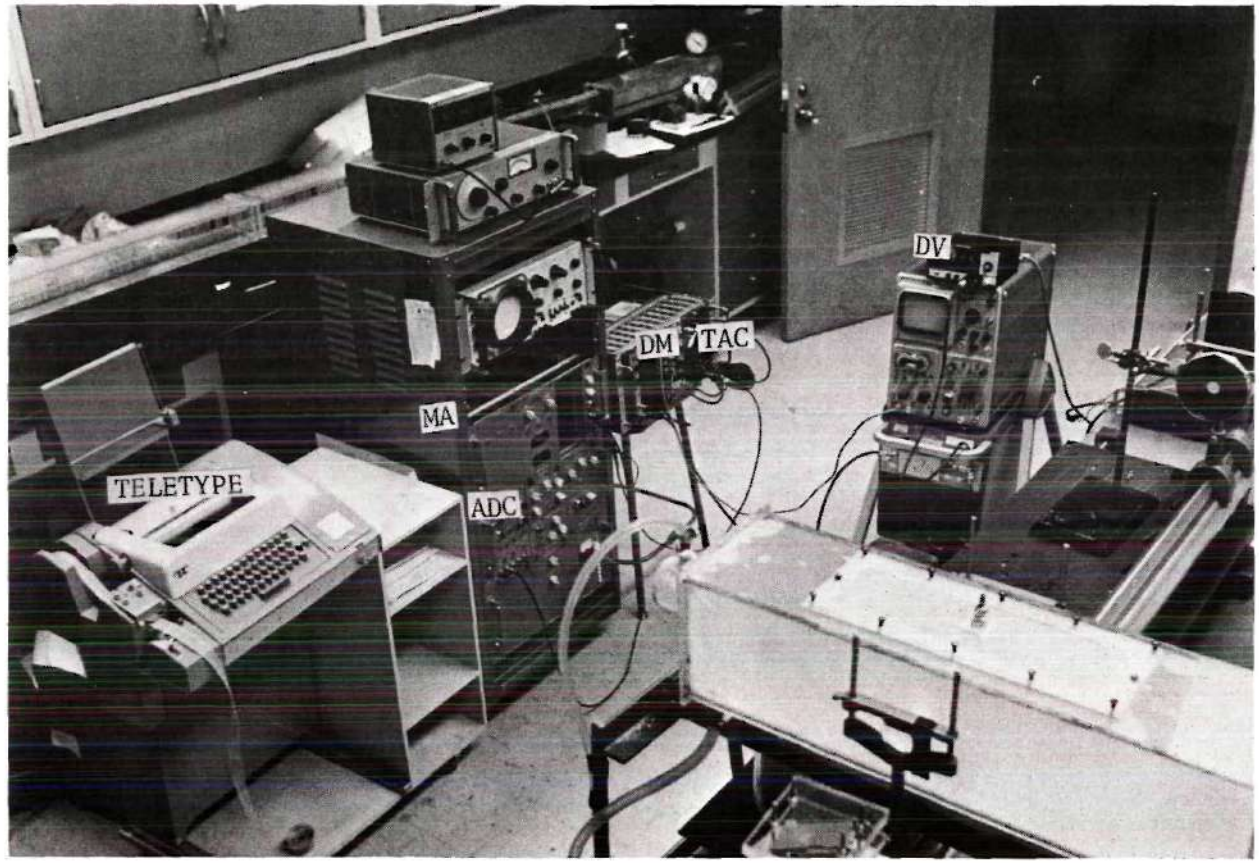

Figure 4.6 The Digital Electronic Readout System

the outputs from various units. Furthermore, a digital voltmeter, DV, was used to monitor PM output signal voltage and a sine-wave generator was utilized to calibrate the readout system. The CRT screen of MA displayed the frequency spectrum of the output in the form of counts versus channel numbers. The teletype was directly linked to the MA and printed out the data in the form of counts versus channel numbers.

4.4 Calibration of the Readout System

Calibration of the readout system was carried out to establish the direct relationship between the channel numbers and the corresponding input signal periods. To accomplish this a sine wave generator was utilized to obtain standard sine wave input signals of periods 1, 2, 4, 8, and 10 microseconds. Each one of the standard input signals was acquired by the readout system for a period of approximately five minutes in order to gather a sufficiently high number of counts for each case. The resulting printout showed five high counts corresponding to the five standard periodic input signals. Since the channel number is directly proportional to the period of the corresponding input, each of the five high counts were identified with the respective standard inputs. These five calibration points were utilized to establish the direct straight line relationship between channel numbers and periods of input signals represented by the channels. For channel numbers beyond 68, the resulting equation is

$$T = 0.0425C - 0.88, \tag{4.9}$$

and the corresponding equation for channel numbers below 68 is

$$T = 0.0435C - 0.96, \tag{4.10}$$

where C represents the channel number and T the period of the signal appearing in that channel. Figure 4.7 is a plot of Equations 4.9 and 4.10. It may be pointed out that a slight change in slope of the linear relationship between channel number versus signal period is experienced at channel number 68. Although such a behavior is in disparity with the ideal operation of the TAC unit, the variance between the actual and ideal operation is considered negligible for practical purposes.

Channel number versus period data of Equations 4.9 and 4.10 was converted to a relationship between channel number and input signal frequency appearing in the channel. This relation was established by substitution of

$$f = \frac{1}{T} \tag{4.11}$$

into Equations 4.9 and 4.10 where f is the frequency of a periodic signal with period T. Doppler frequency relationship given by

$$f_D = \frac{2n\ V_2}{\lambda_1}\ \text{Sin}\ \frac{\theta}{2} \tag{4.12}$$

was subsequently utilized to obtain direct relation between a channel number and the corresponding flow velocity, V_2. For the present LDV system, the angle θ is given by

$$\text{Sin}\ \frac{\theta}{2} = 0.0988, \tag{4.13}$$

and $\lambda_1 = 6328\ \mathring{A}$. Incorporating these values in Equation (4.12) gives

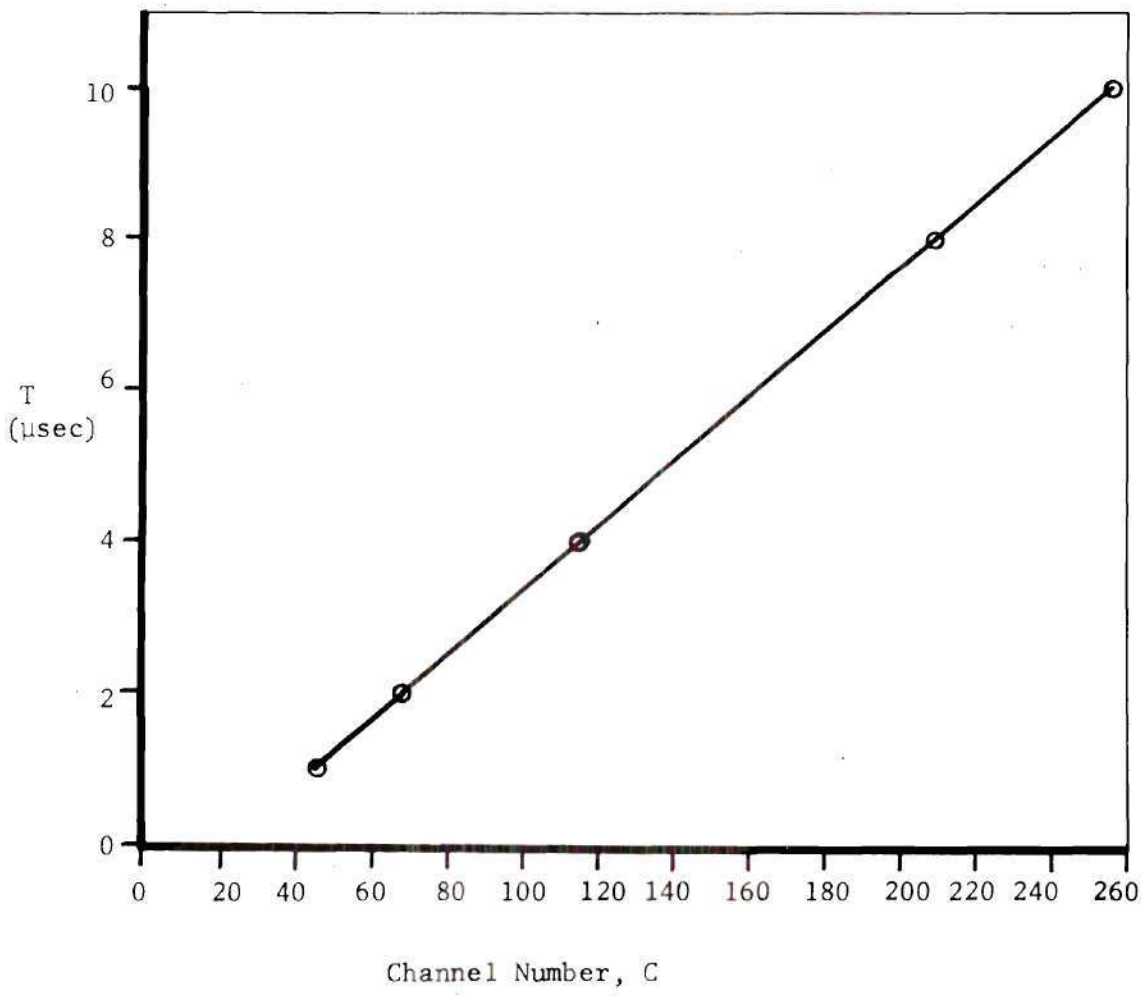

Figure 4.7. Channel Number Versus Signal Period Relationship

$$V_2 = 0.105 \times 10^{-4} f_D, \qquad (4.14)$$

where f_D is in hertz and V_2 is in feet per second. Figure 4.8 shows the scheme of measurement of angle θ and Figure 4.9 presents channel number versus flow velocity information.

The calibration chart of Figure 4.9 was utilized to interpret the output data from velocity measurements made in the flow field. A readout in form of number of counts in various channels was obtained for each point of velocity measurementin the flow field. The readout contained several high counts in closely spaced channels and an arithemetic mean value of those channel numbers was utilized to obtain the average Doppler frequency corresponding to average flow velocity.

4.5 A Brief Description of the Experiments

A laser Doppler velocimeter makes measurements over a small but finite volume, rather than a true point measurement. The accuracy of spatial resolution of a specific LDV system depends on this volume, which is commonly referred to as the heterodyne volume. In a separate study of the experimental system of this investigation, Mathews and Rust [20] have reported measurements of the heterodyne volume. They utilized a conical tip fine needle - approximately 0.002 inch diameter at 0.006 inch from the tip and 0.0005 inch diameter at 0.001 inch from the tip - to probe the heterodyne volume in order to provide a small scattering center. An audio-oscillator driven radio speaker was mounted on the needle stand and the oscillator frequency was varied until it matched the needle resonant frequency. This caused the needle to vibrate and the amplitude of vibrations was controlled by varying the

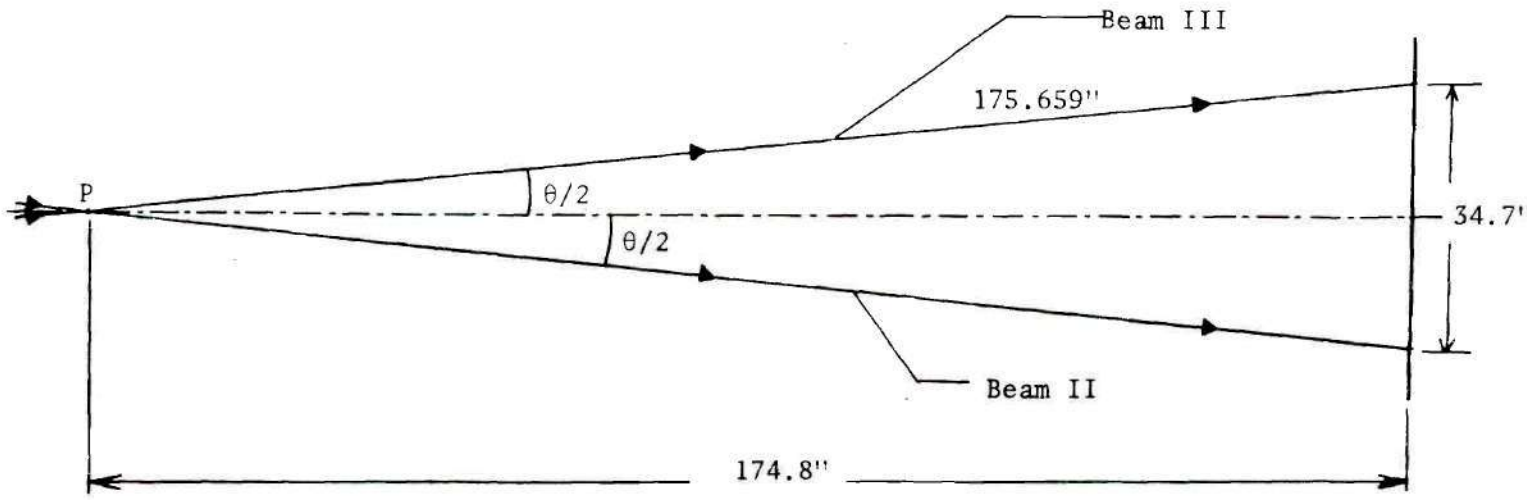

$$\text{Sin } \frac{\theta}{2} = 0.0988$$

Figure 4.8. Scheme of Measuring the Angle Between Incident Beams.

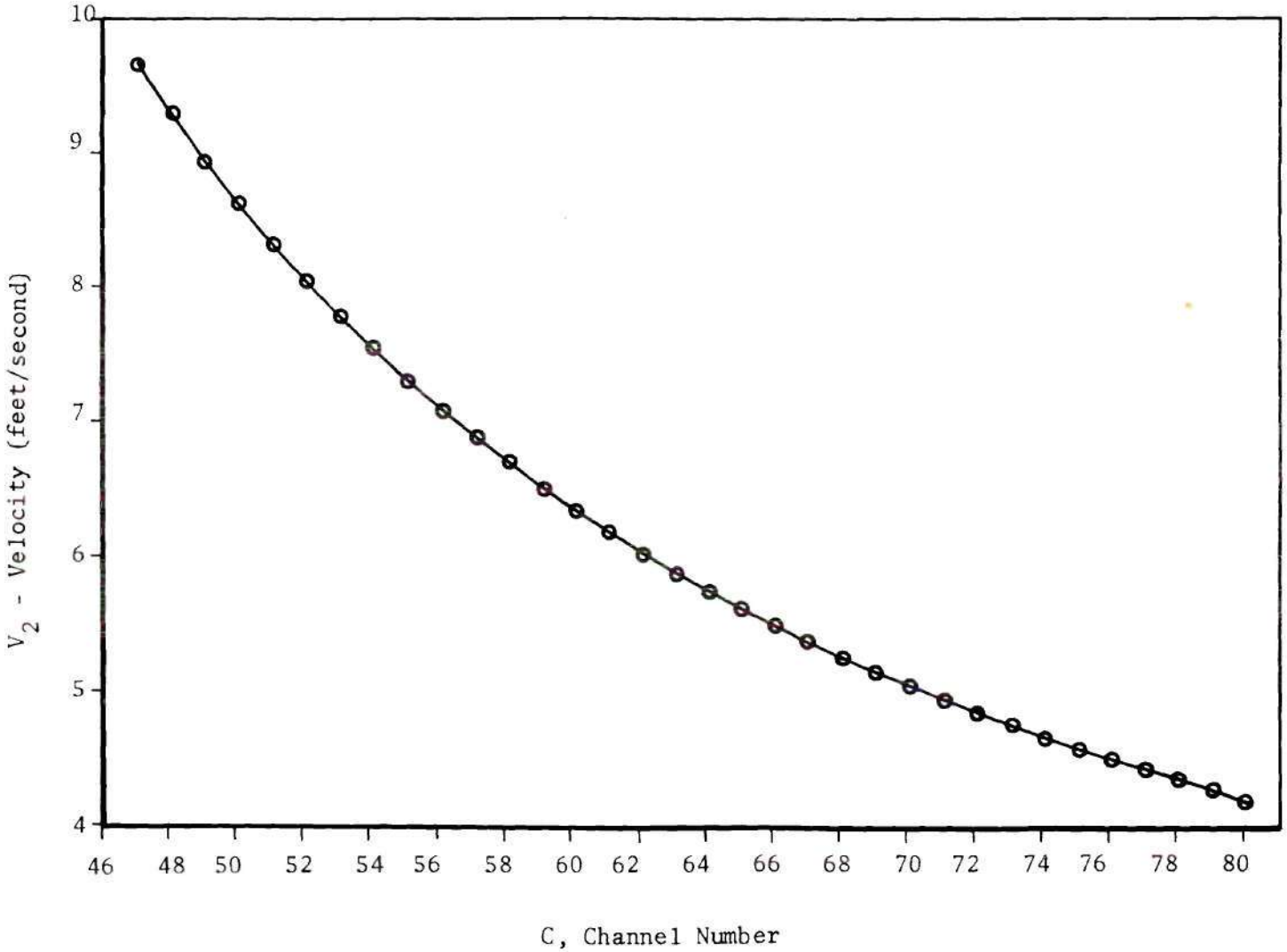

Figure 4.9. Calibration Chart - Channel Number Versus Velocity

power fed to the speaker. The heterodyne volume was traversed axially as well as radially with the vibrating needle and Doppler signal amplitudes were recorded for various axial and radial locations inside the volume. These amplitudes were subsequently normalized with respect to the maximum recorded signal and the results were plotted as contours of equal Doppler amplitudes.

In order to initially establish the basic feasibility of utilizing the present LDV system for axisymmetric liquid jet studies, two brief experiments were carried out. In the first test, the jet flow field was traversed axially and radially and the resulting frequency variation of the Doppler signal was continuously observed during each traverse. The second experiment involved a gradual variation of the flow rate with the help of the flow regulating needle valve and continuous observation of the resulting change in Doppler signal frequency. In both these tests, the Doppler signal was monitored on an oscilloscope screen.

Turbulent velocity fluctuations were obtained from the velocity measurement data by considering variations in counts up to 90 percent of the peak count. Information thus obtained along with the number of counts in the significant channels were subsequently utilized for determination of turbulence intensity variation.

CHAPTER V

DISCUSSION OF RESULTS

5.1 The Heterodyne Volume

Figure 5.1 shows a comparison between the theoretically predicted heterodyne volume by Brayton [21] and experimental results obtained for the LDV system of this investigation [20]. This figure shows the heterodyne volume contours of equal Doppler amplitudes. The amplitudes considered are (a) the maximum Doppler amplitude, (b) 80% of maximum amplitude, (c) 60% of maximum amplitude, (d) 40% of maximum amplitude, and (e) 20% of maximum amplitude. An inherent uncertainty of the order of $\pm$ 5 x 10^{-4} inch to $\pm$ 1 x 10^{-3} inch is associated with these measurements. This uncertainty can be attributed to the finite size of the needle probe utilized. A second factor contributing to the uncertainty is the amplitude of the needle oscillations.

The focusing lens used in the optical configuration of this study has a focal length of 90 millimeters. The experimentally determined size of the heterodyne volume for this configuration was found to be a 0.004" dia. x 0.048" long cylinder.

5.2 Feasibility Test Results

Results of the initial feasibility test runs are shown in Figures 5.2a and 5.2b. A variation of Doppler signal frequency with a decrease in jet centerline velocity is seen in Figure 5.2a as the point of measurement is moved downstream along the jet axis. The expected constancy

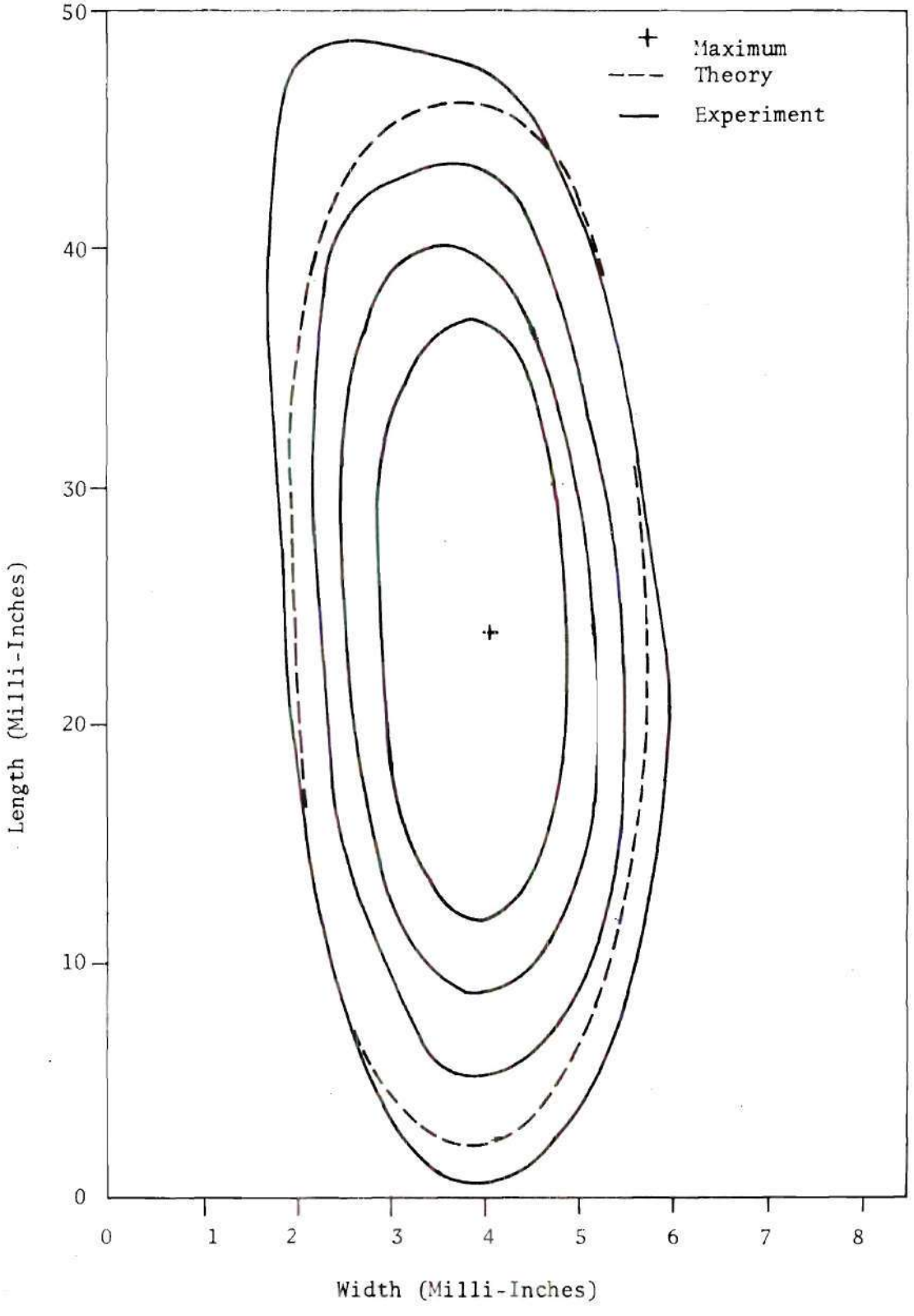

Figure 5.1. Equal Doppler Amplitude Contours In Water For Dual Beam LDV (focal length 90 mm)

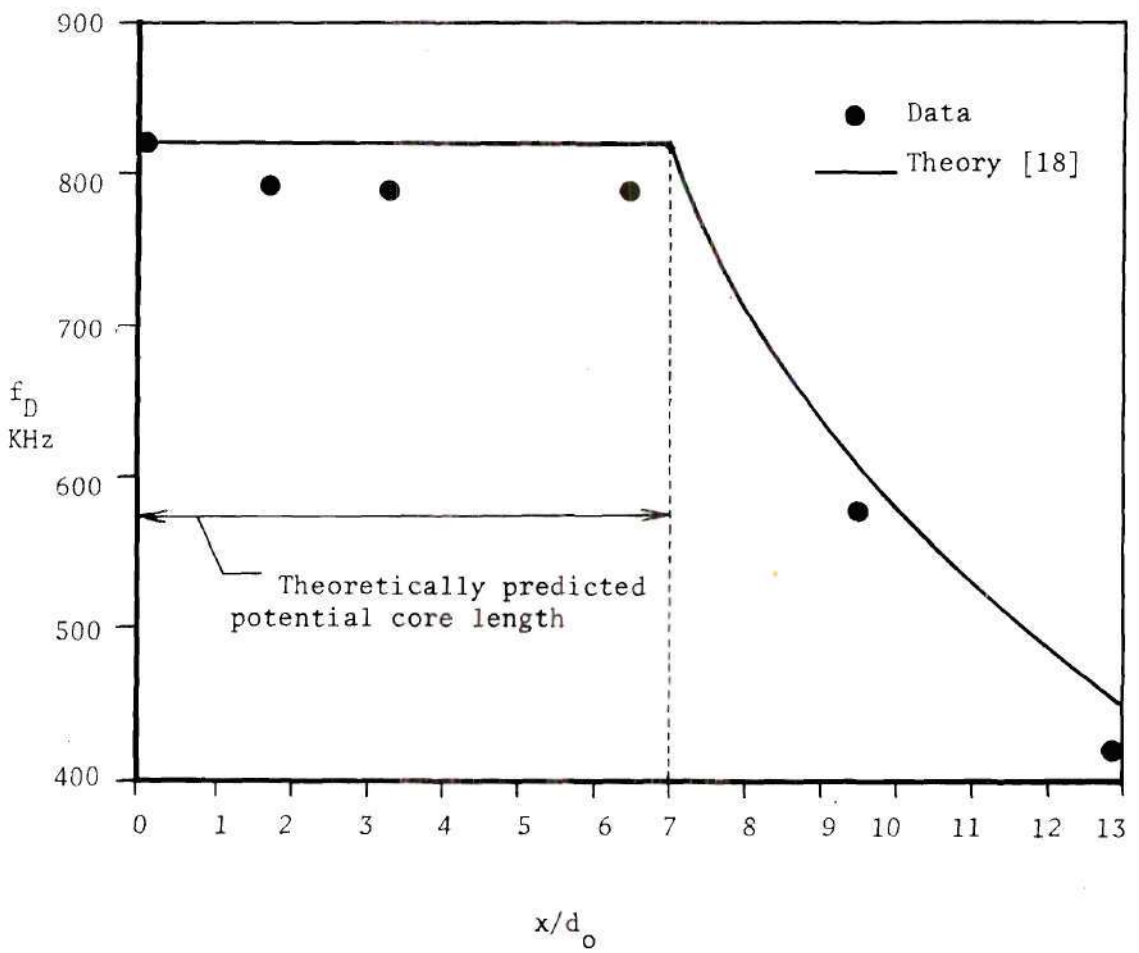

Figure 5.2(a). Variation of f_D Along Jet Centerline

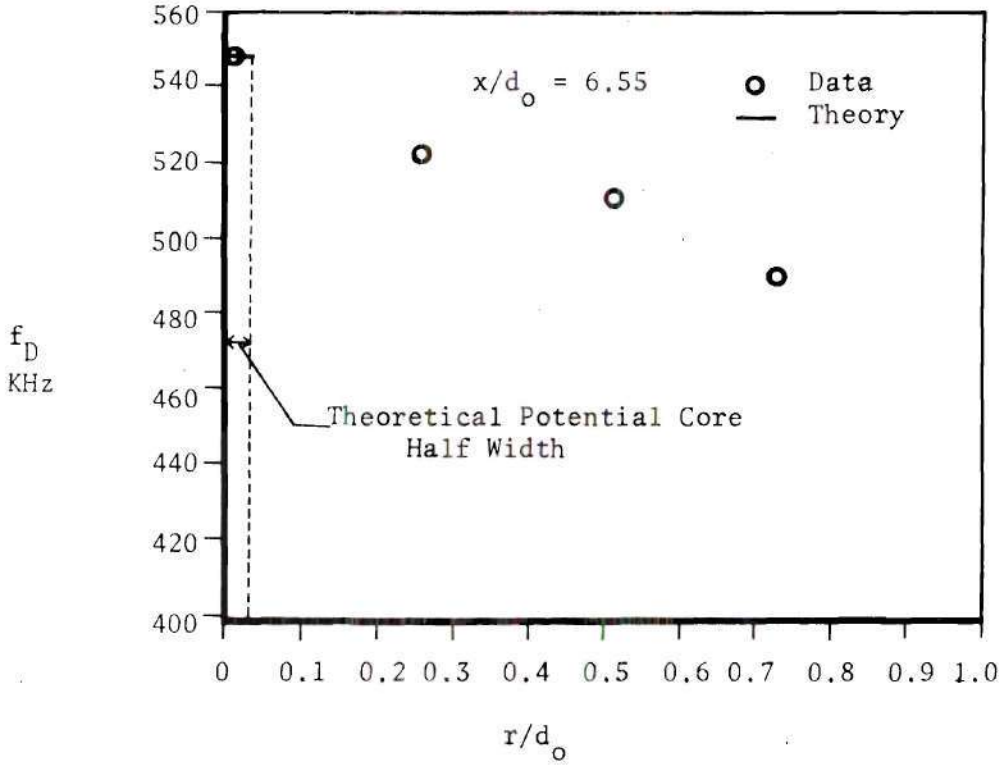

Figure 5.2(b). Radial Variation of f_D In the Transition Region

of the Doppler frequency for axial locations from nozzle exit to the end of the potential core is revealed in this figure. With reference to the relation between Doppler frequency and the associated flow velocity given by

$$f_D = 9.53 \times 10^4 V_2,$$

and the variation of jet centerline velocity along jet axis downstream of the potential core given by

$$\frac{u_{x_{max}}(x)}{u_o} = 6.4 \left(\frac{d_o}{x}\right),$$

an inverse functional relationship is to be expected between the Doppler frequency and the axial coordinate along the centerline. The measured variation of the figure follows this expected trend at axial locations in the transition and fully developed regions of the jet.

A similar variation of the Doppler frequency is expected as the jet flow field outside the potential core is traversed radially from the centerline toward the jet boundary at a specific axial location. The measured values of f_D versus r/d_o, shown in Figure 5.2b, indicate such a behavior for an axial location in the transition flow region.

Further validity of operation of the LDV system designed for this investigation was obtained when the flow rate of water in the jet was varied. At a specific location within the jet an increase in the flow velocity caused by an increased flow rate was followed by a proportionate increase in the resulting Doppler frequency. A similar pattern of decrease in the Doppler frequency was observed for decreasing flow

rates.

The initial test runs thus demonstrated the basic suitability of using the present laser Doppler velocimeter system for velocity measurements within a freely expanding axisymmetric jet of water.

Prior to translating the frequency data to the velocity data, it is worthwhile to recall the discussion presented in section 4.4 regarding the variation in the linear relationship between the channel number and signal period. It is felt that this variation can be attributed to a slight nonlinearity in the functional behavior of the TAC unit. In any case, by making calculations of the velocity values for each channel separately, the influence of this shortcoming was eliminated. In other words, the velocimeter calibration took into account the necessary correction.

5.3 The Jet Structure

5.3.1 The Potential Core

Figure 5.3 shows the jet centerline velocity at three different locations within the potential core. The results agree with the analytically predicted values within four percent.

Figure 5.4 shows the results of radial traverses inside the potential core at three different axial locations. The profiles are seen to be uniform as is to be expected inside the core. In turn, this data gives the axial decay rate of the potential flow field. The expected conical shape of the potential core with its base at nozzle exit is exhibited in this figure. It may be noted that the x_{C_L} = 0.515" curve marks the beginning of the transition zone, or the end of the potential core indicated by a vanishingly small width of the core.

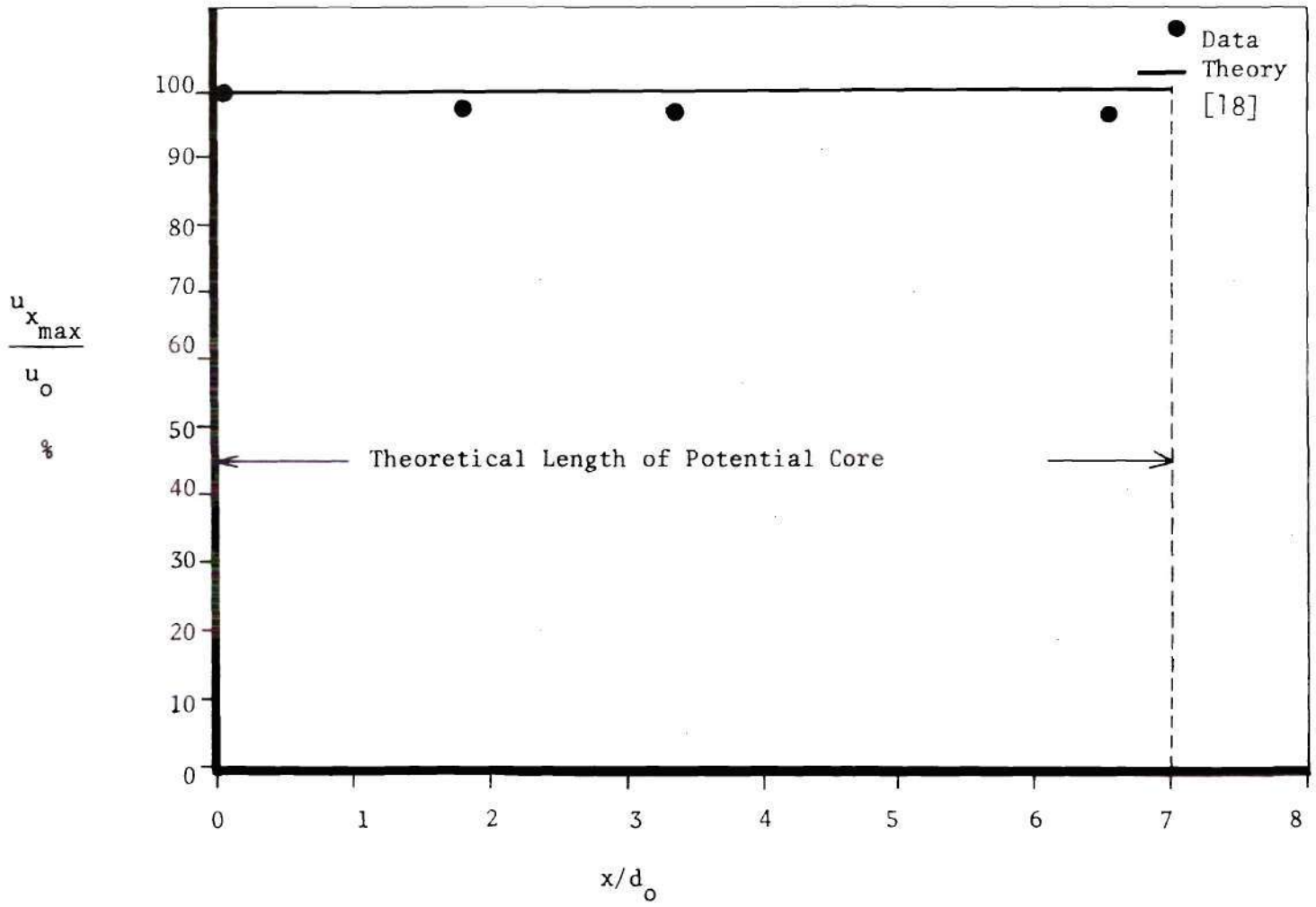

Figure 5.3. Centerline Velocity Inside the Potential Core.

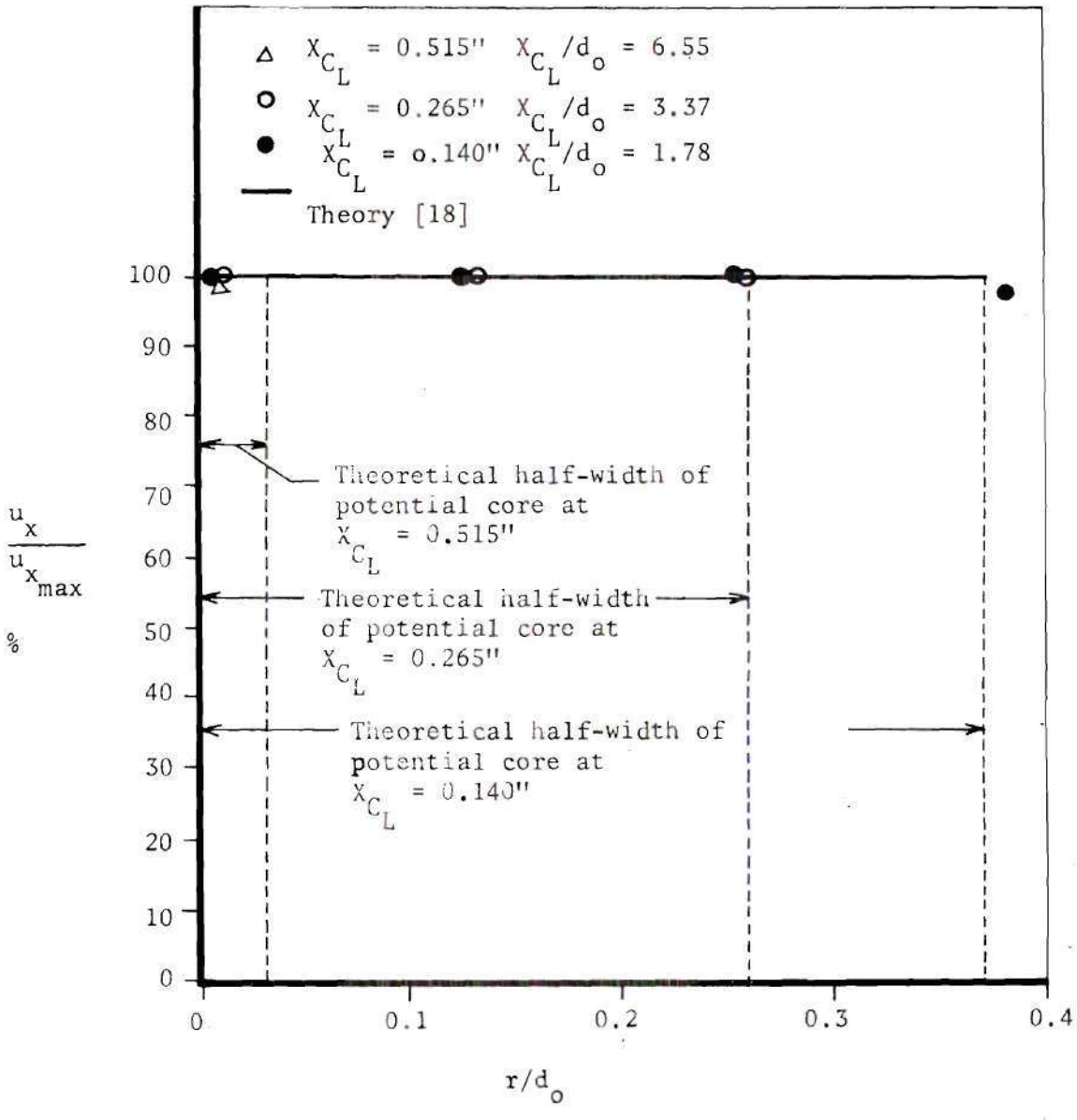

Figure 5.4. Velocity Distribution in Jet Potential Core

The measured half width of the potential core from these plots, defined by the radial location where the profiles become nonuniform, is subsequently shown in Figure 5.5. Extrapolation of the plot to the nozzle exit location gives a nozzle radius of 0.0327 inch which is in good agreement with the actual nozzle radius of 0.0393 inch.

5.3.2. The Jet Centerline Velocity

The centerline velocity for the entire length of the jet is shown in Figure 5.6. The expected constancy of the centerline velocity within the jet potential core has been already pointed out previously. Although the measurements in the fully developed zone were limited, the velocity decay along the jet axis is clearly seen. This is in agreement with the analytical prediction.

5.3.3. The Velocity Distribution in the Transition Zone

Figure 5.7 shows the velocity distribution for an axial location marking the initiation of the transition zone. Since no information regarding the velocity distribution in the jet transition zone is available at present, the data should be accepted with caution. However, the expected trend of radial decay of the velocity can be seen in the figure.

5.3.4. The Free Shear Layer In the Near Jet Field

A free shear layer of a jet is formed due to a shear discontinuity at the nozzle exit. In fact, a jet is defined primarily by this turbulent layer. In the near jet flow field the free shear layer starts at a radial location marking the edge of the potential core and it extends radially out to the outer edge of the jet. Naturally, the thickness of this layer increases with the axial location in the downstream

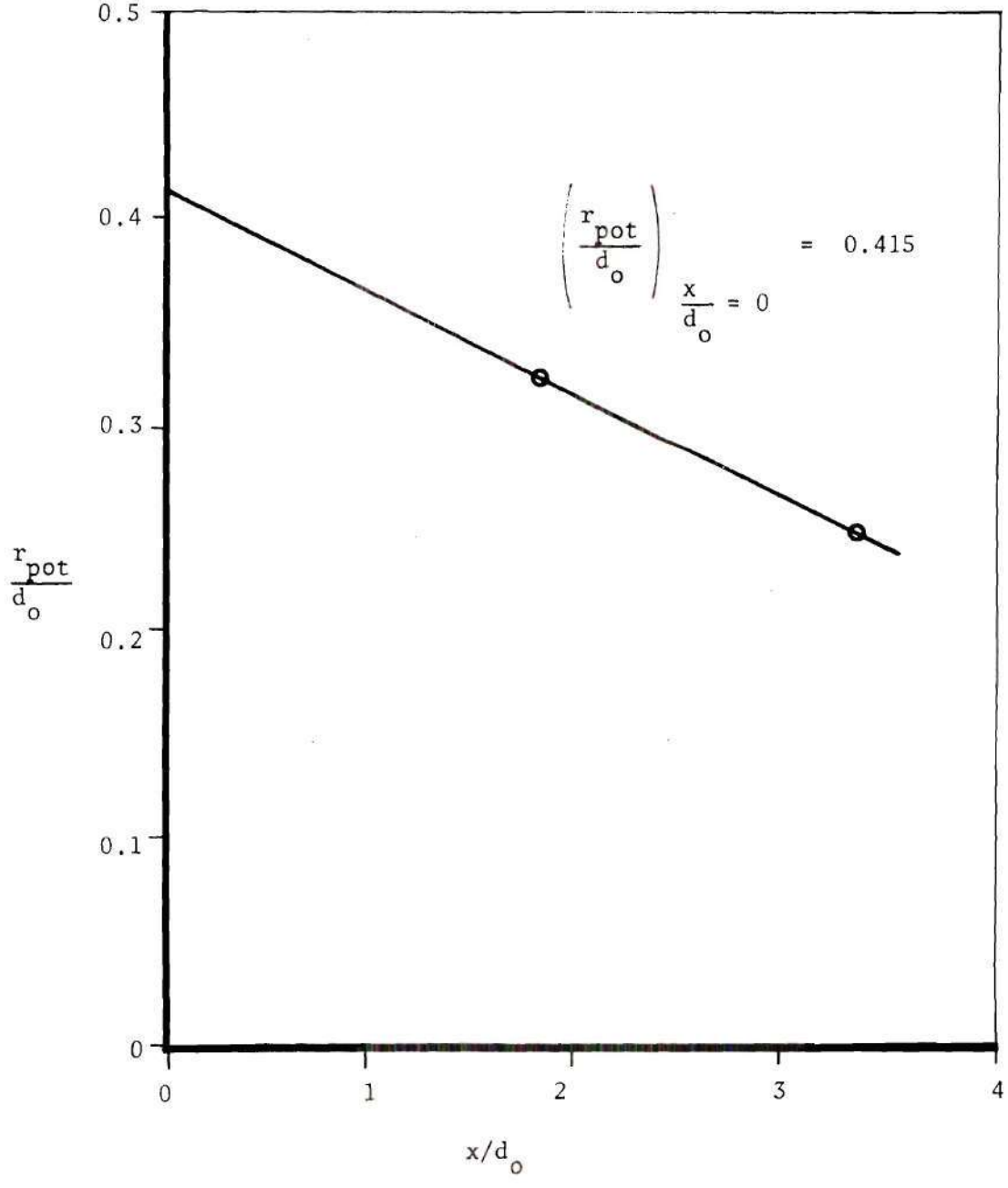

Figure 5.5. The Jet Potential Core Half-Width

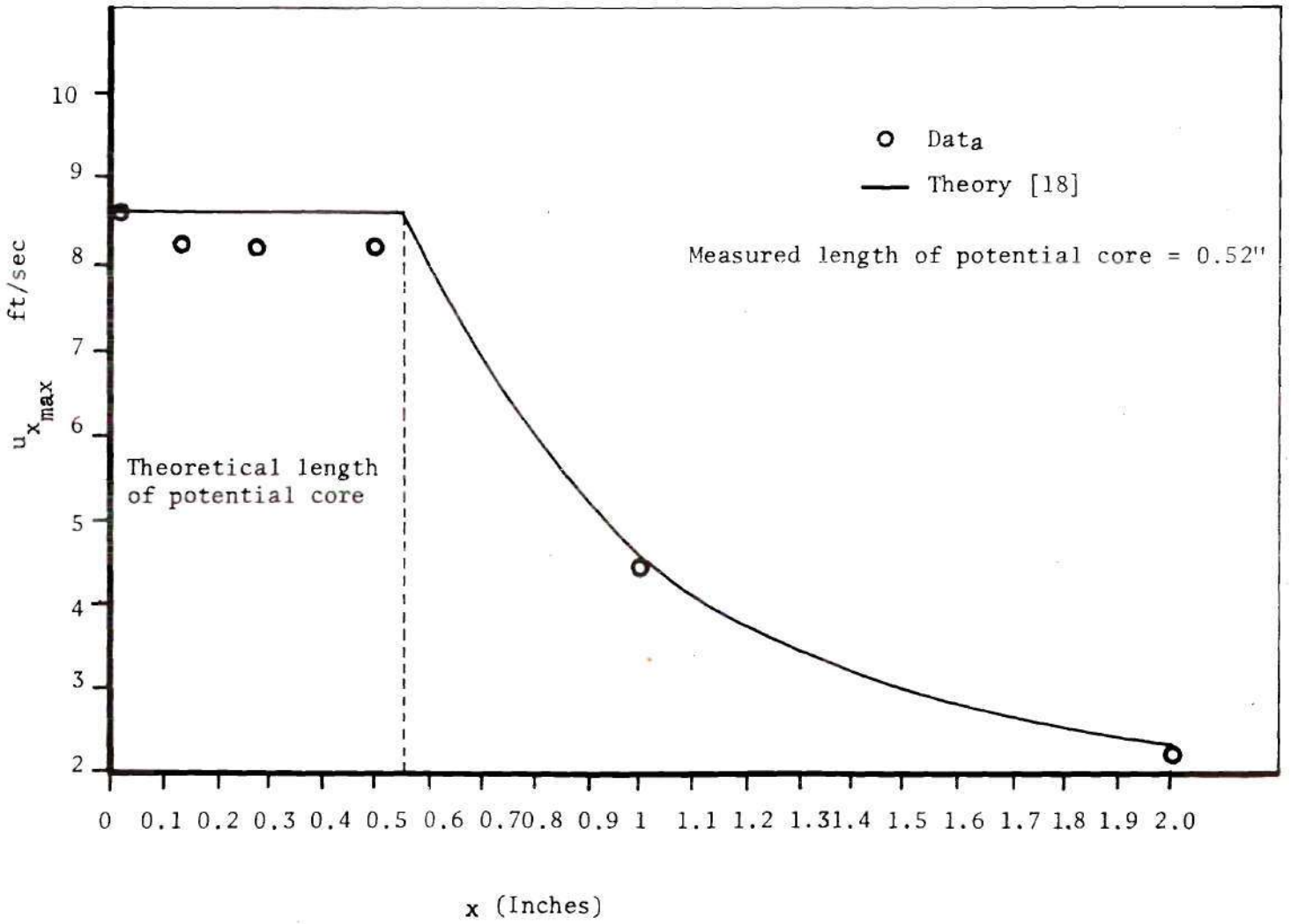

Figure 5.6. The Jet Centerline Velocity

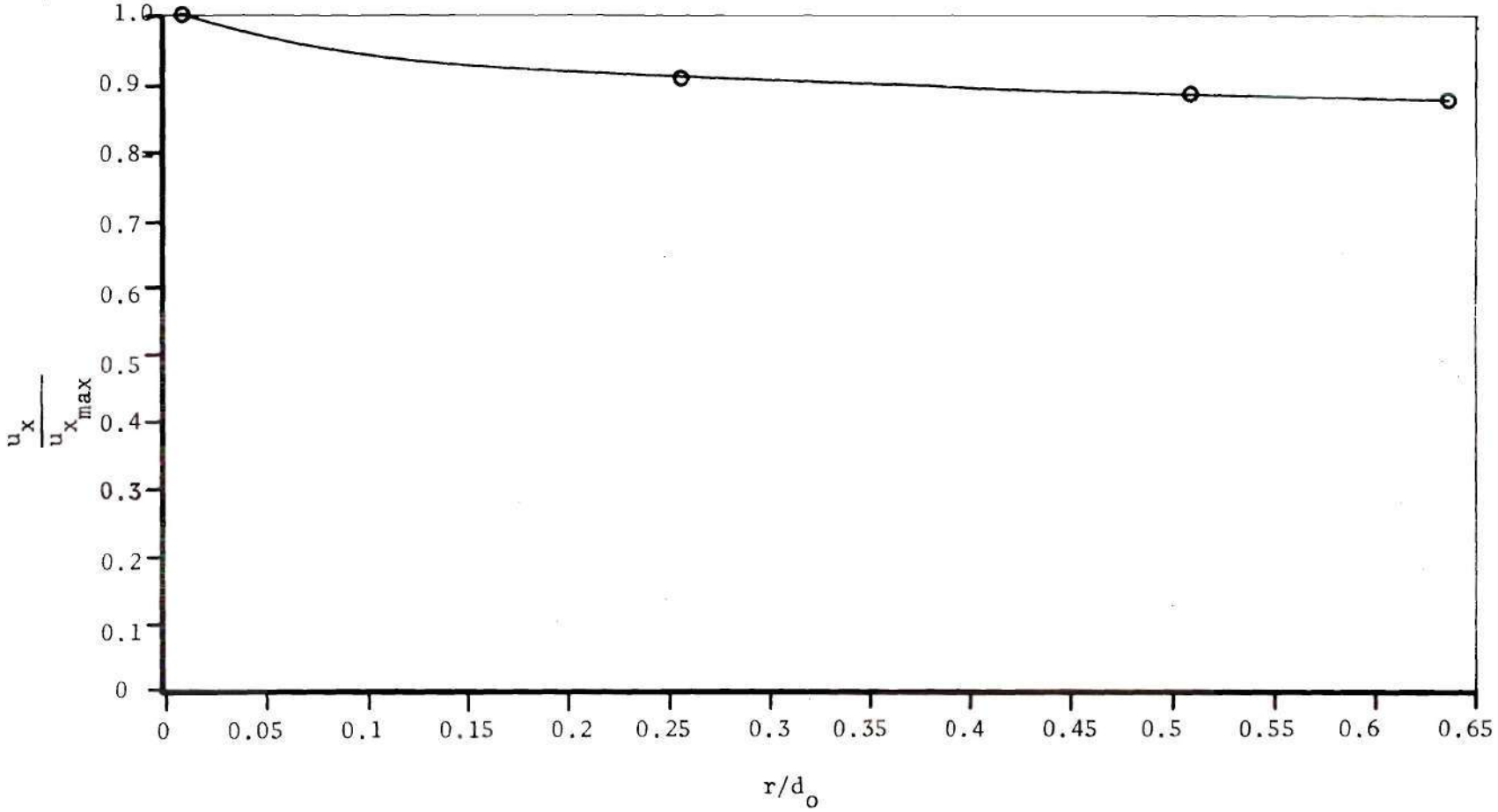

Figure 5.7. Velocity Distribution in the Transition Zone

direction. This layer also exhibits the developing nature of the turbulent jet. When the jet is fully developed, its entire structure may be viewed as a free shear layer. In Figure 5.8 are shown the results of measurements within the free shear layers at two different axial locations. Both the curves exhibit a decreasing velocity as the radial location is moved outward from the axis.

5.3.5 The Jet Turbulence Structure

At the outset it is admitted that considerable difficulty was experienced in making any quantitative turbulence studies. The overall progress in developing turbulence measurement capacity of the present LDV system has been somewhat slow. An extensive amount of further research is needed to generate useful system configurations to make meaningful turbulence studies. A few qualitative results are presented here only for the sake of completeness.

Figure 5.9 shows axial turbulence intensity along the jet centerline. Although the trend of the curve obtained in this investigation is somewhat agreeable in the near jet field with the results of Bradbury [22], the curve drops off for large downstream locations.

Figure 5.10 shows a measured profile of $\overline{u'^2}/u_o^2$ versus the radial distance from the centerline of the jet, in the transition flow region. It is observed that the turbulent fluctuations vary considerably over the radial traverse conducted. Since little is known about the turbulence structure in the transition zone, a comparative study of the data has not been made.

The corresponding $\overline{u'^2}/u_o^2$ in the fully developed jet flow field is shown in Figure 5.11 for an axial location in the fully developed zone

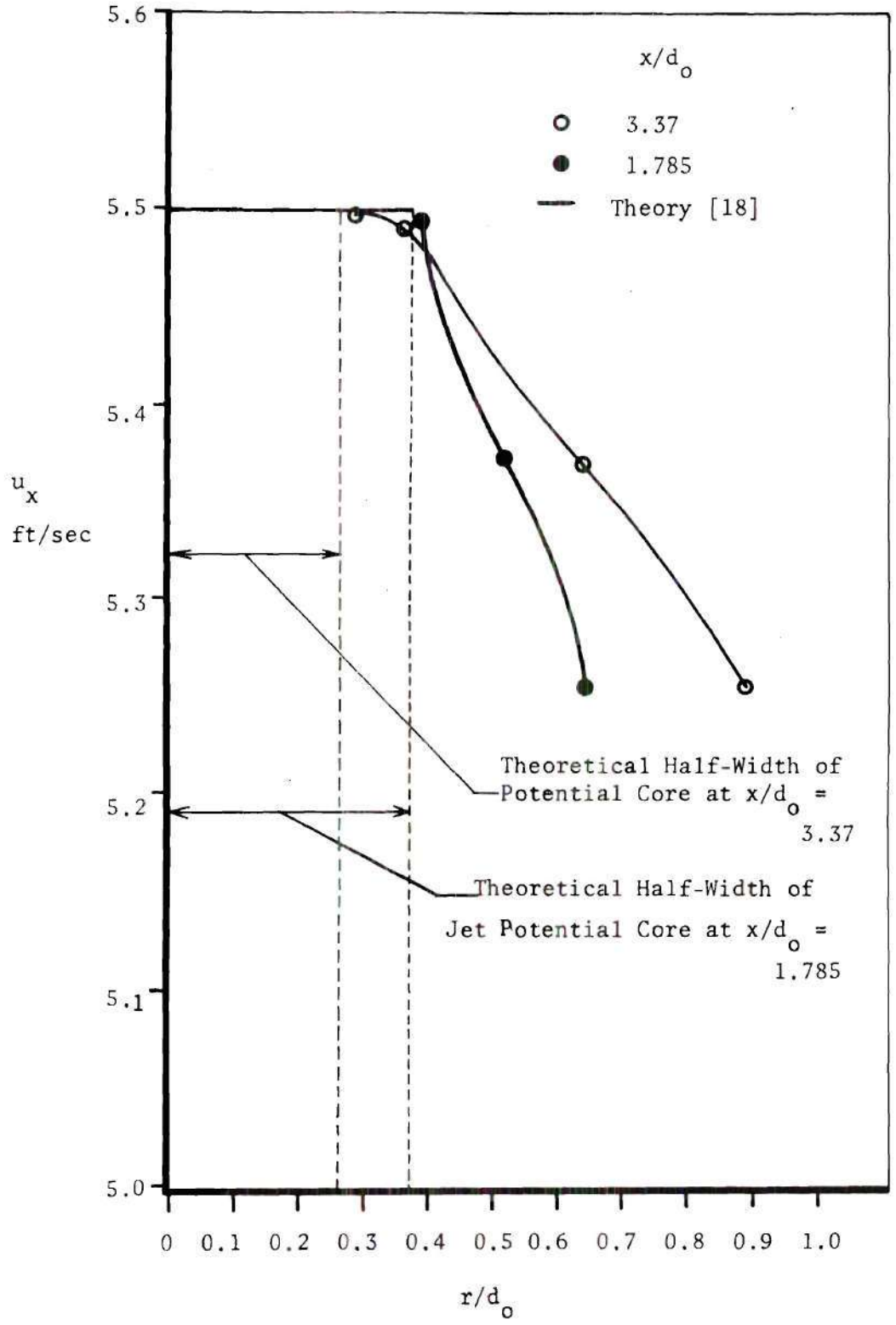

Figure 5.8. Velocity in the Near Field Free Shear Layer

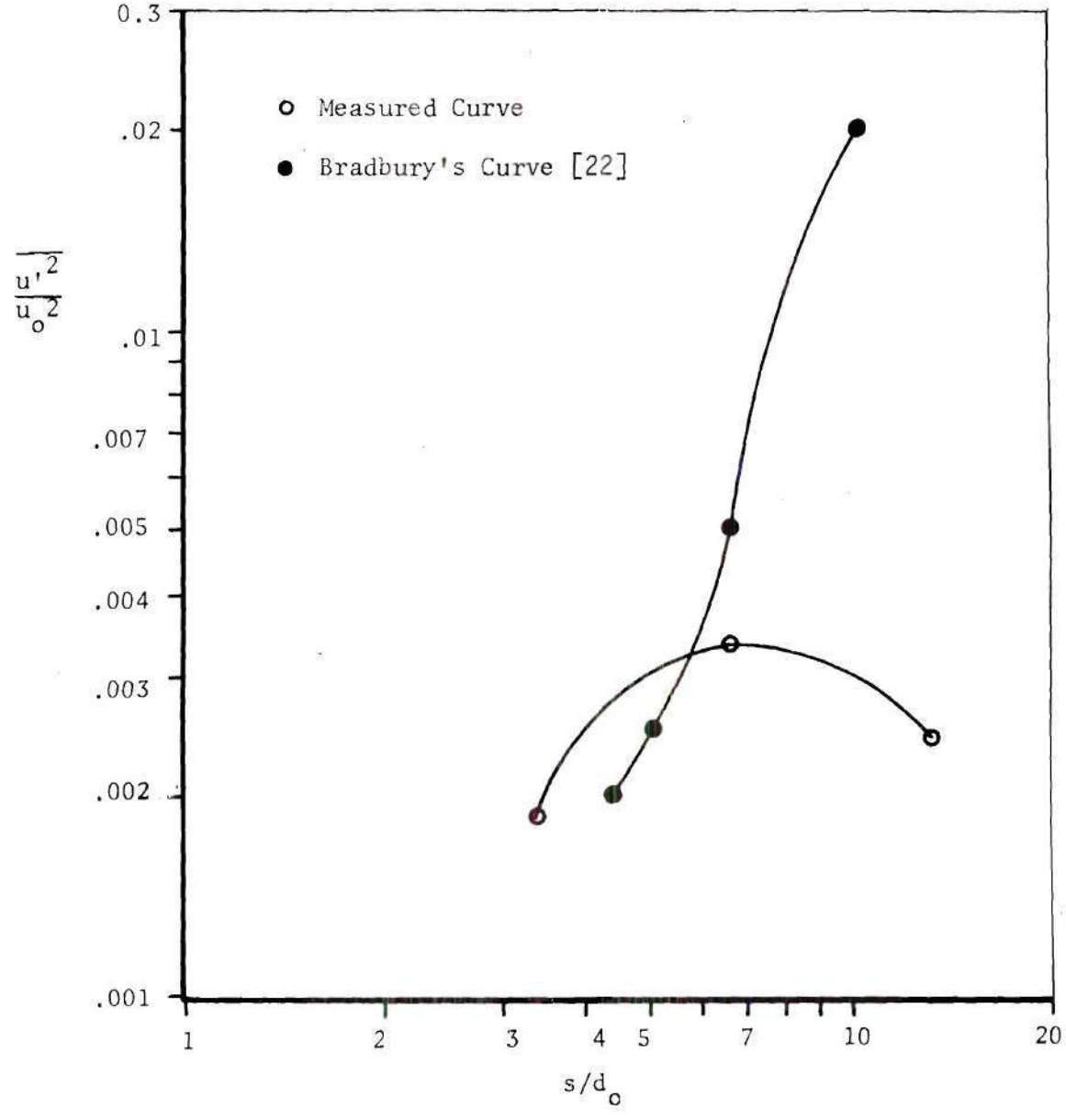

Figure 5.9. $\overline{u'^2}/u_o^2$ Variation Along Jet Centerline

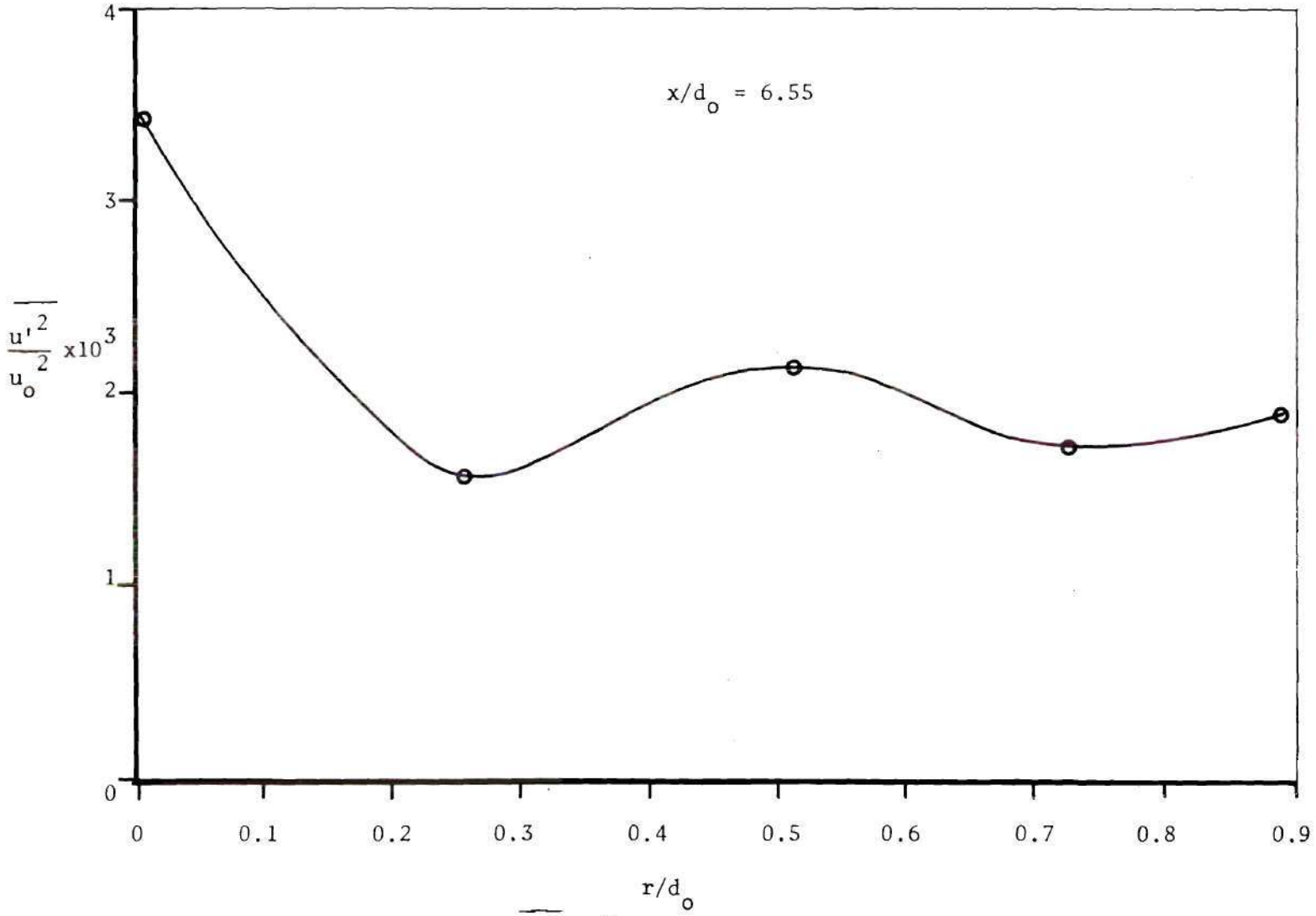

Figure 5.10. Variation of $\overline{u'^2}/u_o^2$ Along the Radial Coordinate In The Transition Zone

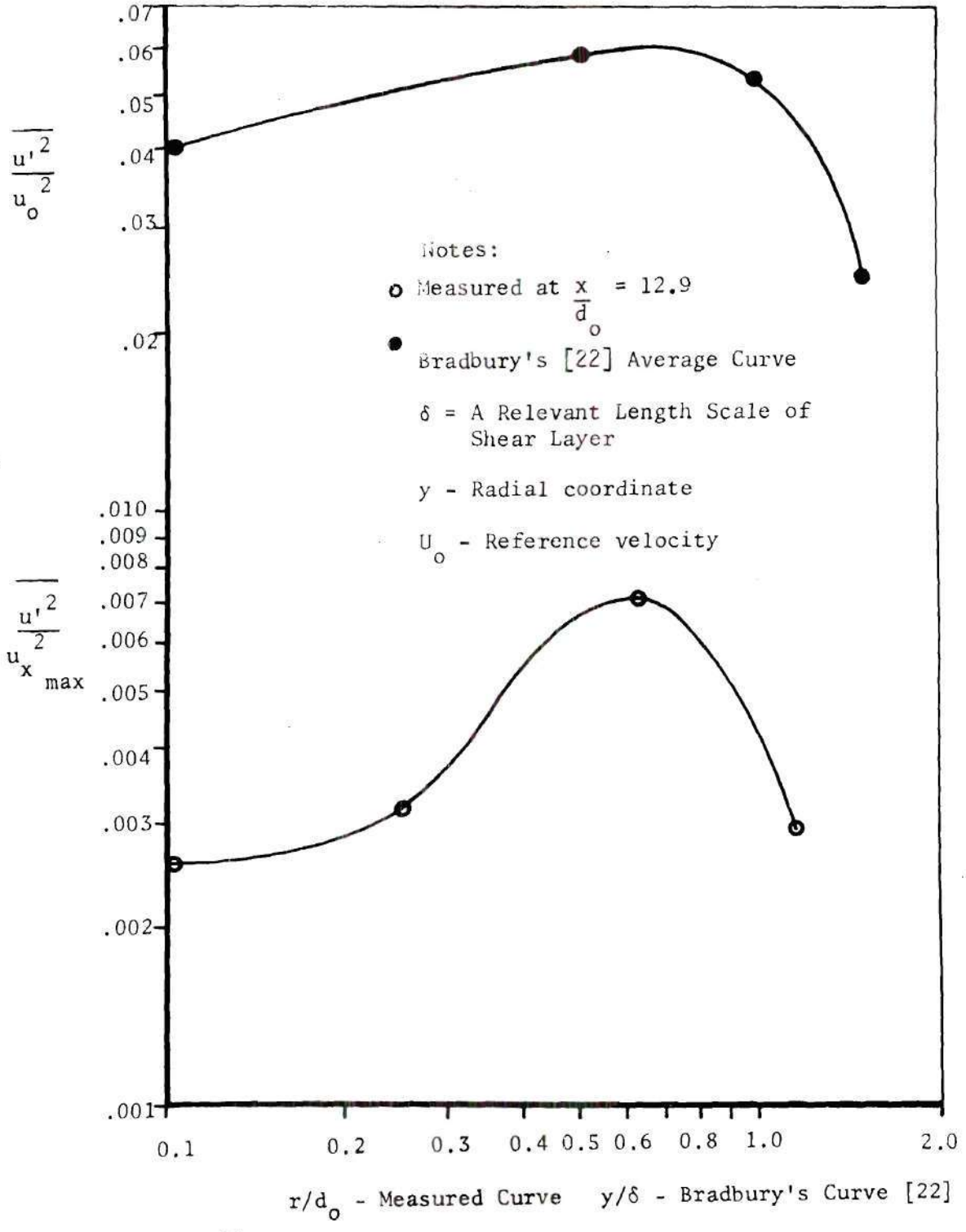

Figure 5.11. $\overline{u'^2}/u_{x_{max}}^2$ Measured Profile In Fully Developed Jet Flow Field and $\overline{u'^2}/u_o^2$ Average Profile Of Bradbury [22] In Fully Developed Jet Flow Field

of the jet. A comparison of this curve with a similar profile developed by Bradbury [22] for a gas jet flow field shows good agreement. The figure shows a measured turbulence structure profile which is close to the state of self-preservation, as seen by its comparison with Bradbury's curves.

CHAPTER VI

CONCLUSIONS AND RECOMMENDATIONS

On the basis of the experiments performed with the newly developed LDV system, and on the basis of a literature survey conducted during this investigation, the following conclusions are made:

(i) A sufficiently small size of the heterodyne volume can be obtained to determine local velocity data with a high instrument resolution and without perturbing the jet flow field.

(ii) The operational characteristics of the readout system yield continuous information on the instantaneous velocity and only a negligible information is lost due to any dropout of the signal.

(iii) The independence of the signal frequency on scattering direction provides a relatively noise free signal.

(iv) The velocimeter is readily calibrated and the calibration holds good for all subsequent measurements in the selected frequency range.

(v) The digital readout system shows its promise for turbulence measurement since the frequency data is obtained in digital form as the number of counts for a given signal period.

(vi) The data obtained shows good agreement with the theoretical predictions within and beyond the jet potential core zone.

(vii) A suitably designed optical configuration results in elimi-

nating cumbersome alignment procedure.

(viii) Quality of the signal is a strong function of the relative intensities of the two incident beams. Signal to noise ratio is considerably improved as the two intensities are brought closer - within 95%.

It is recommended that the following aspects of this research be continued further:

(i) Influence of the size and concentration of scattering particles and the beam separation on the Doppler signal need to be examined in further detail.

(ii) An accurate way of establishing the location of the focal point inside the flow field needs to be developed in order to improve the overall accuracy of the system.

(iii) A quantitative evaluation of the effect of beam refraction through duct walls on the resulting Doppler signal characteristics and the effective focal length needs to be performed.

(iv) A detailed study needs to be undertaken in order to determine the effect of jet pipe vibrations on the resultant jet flow field for relatively high exit velocities.

APPENDIX A

CONTROL SETTINGS

Ortec Amplifier

Positive/negative - positive
Unipolar/Bipolar - unipolar
Coarse gain - 64
Fine gain - 7.5 (compatible with 10-50 mv signals)

Discriminator

Output - C or D
Pulse width - set for 0.1 P-P output at C or D
Gated/ungated - ungated
Normal/clipped mode - clipped
Threshold - 2.10

Hewlett-Packard Amplifier

First/second differentiator - out
Integrator - out
Invert/noninvert - noninvert
Coarse gain - 1
Fine gain - 2.80

TAC

Output - positive
Range - 30 usec. (ext. position provided to extend this as needed for low frequencies)
Pulse width - set for 1.5 usec. width
Dead time - set so that distance between TAC out pulses is approximately 80 usec. when the Noise Generator is being used on 500 kHZ range

Nuclear Data PHA System

PAD:

Coarse gain - 16
Fine gain - full
Discriminator - 0.00

ADC:

Conversion gain - 4096
Upper level discriminator - 10.0

Nuclear Data PHA System (continued)

Lower level discriminator - 1.0
Zero coarse - 10.0

Master Control:

Acquision program - PHA
Overlap - off
Add/substract - add
Display - live
Timer - PHA internal

Data Reduce/Integrate:

Off

Teletype Drive:

Read in/out - out
Address - on
Leader - on

Readout In/Out Display

Autocycle - single
Read in/out - printer
Plotter calibrate - off
Digital readout - all
Scanmaster - 0.0
Scanmaster X-gain - counterclockwise

APPENDIX B

NUMERICAL CALCULATIONS

Turbulence Intensity

Turbulence intensity was calculated from the expression

$$\text{Intensity} = \frac{\sqrt{\overline{u'^2}}}{\bar{u}_x} , \tag{B.1}$$

where

$$\overline{u'^2} = \frac{\sum_j Nj\ (uj - \bar{u}_x)^2}{\sum_j Nj} \tag{B.2}$$

and

$$\bar{u}_x = \frac{\sum_j Nj\ uj}{\sum_j Nj} , \tag{B.3}$$

where j = channel number,

Nj = number of counts in channel j,

and $uj = \bar{u}_x + u'$, with

uj = instaneous flow velocity

and u' = fluctuating component

BIBLIOGRAPHY

1. Yeh, Y., and H. Z. Cummins, "Localized Fluid Flow Measurements With An He-Ne Laser Spectrometer," Applied Physics Letters, Volume 4, 15 May 1964, pp. 176-178.

2. Foreman, J. W., Jr., E. W. George, J. L. Jetton, R. D. Lewis, J. R. Thornton and H. J. Watson, "8C2-Fluid Flow Measurements With a Laser Doppler Velocimeter," IEEE Journal of Quantum Electronics, Volume QE-2, August 1966, pp. 260-266.

3. Davis, D. T., "Analysis of a Laser Doppler Velocimeter," ISA Transactions, Volume 7, 1968, pp. 43-51.

4. Grant, G. R. and R. W. Donaldson, "A Laser Velocity Measurement System for High-Temperature Wind Tunnels," Scientific & Technical Aerospace Reports," Volume 8, June 8, 1970.

5. Huffaker, R. M., "Laser Doppler Detection Systems for Gas Velocity Measurement," Applied Optics, Volume 9, May 1970, pp. 1026-1039.

6. Foreman, J. W., Jr., R. D. Lewis, J. R. Thorton and H. J. Watson, "Laser Doppler Velocimeter For Measurements of Localized Flow Velocities in Liquids," Proceedings of the IEEE, Volume 54, March 1966, pp. 424-425.

7. Lewis, R. D., J. W. Foreman, Jr., H. J. Watson and J. R. Thornton, "Laser Doppler Velocimeter for Measuring Flow-Velocity Fluctuations," Research Notes, July 1967, pp. 433-435.

8. Goldstein, R. J. and D. K. Kreid, "Measurement of Laminar Flow Development in a Square Duct Using a Laser-Doppler Flowmeter," Paper No. 67--APM-37, Journal of Applied Mechanics.

9. Penney, C. M., "Differential Doppler Velocity Measurements," Applied Physics Letters, Volume 16, 15 February 1970, pp. 167-169.

10. Mazumder, M. K. and D. L. Wankum, "SNR and Spectral Broadening in Turbulence Structure Measurement Using a cw Laser," Applied Optics, Volume 9, March 1970, pp. 633-637.

11. Mazumder, M. K., "Laser Doppler Velocity Measurement Without Directional Ambiguity By Using Frequency Shifted Incident Beams," Applied Physics Letters, Volume 16, 1 June 1970, pp. 462-464.

12. Mayo, W. T., Jr., "Simplified Laser Doppler Velocimeter Optics," Journal of Physics E:Scientific Instruments, Volume 3, 1970.

13. Bedi, P. S., "A Simplified Optical Arrangement for the Laser Doppler Velocimeter," Journal of Physics E:Scientific Instruments, 1971 Volume 4, pp. 27-28.

14. Thompson, D. H., "A Tracer-Particle Fluid Velocity Meter Incorporating a Laser," Journal of Physics E:Scientific Instruments, Volume 1, September 1968, pp. 929-932.

15. Grebene, A. B., "The Monolithic Phase-Locked Loop --- A Versatile Building Block," IEEE Journal, March 1971.

16. Grisell, T. L., I. H. Hawley, Jr., B. D. Unter and P. G. Winninghoff, "Design of a Third-Generation RF Spectrum Analyzer," Hewlett-Packard Journal, August 1968.

17. Ross, W. A., "A Multichannel Pulse-Height Analyzer With A Very Fast Analog-Digital Converter," Hewlett-Packard Journal, March 1968.

18. Daily, J. W. and D. R. F. Harleman, Fluid Dynamics, Addison-Wesley Publishing Co., Inc., pp. 419, 1966.

19. Ross, M., Laser Receivers, John Wiley & Sons, Inc., New York, 1966.

20. Mathews, L. K. and J. H. Rust, "Laser Doppler Velocimeters-Performance in Open and Confined Flows," presented at the Flow Symposium, Pittsburgh, May 14, 1971.

21. Brayton, D. B., "A Laser, Doppler Shift, Velocity Meter With Self-Aligning Optics," Proceedings of the Technical Program, Electro-Optical Systems Design Conference, New York, September 1969, pp. 168-177.

22. Bradbury, L. J. S., "The Structure of A Self-Preserving Turbulent Plane Jet," Journal of Fluid Mechanics, Volume 23, Part 1, 1965, pp. 31-64.